This is to certify that the

thesis entitled

Back Extrusion (Annular Pumping) Technique for Measuring Thixotropic Properties

presented by

Fernando Alberto Osorio-Lira

has been accepted towards fulfillment
of the requirements for

Ph.D. degree in Agricultural Engineering
Food Sci. & Hum. Nutr. (Dual Maj)

James F. Steffe
Major professor

Date June 16, 1989

BACK EXTRUSION (ANNULAR PUMPING) TECHNIQUE FOR MEASURING THIXOTROPIC PROPERTIES

By

Fernando Alberto Osorio-Lira

A DISSERTATION

Submitted to
Michigan State University
in partial fulfillment of the requirements
for the degree of

DOCTOR OF PHILOSOPHY

in

Agricultural Engineering

(Dual Major : Food Science)

Department of Agricultural Engineering

Department of Food Science and Human Nutrition

1989

ABSTRACT

MEASUREMENT OF THIXOTROPIC PROPERTIES WITH A BACK EXTRUSION (ANNULAR PUMPING) DEVICE

By

Fernando Alberto Osorio-Lira

Many fluid foods exhibit time-dependent behavior. Several problems have been reported regarding the traditional use of rotational rheometers to evaluate time-dependent behavior. Back extrusion (annular pumping) is presented as a new method for evaluating thixotropy.

A technique was developed to evaluate thixotropy by using a seven parameter model equation for a thixotropic fluid in conjunction with the equations describing the back extrusion of a Herschel Bulkley fluid.

A new mathematical expression was derived to evaluate time-dependent behavior of a thixotropic fluid in a back extrusion device. The model was applied to typical thixotropic fluids: a 7% bentonite suspension, and a 1% Iota-Carrageenan solution. Testing was conducted in both concentric cylinders and parallel plates geometries considering steady shear and oscillatory modes (parallel plate only). The results of these tests were compared to the results obtained with the back extrusion technique.

One of the main advantages of the back extrusion technique is that it allows one to follow the changes that occur in yield stress over time after the sample has been disturbed and allowed to rest. This fact means that the future potential for this technique is excellent.

To : Alicia

Carolina

Pilar

Denisse

Aurora

and

H. Rolando

ACKNOWLEDGMENTS

I am deeply indebted to Dr. James F. Steffe, my major professor, for his advice, interest and continuous support throught the course of this study.

Sincere appreciation is extended to the guidance committee members: Dr. Mark Uebersax, Dr. Ajit Srivastava, Dr. Robert Ofoli, Dr. Kris Berglund and Dr. Ron Morgan.

Special thanks is expressed to ODEPLAN - CHILE for their financial support during the first three years of my studies.

TABLE OF CONTENTS

LIST OF TABLES

LIST OF FIGURES

NOMENCLATURE

a = radius of the plunger, m

a_1 = constant defined in Eq. [66]

A = constant defined in Eq. [55]

$\bar{A}$ = level of fluid measured from the fluid surface to 0, m

A_1 = constant defined in Eq. [69]

b = constant defined in Eq. [66]

B_1 = constant defined in Eq. [69]

C = function defined in Eq. [61]

C_Λ = function defined by Eq. [61]

$\bar{C}$ = averaged value of function C in Eq. [68]

$\frac{dv}{dr}$ = shear rate, s^{-1}

D = diameter, m

F = force applied to the plunger, N

F_b = buoyancy force, N

F_{cb} = force corrected for buoyancy, N

F_T = recorded force while plunger is traveling down, N

F_{Te} = recorded force after the plunger is stopped, N

g = acceleration due to gravity, m/s^2

G = function defined in Eq. [49] defining a material as a shear type

G' = storage modulus or dynamic rigidity, Pa

G'' = loss modulus, Pa

h = function defined in Eq. [50] determining the state of

thixotropic fluid

K = ratio of radius of plunger to that of outer cylinder, dimensionless

L = length of annular region = $\overline{AO} + \overline{OB}$, m

m = exponent defined in Eq. [57]

M = function defined in Eq. [57]

n = flow behavior index, dimensionless

O = initial level of fluid when the plunger has not been forced down into the sample, m

$\overline{OB}$ = position of the plunger bottom, measured with respect to O, m

p = static pressure, Pa

p_1 = pressure in excess of hydrostatic pressure at the plunger base, Pa

p_o = pressure at entrance to annulus, Pa

P = pressure drop per unit of length, Pa/m

$P|_o$ = pressure drop per unit of length right after a step change in plunger velocity, Pa/m

$P|_\infty$ = pressure drop per unit of length at equilibrium at a given plunger velocity, Pa/m

Q_T = total volumetric flow rate through the annulus, m^3/s

r = radial coordinate, measured from common axis of cylinder forming annulus, m

s = constant defined in Eq. [55]

R = radius of outer cylinder of annulus, m

t = time, s

t_f = time at the end of the test, s

T = dimensionless shear stress, defined by Eq. [36]

T_0 = dimensionless yield stress, defined in Eq. [37]

Tw = dimensionless shear stress at the plunger wall

u_r = radial component of the velocity inside the annulus, m/s

u_z = axial component of the velocity inside the annulus, m/s

v_p = velocity of the plunger, m/s

x = ordinate, m

y = abscissa, m

z = axial coordinate, m

GREEK SYMBOLS

α = parameter defined in Eq. [58]

γ = strain, dimensionless

$\dot{\gamma}$ = shear rate, s^{-1}

$\dot{\gamma}_{HB}$ = shear rate at the plunger wall for a Hershel Bulkley fluid, s^{-1}

$\dot{\gamma}_N$ = Newtonian shear rate for a fluid in a back extrusion device, s^{-1}

Γ = inverse time constant for a thixotropic fluid in a back extrusion device, s^{-1}

ϵ = parameter defined in Eq. [95]

η = consistency coefficient, Pa s^n

η' = dynamic viscosity, Pa s^{-1}

η^* = complex viscosity, Pa s^{-1}

κ = structural parameter, dimensionless

$\dot{\kappa}$ = substantial derivative of structural parameter, s^{-1}

κ_e = equilibrium structural parameter defined in Eq. [58]

κ_o = initial value of structural parameter

λ = a value of dimensionless radial coordinate ρ for which the shear stress is zero

λ_+ = limit of plug region in Herschel Bulkley flow, near the cylinder wall, as shown in Fig. 4

λ_- = limit of plug region in Herschel Bulkley flow, near the plunger wall, as shown in Fig. 4

Λ = function defined in Eq. [62]

$\rho = \frac{r}{R}$ = dimensionless radial coordinate

σ = shear stress, Pa

$\dot{\sigma}$ = substantial derivative of shear stress, Pa s

σ_e = equilibrium shear stress at a given shear rate, Pa

σ_0 = equilibrium yield stress defined in Eq. [51], Pa

σ_y = structural parameter κ dependent yield stress, Pa

σ_w = shear stress at the plunger wall, Pa

ϕ = dimensionless velocity defined in Eq. [38]

ϕ_p = dimensionless velocity at the plunger wall

Φ = dimensionless flow rate

ψ = function defined in Eq. [66]

ω = frequency, rad/s

CHAPTER 1

INTRODUCTION

1.1 Research Justification

Many fluid foods exhibit time-dependent behavior. Knowledge of rheological properties of thixotropic food stuffs is required to solve food industry problems in numerous areas : process and equipment design, quality control, evaluation of processing parameters, product development and shelf-life studies, evaluation of consumer acceptance or texture.

Several rotational instruments : concentric cylinders, mixer viscometer, parallel plates and cone and plate have been used to evaluate time-dependency. Techniques such as step change in shear stress, step change in shear rate, hysteresis loop, and oscillatory testing have been developed and used with the mentioned instruments.

Several problems have been reported in the literature regarding the use of rotational rheometers to evaluate thixotropy : sample creeping out of the gap (Mewis, 1979); partially sheared time-dependent yield stress sample undergoing shear at a steady rotational speed in the gap of a rotational rheometer; strong dependence of the shear rate, at a given rotational speed, on the time-dependent change of the fluid properties (Nguyen and Boger, 1987). An additional problem is that many

food materials contain large particles which cannot be accommodated in the narrow gap of rotational instruments.

One of the most used techniques to evaluate thixotropy with rotational rheometers is the rate step change, where the rate of rotation of the bob is changed to a given value and the shear stress is measured with time until equilibrium is reached. Nguyen and Boger (1987) concluded that meaningful transient data cannot be obtained with the constant speed experiment using the concentric cylinder geometry for time-dependent fluids with yield stress.

It is obvious from the above discussion that there exists a need for developing new techniques to study thixotropy. The back extrusion (annular pumping) test method presents advantages: all the material present in the gap is sheared during the test; loading problems are minimized so that the sample is not disturbed before testing; and flushing effects may reduce sedimentation problems. Hence, the development of a method to investigate thixotropy based on the back extrusion geometry is a valuable contribution to the field of rheology.

1.2 Objectives

The objectives of this study were : (1) To develop a technique to evaluate the thixotropic characteristics of fluids by using back extrusion testing; (2) To evaluate materials with known thixotropic behavior in a back extrusion device. To accomplish these objectives the following were also conducted: (1) A review of methods of measuring thixotropy; (2) Selection of a model mathematical equation to describe thixotropic behavior; (3) Analysis of the flow characteristics of materials obeying this model in back extrusion geometry.

CHAPTER 2

LITERATURE REVIEW

2.1 Definition of Thixotropy

The term thixotropy was first used to describe an isothermal, reversible, gel-sol (liquid-liquid) transition due to mechanical agitation (Mewis, 1979). At present, the term thixotropy is used to describe the continuous decrease of apparent viscosity with time under constant shear rate, and the subsequent recovery of viscosity when the flow is discontinued (Bauer and Collins, 1967; Reiner and Scott Blair, 1967). The opposite effect also exits and is known as antithixotropy (Cheng and Evans, 1965), rheopexy (Van Wazer,1963; Skelland,1967) or negative thixotropy (Whorlow,1980).

From its definition, thixotropy is associated with time-dependent effects. Time effects are reflected in shear rate effects but the relationship might be complicated. As viscoelasticity deals with similar effects, the relative positions of both needs to be explained. First, the definition of thixotropy does not exclude elastic effects; one important difference is that the time-dependent behavior of viscoelastic fluids arises because the response of stresses and strains in the fluids to changes in imposed strains and stresses respectively is not instantaneous; in a thixotropic fluid such response is instantaneous and the time-dependent behavior arises only because of changes in the structure of the fluid as a result of shear (Cheng and Evans, 1965).

Therefore, the time scale of thixotropy is not necessarily associated with the time scale for viscoelastic relaxation (Mewis, 1979).

2.2 Mechanism of Thixotropy

The material for this section is mostly based on the excellent review paper by Dr. Cheng (1987).

The phenomenon of thixotropy results from the microstructure of the liquid system (Kemblowski and Petera, 1981). Thixotropy may be explained as a consequence of aggregation of the suspended particles (Gillespie, 1960; Michaels and Bolger, 1962; Firth and Hunter, 1976; Van de Ven and Hunter, 1977). In these systems interaction occurs between the particles as a result of the attraction due to Van der Waals forces on the one hand, and the repulsion due to electrostatic effects on the other. The stability of the system depends upon the existence of a potential energy barrier which prevents the particles from approaching close to one another. In this way, the comparatively weak physical bonds between the particles give rise to aggregation.

If the suspension is at rest, the particle aggregates can form a spatial network and the suspension develop an internal structure; the network has to be strong enough to resist destruction by the disintegrating effects of Brownian motion. When the suspension is sheared, the weak physical bonds are ruptured and the network breaks down into separate aggregates, which can disintegrate further into smaller fragments called flow units (flocks). Brownian motion causes collisions

between the flow units, and a subsequent growth in the number of aggregates. After some time at a given shear rate, a dynamic equilibrium is established between aggregate destruction and growth, and at higher shear rates the equilibrium is shifted in the direction of greater dispersion.

The energy dissipated in the flow process which has just been described can be divided into two parts,

a) that attributable to the viscous flow of the liquid around the flow units, and

b) the additional energy dissipated because of the breakdown of the bonds between flow units, either within or between the aggregates. The main reason for the decrease of the apparent viscosity of the system with increasing shear rate is the decrease of that part of the energy dissipation which is attributable to the rupture of interparticle bonds (the number of bonds is lower at higher shear rates).

Interparticle forces are derived from the interatomic and intermolecular forces on the surface of particles. It is usual to describe these forces in terms of intermolecular potential energy, the derivative of which gives the force. Positive slope gives attraction, negative slope gives repulsion. The potentials have the form shown in Fig. [1]. At large molecular separations there is Van der Waals' attraction. When the molecules are very close together, the steep Born repulsion comes into play. Under the influence of the attraction, particles come together until the repulsion is felt. Under equilibrium the

particle separation is given by the minimum in the potential function, the potential well, at which distance the interparticle force is zero.

If the particles are sufficiently small, Brownian motion tends to move the particles up the potential curve, then separates and disperses them. For larger species, however, Brownian motion is weak and as particles collide, the attraction holds them in the potential well and they are said to be coagulated. In practical terms, this means that the particles in the dispersion do not remain dispersed for long and they coagulate to form large agglomerates which settle out under gravity. Under this condition, the particles and the dispersion are said to be unstable.

A solid particle is often negatively charged on the surface. In a suspending liquid containing electrolytes, the surface may carry specifically adsorbed co-ions (forming the inner Helmholtz layer). To balance this negative charge, positive counter-ions are attracted to the particle, as shown in Fig. [2]. Close to the surface, the counter-ions are strongly held to form the outer Helmholtz or Stern layer. Further from the surface, the counter-ions are less strongly held: the ionic concentration decreases gradually with distance (the Gouy diffuse layer). If the particle is made to move in the liquid, the strongly held Stern layer moves with it, while the ions in the Gouy layer are left behind. A shear plane therefore marks out the boundary between the Stern and the Gouy layer. The potential at the shear boundary is the zeta-potential, ζ . Neither the position of the shear plane nor the value of the potential are well defined in the literature.

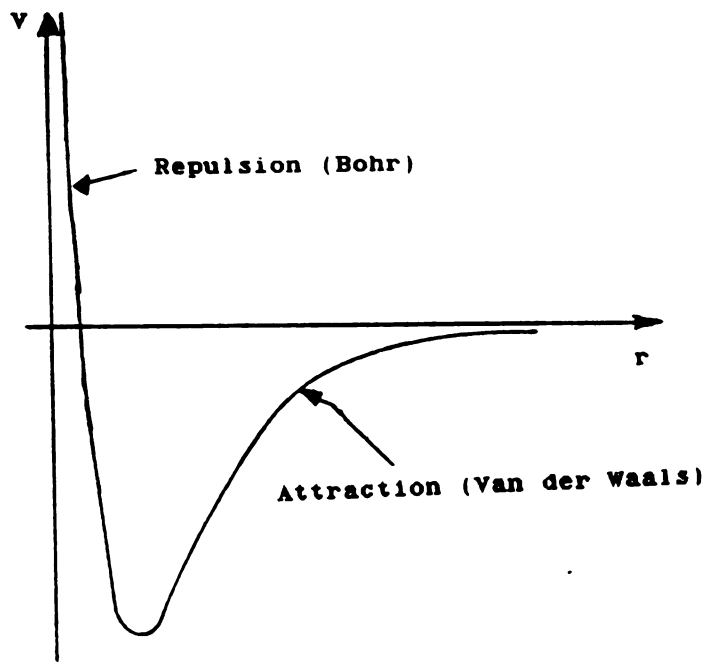

Figure 1. Forces between atoms/molecules expressed as pair potential energy, V. (From Cheng, 1987).

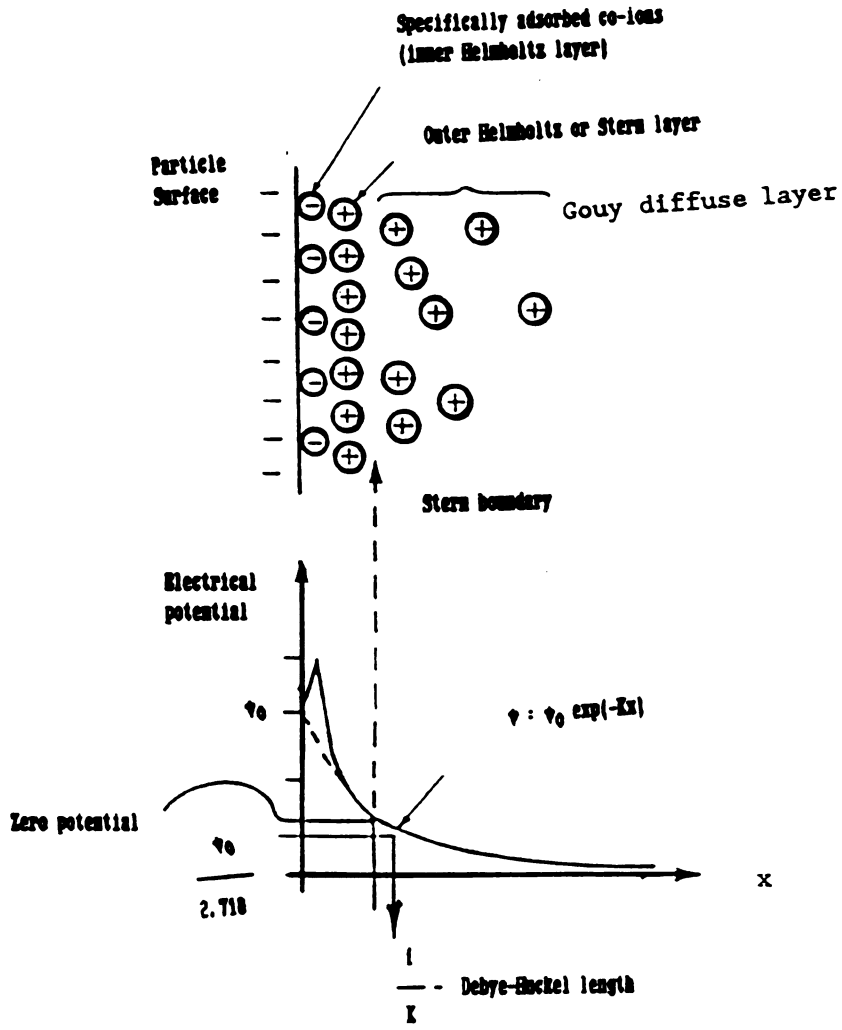

Figure 2. Electrical double layer. (From Cheng, 1987)

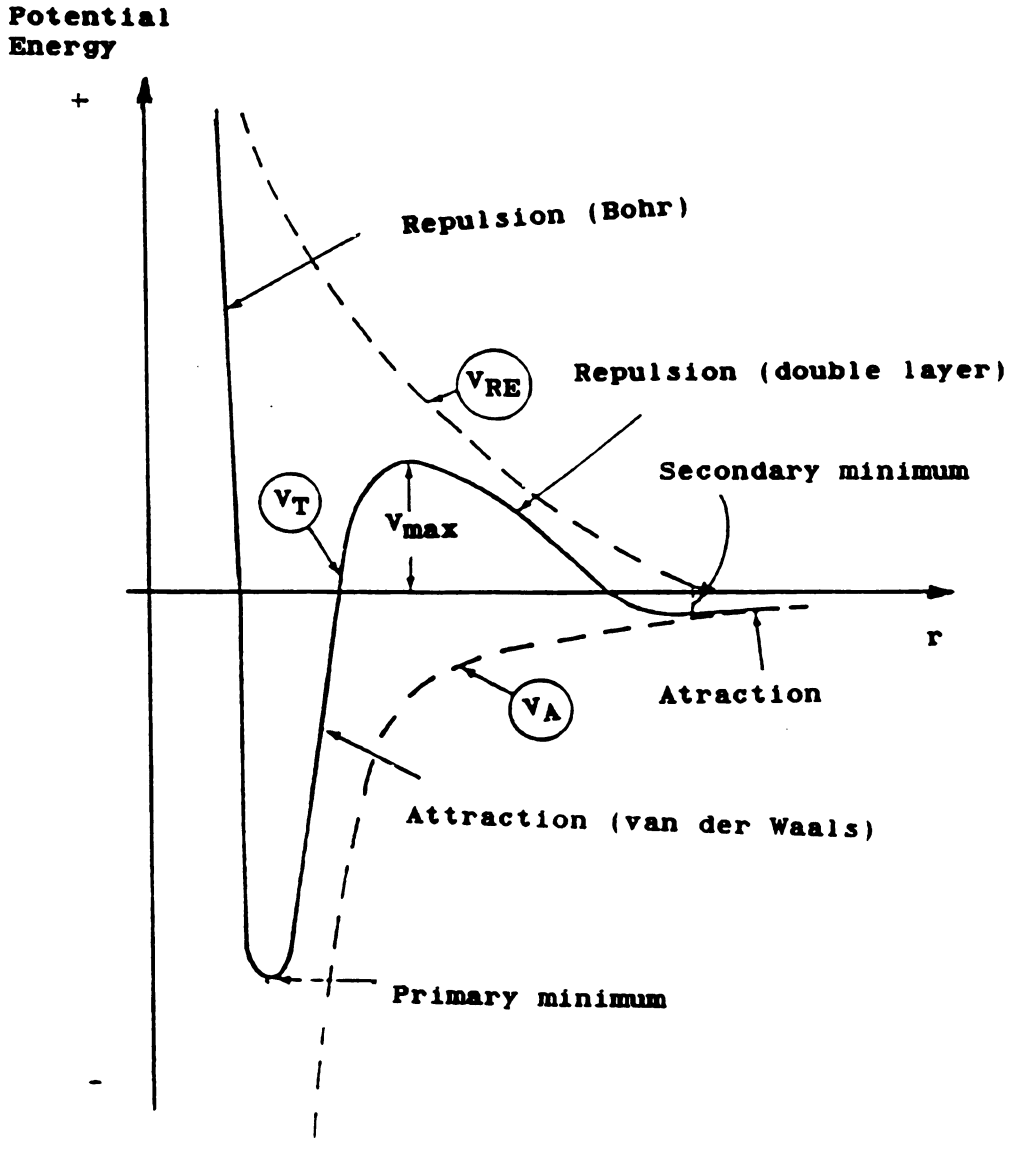

Figure 3. Potential energy for electrostatic stabilization.

(From Cheng, 1987)

When two particles meet, the electrical double layers interact and a repulsive potential is developed. The total potential takes the form shown on Fig. [3] and it has three special features. First is the secondary minimum at a large separation into which particles flocculate. If the minimum is shallow, the flocs formed are weak and can be readily defflocculated by shear. If the minimum is deep, strong flocs are formed.

Second is the primary minimum at small separation. This is usually very deep and particles that aggregate into this form very strong clusters. The process is referred to as coagulation to distinguish it from flocculation associated with the secondary minimum.

The third feature is the potential maximum, Vmax, which constitutes a barrier to coagulation. If it is high, neither Brownian motion nor kinetic energy imparted on the particles by shear can make them come close together. If Vmax is less than the kinetic energy, shear can cause coagulation. If Vmax is less than kT, Brownian motion can cause coagulation (k =Boltzman constant; T = absolute temperature).

As the zeta-potential is increased, the potential barrier increases and the secondary minimum becomes shallower. Thus, high surface charge promotes stability, prevents coagulation and is conducive to weak flocs.

Brownian motion of individual particles within a flow unit (or floc; a floc is composed of only a small number of particles) can lead

to its break-up, as can violent collisions between flow units brought about by Brownian encounter. On the other hand, less violent encounter of flow units can result in aggregation.

Both shear and Brownian motion can lead to structural breakdown or build-up. In the case of Brownian build- up and shear breakdown, thixotropy is obtained. Negative thixotropy results from Brownian breakdown and shear build-up.

Immobilization of fluid in the flocs is usually considered one of the main contributions to low shear viscosity. At higher shear rates the flocs decrease in size thereby reducing the amount of immobilized liquid (Mewis, 1980).

2.3 Rheological Equations of Thixotropy

The general principles of thixotropic and antithixotropic behavior are understood. Although these phenomena occur in a large number of important materials, it remains extremely difficult to make any predictions. The specific mechanisms which determine the response of individual systems or classes of systems have not been analyzed in a systematic manner (Mewis, 1979).

Various approaches can be followed to develop a theoretical description for thixotropic materials. One should be able to calculate

the mechanical properties of the system from the fundamental characteristics and the composition of the constituents. At present the qualitative aspects are well covered and the quantitative ones are progressing for very dilute and for some very concentrated systems (Mewis, 1980).

The rheological characteristics of materials such as polymers, suspensions, dispersions and emulsions have been studied extensively using some of the following (De Kee et al, 1983) : phenomenological methods, microrheological methods and empirical methods.

The phenomenological methods can be separated further into two broad classes (i) continuum theory equations, and (ii) a structural kinetics approach. Using continuum mechanics theory to develop a theoretical description for thixotropic materials presents some problems because simplifications, valid in polymer rheology, cannot be applied to thixotropy without further verification. For example, some thixotropic materials behave solid-like at low stress levels and liquid-like at high stress levels; as a result the consecutive order approximations must fail, also the structural recovery is based on interactions which can have a non-negligible range of action. Whether the presence of such interactions eventually invalidates the principle of local action is not known.

A large number of theoretical analyses use the structural kinetics approach. This means that the change, over time, of rheological parameters is caused by changes in the internal structure of the

the mechanical properties of the system from the fundamental characteristics and the composition of the constituents. At present the qualitative aspects are well covered and the quantitative ones are progressing for very dilute and for some very concentrated systems (Mewis, 1980).

The rheological characteristics of materials such as polymers, suspensions, dispersions and emulsions have been studied extensively using some of the following (De Kee et al, 1983) : phenomenological methods, microrheological methods and empirical methods.

The phenomenological methods can be separated further into two broad classes (i) continuum theory equations, and (ii) a structural kinetics approach. Using continuum mechanics theory to develop a theoretical description for thixotropic materials presents some problems because simplifications, valid in polymer rheology, cannot be applied to thixotropy without further verification. For example, some thixotropic materials behave solid-like at low stress levels and liquid-like at high stress levels; as a result the consecutive order approximations must fail, also the structural recovery is based on interactions which can have a non-negligible range of action. Whether the presence of such interactions eventually invalidates the principle of local action is not known.

A large number of theoretical analyses use the structural kinetics approach. This means that the change, over time, of rheological parameters is caused by changes in the internal structure of the

material. The nonlinear, time-dependent behavior can be described by a set of two equations: the first gives the instantaneous stress as a function of the instantaneous kinematics for every possible degree of structure, the second is a kinetic equation which describes the rate of change for the degree of structure as a function of the instantaneous value of the structure and the instantaneous kinematics. A structural parameter ,κ, was introduced by Cheng and Evans (1965). The constitutive relation involving this parameter is given by a pair of equations, i.e., the equation of state:

$$\sigma = \eta(\dot{\gamma},\kappa)\ \dot{\gamma} \qquad [1]$$

and the rate equation

$$\frac{d\kappa}{dt} = g(\dot{\gamma},\kappa) \qquad [2]$$

After differentiating Eq [1] and substituting Eq [2] Cheng (1973) obtained,

$$\frac{d\sigma}{dt} = \alpha'(\sigma,\dot{\gamma})\frac{d\dot{\gamma}}{dt} + \beta'(\sigma,\dot{\gamma}) \qquad [3]$$

Normal stress effects are not considered in this model, which has only been applied in shear flow.

Another approach is to start from the microstructure to calculate the rheological properties. For thixotropic materials, a few attempts

have been made (Mewis,1979). They refer to dispersions and try to give a more detailed picture of the microstructure than the structural kinetics models.

Mercer and Weymann (1974a, 1974b) developed a set of coupled differential equations giving the rate of change of the aggregate size distribution for spheres.

The main difficulty with these models is the lack of knowledge of the structure of thixotropic materials. Different materials have different microstructure: entangled and gelled macromolecules, particulate chains and networks, spherical aggregates, and card-house structure. It is not quite clear how a single explicit model could cover the detailed behavior of the various microstructures (Mewis, 1979).

Different types of equations that have been developed for thixotropic fluids (Table 1). Some of the equations have been developed using continuous mechanics theory, others using structural kinetics approach, and some are empirical equations.

TABLE 1. Equations for Thixotropic Models

Reference	Note	Equation	Equation Number
Slibar and Paslay (1964)	The authors developed a memory function model to analyse breakdown and recovery. No experimental confirmation given.	$\sigma_{ij}(t)\,\dfrac{\left[\mathrm{II}_{\sigma}(t)\right]^{\frac{1}{2}} - \sigma_{crit}(t)}{\left[\mathrm{II}_{\sigma}(t)\right]^{\frac{1}{2}}} = 2\,\eta\,\dot{\gamma}_{ij}(t)$	[4]
		if $\left[\mathrm{II}_{\sigma}(t)\right]^{\frac{1}{2}} > \sigma_{crit}(t)$	[5]
		with $\dfrac{\sigma_i - \sigma_{crit}(t)}{\sigma_i - \sigma_0} = \dfrac{\int_{\infty}^{t}\left[\mathrm{II}_{\cdot}(t')\right]^{\frac{1}{2}}\exp[-\alpha\,(t-t')]\,dt'}{\beta + \int_{-\infty}^{t}\left[\mathrm{II}_{\dot{\gamma}}(t')\right]^{\frac{1}{2}}\exp[-\alpha\,(t-t')]dt'}$	[6]
Harris (1967)	The author applied continuum theory to obtain integral equations for describing time dependent inelastic flow. No experimental confirmation given.	$\eta(t) = \eta_1 - \int_{-B}^{t} f_1(\mathrm{II}_{\dot{\gamma}}(t), \mathrm{III}_{\dot{\gamma}}(t'))M(t-t')dt'$	[7]

Table 1 (cont'd.).

Tung et al. (1970)	Concentric cylinder experiments with fresh, aged and gamma irradiated egg white	$\sigma = A_1 - B_1 \log t$	[8]
		$\log(\sigma - \sigma_e) = A_2 - B_2 t$	[9]
De Kee et al. (1983)	Experiments were conducted on a cone and plate viscometer with honey, yogurt, mayonnaise, salad dressing, and tomato juice	$\sigma = \kappa \left\{ \sigma_0 + \dot{\gamma} \sum_{p=1}^{\infty} \eta_p \exp(-t_p \dot{\gamma}) \right\}$	[10]
		$\frac{d\kappa}{dt} = - k (\kappa - \kappa_e)^n$	[11]
		where $k = a \dot{\gamma}^b$	[12]
Moore (1959) In:Cheng (1987)	Was the first author to propose an equation of state and a rate equation to study thixotropy	$\sigma = (\eta_\infty - c \kappa) \dot{\gamma}$	[13]
		$\frac{d\kappa}{dt} = a (1 - \kappa) - b \kappa \dot{\gamma}$	[14]
Wilson (1986)	The author developed this expression to use it in scale up test for turbulent flow. No experimental confirmation given.	$\sigma = \sigma_{i\infty} + \eta \frac{dU}{dy} + (\sigma_{i0} - \sigma_{i\infty}) \exp(-k_2 t)$	[15]
Hahn et al. (1959)	Model applied to silicone oil, printing inks, shaving cream, mayonnaise, and grease. Model checked for heavy mineral oil within a shear rate range of 71 to 330 s^{-1}	$\ln(\sigma - \sigma_e) = p - a'' t$	[16]
		where: $\sigma_e = \frac{b}{a''} \left[\frac{\sinh^{-1} \beta_2 \dot{\gamma}}{\alpha_2} - \frac{\beta_1}{\alpha_1} \dot{\gamma} \right] + \frac{\beta_1}{\alpha_1} \dot{\gamma}$	[17]

Table 1 (cont'd.).

$$p = \ln\left[\left\{\sinh^{-1}\left[\frac{\beta_2\dot{\gamma}}{\alpha_2}\right] - \frac{\beta_1}{\alpha_1}\dot{\gamma}\right\}\left\{\chi_{20} - \frac{b}{a}\right\}\right] \quad [18]$$

Fredrickson (1970)

The author presents a model for thixotropic systems composed of suspensions of solid particles in liquids. No experimental confirmation given.

$$\frac{d\psi}{dt} = -\frac{1}{\lambda'}(\psi - \psi_0) + 4k\dot{\gamma}^2\frac{[\psi_\infty - \psi]}{\psi} \quad [19]$$

where:

ψ = fluidity (inverse of viscosity),
ψ_0, ψ_∞ = equilibrium fluidity at zero and infinity shear rates respectively,

λ', k = material parameters.

Godfrey (1973)

Cone and plate viscometer, used in the range of 0.9 to 90 s^{-1} with fuel oil

$$\mu(t) = \mu_\infty + \Delta\mu_1\exp(-t/\lambda_1) + \Delta\mu_2\exp(-t/\lambda_2) \quad [20]$$

$$\Delta\mu = \Delta\mu'\dot{\gamma}^n \quad [21]$$

where:

λ_1 , λ_2 = material parameters,

$\Delta\mu_1$, $\Delta\mu_2$ = viscosity deficits.

Petrellis and Flumerfelt (1973)

Weissenberg rheogoniometer with both coaxial and cone and plate configuration in the shear rate range of 0.001 to 100 s^{-1}, with several types of crude oil at different temperatures

$$\frac{1}{\eta - \eta_e} = \frac{1}{\eta_0 - \eta_e} + \frac{\beta'\dot{\gamma}^{k+1}t}{\sigma_y + \left[\hat{\mu} - \mu_s\right]\dot{\gamma}} + B\dot{\gamma}^m \quad [22]$$

where:

$k, \mu_s, \sigma_y, \hat{\mu}, \beta'$, B and m = material parameters,

η, η_0 and η_e = instantaneous, initial and equilibrium viscosities at a particular shear rate.

Storey and Merill (1958)

Experiments were conducted with amylose solutions on a coaxial cylinder viscometer in the shear range of 0 to 10^4 s^{-1}

$$\frac{\sigma}{\dot{\gamma}} = \alpha N_0\exp[-(k_2+k_1\dot{\gamma})t] + \frac{\alpha N_0}{1+\frac{k_1}{k_2}\dot{\gamma}} + \frac{\alpha N_0\exp[-(k_2+k_1\dot{\gamma})t]}{1+\frac{k_2}{k_1}\dot{\gamma}} + \eta_s \quad [23]$$

Table 1 (cont'd.).

		where α, k_1, k_2 and N_0 are material parameters' η_0 is the Newtonian viscosity obtained after prolonged shearing at high shear rates.
Ritter and Govier (1970)	Experiments were conducted on a coaxial cylinder viscometer with pembina crude oil in the shear rate range of 10 to 500 s^{-1}	$\log\left[\frac{\sigma_s - \sigma_\infty}{\frac{\sigma_{s^0}^2}{\sigma_{s\infty}} - \sigma_s}\right] = -K_0\left[\frac{\sigma_{s^0} + \sigma_{s\infty}}{\sigma_{s^0} - \sigma_{s\infty}}\right] \log t - \log K_{DR}$ [24] where $K_{DR} = \frac{\sigma_{s^0}^2 - \sigma_{s^1}\sigma_{s\infty}}{\sigma_{s^1}\sigma_{s\infty} - \sigma_{s\infty}^2}$ [25] $\sigma_s = \sigma - \sigma_\mu$ σ_μ = equilibrium shear stress at high shear rates σ_s = structural stress σ_{s^0}, σ_{s^1}, $\sigma_{s\infty}$ = structural stresses at 0, 1 and ∞ minutes K_D = rate constant of a network decay process.
Camina and Roffey (1971)	Data for highly pigmented paints within a shear rate 0.05 to 10 s^{-1}	$\sigma = \sigma'\left[\frac{\dot{\gamma}}{\dot{\gamma}'}\right]^{\frac{1}{n}}$ [26] where σ', $\dot{\gamma}'$ = material parameters, n = function of time

Table 1 (cont'd.).

Cheng and Evans (1965)	Cone and plate viscometer with 6.5 % bentonite suspensions. Shear range of 2.4 to 734 s^{-1}. Also an alkaline perbunan latex in the range of 8.5 to 734 s^{-1}	$\frac{d\sigma}{dt} = \alpha' (\sigma, \dot{\gamma}) \frac{d\dot{\gamma}}{dt} + \beta' (\sigma, \dot{\gamma})$ [27] where $\alpha' = \left[\frac{\partial \sigma}{\partial \dot{\gamma}} \right]_{\kappa}$; $\beta' = \left[\frac{\partial \sigma}{\partial \kappa} \right]_{\dot{\gamma}} \frac{d\kappa}{dt}$ [28]
Zitny et al. (1978)	Bentonite in water, shear rate rate range of 48.6 to 1312 s^{-1}	$\sigma = K_0 \dot{\gamma}^n - p (K_0 - K_\infty) \int_{-\infty}^{t} \dot{\gamma}^n \exp(-p (t - \sigma^*)) d\sigma^*$ [29]
Tiu and Boger (1974)	Mayonnaise samples. Shear rate range of 0.41 to 205 s^{-1}	$\sigma = \kappa (\sigma_y + K \dot{\gamma}^n)$ [30] where: $\frac{d\kappa}{dt} = k_1 (\kappa - \kappa_e)^2$ [31] and $k_1 = k_1 (\dot{\gamma})$

Table 1 (cont'd.).

Godfrey In:Sestak et al. (1982)	Bentonite in water. Shear rate range of 48.6 to 1312 s^{-1}	$\sigma = K_\infty \dot{\gamma}^{n\infty} + (K_1+K_2)\dot{\gamma}^n - \int_{-\infty}^{t} \dot{\gamma}^n \left(A_1 + B_1 \right) d\sigma^*$ where: $A_1 = \frac{K_1}{\lambda_1} \exp\left[- \frac{(t - \sigma^*)}{\lambda_1} \right]$ $B_1 = \frac{K_2}{\lambda_2} \exp\left[- \frac{(t - \sigma^*)}{\lambda_2} \right]$	[32]
Carleton et al. (1974)	Bentonite in water. Shear rate range of 27 to 1312 s^{-1}	$\sigma = \sigma_{y0} + \sigma_{y1}\, \kappa + K\, \dot{\gamma}^n$ where: $\frac{d\kappa}{dt} = a \left(1 - \kappa \right) - b\, \dot{\gamma}\, \kappa$	[33] [34]

2.4 Techniques for Measuring Thixotropy

Transient measurements should provide useful information when studying time effects, but it should be kept in mind that several parameters will affect the measured time function (Mewis, 1979). According to Cheng (1980), experimental techniques to measure thixotropy can be divided into three major categories: rotational methods, tube flow methods and miscellaneous methods.

2.4.1 Rotational Methods

Many experiments can be performed using rotational viscometers and rheometers:

1) A step function in shear stress or shear rate.
2) Successive step functions in shear rate: The high shear/low shear test; test in which at each shear rate the sample is sheared until equilibrium is reached and then rested for different periods; the step shear rate test where the sample is sheared to equilibrium at a constant shear rate before a step change to another shear rate, and so on.
3) The hysteresis loop test involving consecutive increase and decrease in shear rate: changes in shear rate step wise and at regular time intervals; changes in shear rate is continuous at controled acceleration; the top shear rate is held constant for some time before the decrease is

initiated.

4) Oscillatory test: sinusoidal change in shear.

5) Stress relaxation test used in two ways: The measuring element is displaced against the torsion spring and then allowed to swing back under the action of the unwinding spring; the outer driven cylinder is set into motion, and the transient response of the inner cylinder is recorded.

2.4.2 Tube Flow Methods

Testing involving flow through tubes is not often used for thixotropic measurements because the large variations of shear stress and shear rate render data interpretation difficult, although not impossible. For certain materials such as those containing large particles or rheological species which cannot be accommodated in the narrow gaps of rotational instruments, the tube flow method has to be used.

2.4.3 Miscellaneous Tests

Ad hoc testing may be carried out by a number of means. They include penetrometer, falling plunger in a close-fitting tube and rotating paddle.

Nondestructive techniques have been developed to supplement or to replace mechanical measurements on thixotropic systems. For sufficiently transparent materials, optical measurements can be used. Ross (1970) applied light scattering to bentonite suspensions to investigate

its optical transmission dependence on shear rate, temperature and concentration.

Dielectric techniques have been used but they are limited to materials containing conductive elements in a nonconductive medium (Mewis,1979).

Mixer viscometer technique has been used by Steffe and Ford (1985) to evaluate shelf-stability of starch-thickened, strained apricots, by measuring torque decay as a function of time over various storage periods. Ford and Steffe (1986) quantified thixotropy in starch-thickened, strained apricots and found that it showed irreversible thixotropy. They used a modified Tiu and Boger (1974) method.

A rapid testing method for characterizing the rheological behavior of gelatinizing corn starch slurries was developed by Steffe et al (1989). Results gave sample temperature and torque response as a function of time.

Steffe and Osorio (1987) used a subjective method to evaluate time dependency with help of the back extrusion technique. They tested numerous baby food products in a cylindrical container and both hollow and solid rods. Using an Instron Universal Testing Machine, the sensor was thrust through an undisturbed sample. Then the probe was withdrawn and the sample thoroughly mixed to allow complete mechanical degradation of the material. When the mixing was complete, the force was recorded while the sensor was pushed into the material a second time. Curves for

the first and second thrust were significantly different and provided a measure of thixotropy.

2.4.4 Problems when Measuring Thixotropy

It is assumed that the rheological data is obtained in properly designed experiments. Some important problems are enumerated below. Because time effects are normally very slow, instruments with a shear rate gradient in the sample, as in capillaries, are not recommended. Large entrance effects can be expected and only the equilibrium behavior can be adequately derived from the data (Mewis, 1979).

For the analysis of the time effects, a constant shear rate through the sample is essential. Thixotropic samples are most often strongly nonlinear at low shear rates and even show a yield stress. For a coaxial viscometer, this can lead to severe restrictions on the radii ratio (Van Wazer et al., 1963).

Some authors have considered superanomalous behavior (Sestak et al., 1982) where there exits a region where the equilibrium shear stress decreases with increasing shear rate. It can be considered as a region with a negative power law index, which would give rise to stability problems in any measuring device. With heterogeneous materials slip might occur.

Many thixotropic materials have a tendency to show shear fracture (Hutton,1963). Also, at higher shear rates they creep out of the gap thereby reducing the cross section of sheared material. The effect is most pronounced in plate-and-cone viscometers and in parallel plate instruments but it can also occur in coaxial cylinders.

For the determination of transients, if the variable structure responsible of thixotropy is not deformable enough, the structural changes can be inhomogeneous through the sample (Mewis, 1979).

Nguyen and Boger (1985) found that due to the initial solid-like behavior of their sample--concentrated bauxite residue suspensions--standard methods and viscometric instruments normally recommended and used for thixotropic fluids were unsuitable. By using a concentric cylinder viscometer, the transient data obtained were not reproducible due to serious wall slippage and a flow discontinuity near the shearing surface. Cheng (1984) reported similar observations with other concentrated suspensions.

2.5 Back Extrusion Theory

The term back extrusion has been generally used to describe the situation were a solid rod is thrust downward into a cylindrical cup containing the experimental sample (Fig. [4]). Downward movement of the

rod displaces material, causing it to be extruded in the direction opposite to that of the rod, i.e., backward; hence, the name back extrusion (Steffe and Osorio, 1987).

2.5.1 Analysis of Time-Independent Fluids

The Herschel Bulkley model describes the flow characteristics of a large number of industrially important materials. Special cases of this model are the Newtonian model, power law model, and Bingham plastic model. A Herschel Bulkley fluid can be written as,

$$\sigma = \sigma_0 + \eta \left| \frac{dv}{dr} \right| \qquad [35]$$

where:

σ = shear stress, Pa

σ_0 = yield stress, Pa

η = consistency coefficient, Pa s^n

$\frac{dv}{dr}$ = shear rate, s^{-1}

n = flow behavior index, dimensionless

During the analysis of a Herschel Bulkley fluid in a back extrusion device, the following assumptions were made (Osorio-Lira, 1985) :

a. The density is constant;

b. The fluid is homogeneous;

c. The fluid has achieved steady state flow;

d. There is no elasticity or time-dependent behavior;

e. The flow is laminar and fully developed;

f. The cylinders are sufficiently long that end effects may be

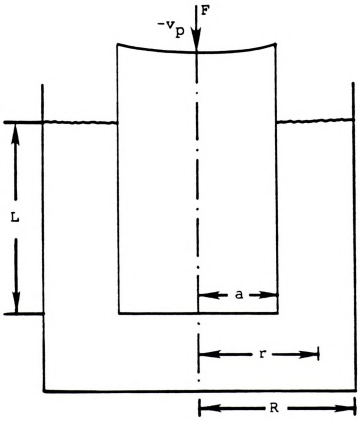

Figure 4. Schematic representation of the back extrusion device.

neglected;

g. The temperature is constant.

In addition, the following boundary conditions were assumed for the time-independent analysis:

a. There is no slip at the walls, or $v(a) = -Vp$ and $v(R) = 0$;

b. The definition of a Herschel Bulkley fluid implies a region of "plug flow" (Fig. [5]) where the shear stress, σ, must reduce to zero at the boundary and inside the plug.

To analyze the time independent flow characteristics of a Herschel Bulkley fluid in a back extrusion device, four dimensionless numbers are defined:

$$T = \frac{2\,\sigma}{P\,R} = \text{dimensionless shear stress;} \qquad [36]$$

$$T_o = \frac{2\,\sigma_o}{P\,R} = \text{dimensionless yield stress;} \qquad [37]$$

$$\emptyset = \left[\frac{2\,\eta}{P\,R^{n+1}}\right]^{\frac{1}{n}} v = \text{dimensionless velocity;} \qquad [38]$$

where:

$$P = \left|\frac{P_o - P_1}{L}\right| = \text{pressure drop per unit of length, Pa/m;}$$

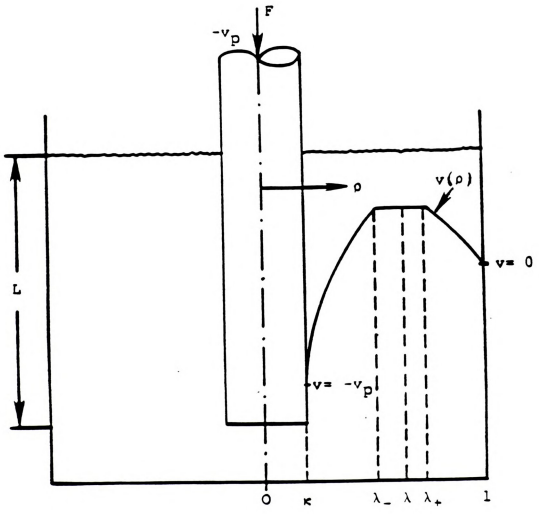

Figure 5. Schematic representation of coordinates describing the axial flow in a back extrusion device.

The analysis of a fluid that follows the Ostwald-de-Waele model, also called the power law model, in a back extrusion device has been done by Osorio and Steffe (1987). The behavior of a Bingham plastic fluid in a back extrusion device has been studied by Osorio et al (1989). They developed mathematical expressions to find the effects of plunger velocity and yield stress on the velocity profile.

2.5.1.1 Basic Equations

This is a brief summary of the basic equations required to understand the theory of back extrusion. Refer to Osorio-Lira (1985) for a complete development of the theory.

Applying a force balance in a core of fluid in the annular gap of a back extrusion device gives an expression for the shear stress in the annulus:

$$\sigma = \frac{P R}{2} \left[\rho - \frac{\lambda^2}{\rho} \right] \qquad [39]$$

where the radial distance $r = \lambda R$ represents a position at which $\sigma = 0$. $\rho = r/R$ is the dimensionless radius. λ_+ and λ_- represent the bounds on the plug flow region. They are those values of ρ for which $|T| = T_0$ in the region $\lambda_- < \rho < \lambda_+$.

The following two conditions need to be met when characterizing the flow behavior of a Herschel Bulkley fluid in a back extrusion device,

$$\int_{\lambda_+}^{1} \left[\rho^2 - \lambda^2 - T_0 \rho \right]^{\frac{1}{n}} \rho^{\left[2-\frac{1}{n}\right]} \, d\rho = \int_{K}^{(\lambda_+ - T_0)} \left[\lambda^2 - \rho^2 - T_0 \rho \right]^{\frac{1}{n}} \rho^{\left[2-\frac{1}{n}\right]} \, d\rho \qquad [40]$$

and

$$\int_{K}^{(\lambda - T_0)} \left[\lambda^2 - \rho^2 - T_0 \rho \right]^{\frac{1}{n}} \rho^{(-\frac{1}{n})} d\rho - \int_{\lambda_+}^{1} \left[\rho^2 - \lambda^2 - T_0 \rho \right]^{\frac{1}{n}} \rho^{(-\frac{1}{n})} \, d\rho = \phi_p \qquad [41]$$

where:

$$\lambda^2 = \lambda_+ (\lambda_+ - T_0) \qquad [42]$$

and the dimensionless flow rate is given by

$$\Phi = \phi_p K^2 \qquad [43]$$

From the above first two expressions, the value of λ_+ and T_0 are obtained when the rheological parameters are known.

From $T_0 = \frac{2 \sigma_0}{P R}$, the pressure drop per unit of length, P, is determined.

2.5.1.2 Dimensionless Shear Stress at the Plunger Wall

The dimensionless shear stress at the plunger wall is given by,

$$T_w = \frac{\lambda_+(\lambda_+ - T_0)}{K} - K \qquad [44]$$

2.5.1.3 Shear Stress at the Plunger Wall

The shear stress at the plunger wall is obtained from,

$$\sigma_w = \frac{P\ R\ T_w}{2} \qquad [45]$$

2.5.1.4 Dimensionless Shear Rate at the Plunger Wall

The dimensionless shear rate at the plunger wall is given by,

$$\left[\frac{d\ \phi}{d\ \rho}\right]_{\rho=K} = \left[\frac{\lambda_+(\lambda_+ - T_0)}{K} - K - T_0\right]^{\frac{1}{n}} \qquad [46]$$

2.5.1.5 Shear Rate at the Plunger Wall

The shear rate at the plunger wall for a Herschel Bulkley fluid is,

$$\dot{\gamma}_{HB} = \left[\frac{P\ R}{2\ \eta}\right]^{\frac{1}{n}} \left[\frac{d\ \phi}{d\ \rho}\right]_{\rho=K} \qquad [47]$$

2.5.2 Force Balance on Plunger

When the plunger is forced down into the sample, fluid flows upward in the annulus. At a constant plunger velocity, the total force applied in the plunger is equal to the force due to the shear stress on the plunger wall plus the force due to static pressure pushing upward on the bottom surface of the plunger. The static force at the base of the plunger is composed of the buoyancy force and the force responsible for fluid flow in the upward direction (Morgan et al., 1979).

The following important expression relates the force corrected for buoyancy (F_{cb}) (being applied on the plunger) to the following variables : (i) dimensionless shear stress at the wall (T_w); (ii) pressure drop per unit of length (P); and (iii) the geometric dimensions of the rod and cylinder containing the fluid (K). This expression was obtained from the force balance on the plunger.

$$\frac{F_{cb}}{\pi\ L\ a\ R} = P\ (\ T_w + K\ ) \qquad [48]$$

To obtain the unknown rheological properties of a Herschel Bulkley fluid in a back extrusion device, the procedure developed by Osorio-Lira (1985), summarized in the next section, is followed.

2.5.3 Determination of Rheological Properties of a Herschel Bulkley Fluid

The rheological properties of a Herschel Bulkley fluid may be determined from the following steps (Osorio-Lira, 1985):

1. For a given plunger velocity v_p, determine the expression $F_{cb}/\pi LaR$. This quantity may be expressed in terms of P, T_w and K as,

$$\frac{F_{cb}}{\pi\ LaR} = P\ (\ T_w + K\ )$$

2. Assume a value for the flow behavior index n;

3. Assume a value for the dimensionless yield stress T_0;

4. Using Eq. [37] determine the pressure drop per unit of length P, with the value of yield stress σ_0 calculated with the following equation,

$$\sigma_0 = \frac{F_{T_e} - F_b}{2\ \pi\ a\ L}$$

where:

σ_0 = yield stress, Pa

F_{T_e} = recorded force after the plunger is stopped, N

F_b = buoyancy force, N

a = radius of the plunger, m

L = length of annular region, m

5. With T_0, n and K solve Eqs. [40] and [41] to evaluate Φ with Eq. [43], and get the value of λ_+.

6. Use Eq. [44] to evaluate T_w.

7. Determine the consistency coefficient from the following expression,

$$\Phi = \left[\frac{2\eta}{P R} \right]^{\frac{1}{n}} \frac{v_p}{R} K^2 \qquad [48.a]$$

8. Compute the expression $P (T_w + K)$

9. Return to step 3, to obtain at least three values of $P (T_w + K)$ and η at a given n.

10. Return to step 2, to plot the necessary curves at different n values that cover the range needed to obtain the correct n value.

11. Plot the values of $P (T_w + K)$ versus η with n as a parameter.

12. Draw the line corresponding to the value of $F_{cb}/(\pi LaR)$ computed in step 1.

13. Use a new plunger velocity v_p and repeat steps 1 to 12 for this new value of v_p.

The rheological properties of the fluid are found when, for a specific flow behavior index n, the consistency coefficient is the same in the the curves corresponding to different plunger velocities.

With n and η known, the shear stress at the wall may be computed using the values of T_0 and λ_+ obtained at a given plunger velocity v_p for the known flow behavior index n. Eqs. [46] and [47] are used to calculate the dimensionless shear rate and actual shear rate, at the plunger wall. Also, Eqs. [44] and [36] are used to determine the dimensionless shear stress and the actual shear stress, at the plunger wall, respectively.

CHAPTER 3

THEORETICAL DEVELOPMENT

3.1 Selection of Rheological Model

The criteria used to select the rheological model for a time dependent fluid in a back extrusion device were based on the following:

a. it should be simple;
b. it should describe time independent behavior when the sample is under a constant shear rate for a long period of time
c. it should consider the presence of yield stress;
d. it should take into account the fact that yield stress changes with time for a time-dependent fluid.

The Kemblowski and Petera model (1979, 1980) was selected because it was developed from basic principles following the 'simple fluid' approach developed by Noll (1958,1972). Also, this model takes into account the presence of a yield stress which changes with structural changes in a time-dependent fluid. The model collapses to a time independent model (the Herschel Bulkley model) when the time dependency is overcome.

The fact that the Kemblowski and Petera model collapses to a Herschel Bulkley fluid enables the use of back extrusion theory in a logical way to accommodate both time-dependent and time independent behavior.

3.1.1 Kemblowski and Petera Model (1979, 1980).

Using Noll's (1958,1972) approach, the constitutive equation of a thixotropic fluid can be written as

$$\dot{\sigma} = G\ (\dot{\gamma},\sigma) \qquad [49]$$

where:

$\dot{\sigma}$ = time derivative of the shear stress, Pa/s

σ = shear stress, Pa

$\dot{\gamma}$ = shear rate, s^{-1}

Eq. [49] describes elastico-viscous fluids as well as thixotropic fluids. For elastico-viscous fluids of the rate type the response of the shear stress to the change of shear rate is delayed. For inelastic thixotropic fluids the response to the change of shear rate is immediate. Therefore, the shear stress has to be a function of the shear rate

$$\sigma = h\ (\dot{\gamma},\kappa) \qquad [50]$$

where κ denotes some additional variables characterizing the state of thixotropic fluid.

The state of the material in viscometric flow (i.e. laminar shearing flow) is determined at a given time t by an ordered pair $(\dot{\gamma},\sigma)$ as seen from Eq. [49]. If the fluid is sheared long enough at a constant shear rate, an equilibrium value of shear stress is obtained.

Eq. [50] has to fulfill Eq [49] and is called the rheological equation of state. Eq. [49], after introducing Eq. [50] into it, leads to a differential equation of the function $\kappa(\dot{\gamma},t)$ which is called the rate equation.

It is assumed that the thixotropic material has a yield stress, below which the material behaves as an elastic solid. The value of the yield stress depends on the value of the structural parameter κ and it may be denoted as $\sigma_y(\kappa)$.

In the case of a fully recovered structure of the material ($\kappa \to \infty$) the yield stress assumes the value

$$\sigma_0 = \lim_{\kappa\to\infty} \sigma_y(\kappa) = \lim_{\dot{\gamma}\to 0} \sigma_e(\dot{\gamma}) \qquad [51]$$

In the case of a fully destroyed structure of the material ($\kappa \to 0$)

$$\lim_{\kappa\to 0} \sigma_y(\kappa) = 0 \qquad [52]$$

In general,

$$\sigma_y(\kappa) = \lim_{\dot{\gamma}\to 0} h(\dot{\gamma},\kappa) \qquad [53]$$

The function $\sigma_y(\kappa)$ is a monotonically increasing function and fulfills the following inequality,

$$0 \le \sigma_y(\kappa) \le \sigma_0 \qquad \text{for } \kappa \ge 0 \qquad [54]$$

Considering the above, it can be assumed that the function $\sigma_y(\kappa)$ may be described by an exponential equation:

$$\sigma_y = \sigma_0 \left(1 - \exp(- A \kappa^s) \right) \qquad [55]$$

where A and s are constants. Eq. [55] fulfills the conditions given by Eqs. [51], [52] and [54].

To obtain a generalized equation of state of a thixotropic material with a yield stress, the following assumptions are made,

i- the equilibrium flow curve is described by the Herschel Bulkley equation

$$\sigma = \sigma_0 + \eta \dot{\gamma}^n \qquad [56]$$

ii- the equation of the family of curves of constant κ may be written as

$$\sigma = \sigma_0 \left(1 - \exp(- A \kappa^s) \right) + M \dot{\gamma}^m \qquad [57]$$

with $M = M (\kappa)$

iii-the equilibrium function of the structural parameter is given by

$$\kappa_e = (\propto \dot{\gamma})^{(n-m)} \qquad [58]$$

where:

$\propto$ = a constant = 1 s

m = exponent defined by this equation, dimensionless

Eq. [58] shows that when the shear rate increases to a very high value, the structural parameter decreases to a very small value, and in the limit when the shear rate is infinite, the value of the structural parameter is zero (i.e., when $\dot{\gamma} \rightarrow \infty$, a fully destroyed structure is obtained). On the other hand, if the shear rate is decreased to a limiting value of zero, the structural parameter gets very high, indicating a fully recovered structure (i.e, for $\dot{\gamma} \rightarrow 0$, a fully recovered structure, $\kappa \rightarrow \infty$, is obtained). Also Eq. [57] , when $\dot{\gamma} \rightarrow 0$, fulfills Eq. [53].

From assumptions i to iii, the generalized equation of state may be written as (Appendix B),

$$\sigma = \sigma_0(1 - \exp(- A \kappa^s)) + \eta \dot{\gamma}^m \left[\kappa + \frac{\sigma_0 \kappa^{\frac{m}{m - n}}}{\eta} \right] \exp(- A\kappa^s) \qquad [59]$$

Eq. [59] has the following properties:

i- in the case of $\kappa = \kappa_e = (\alpha \dot{\gamma})^{(n - m)}$,
with $\alpha = 1$ s, Eq. [59] collapses to Eq. [56].

ii- when $\sigma_0 = 0$, Eq. [59] reduces to the power law model.

iii- when $\kappa \to 0$, Eq. [59] reduces to the power law case, and

iv- when $\kappa \to \infty$, Eq. [59] reduces to

$$\sigma = \sigma_0 + \eta \kappa \dot{\gamma}^m \qquad [60]$$

which, after introducing the equilibrium value of κ given by Eq. [58] leads to Eq. [56].

The Rate Equation.

To take into account the difference in destruction and recovery rate of the material structure, the function C_Λ is defined as,

$$C_\Lambda = \begin{cases} \frac{1}{\Lambda} x \; ; & \text{when } x \leq 0 \\ \frac{C}{\Lambda} x \; ; & \text{when } x > 0 \end{cases} \qquad [61]$$

where:

$\Lambda = \Lambda(\dot{\gamma})$,

$C = C(\dot{\gamma})$,

x = arbitrary real value, and

$$\Lambda = -\frac{1}{\psi} \qquad [62]$$

with $\psi = \psi(\dot{\gamma})$ having the dimension of time and called the natural time function of the thixotropic material.

The rate equation may be written as

$$\dot{\kappa} = C_{\Lambda}(\kappa_e - \kappa) \qquad [63]$$

where $\dot{\kappa}$ is a substantial derivative. It is assumed that the rate of building and destruction can be expressed as a first order reversible reaction.

Integration for $\dot{\gamma}$ = constant leads to,

$$\kappa = \kappa_e + (\kappa_0 - \kappa_e)\exp\left(-\frac{t}{\Lambda}\right) \qquad [64]$$

for $\kappa_e \leq \kappa_0$ with $\kappa_e = \kappa_e(\dot{\gamma})$

and

$$\kappa = \kappa_e + (\kappa_0 - \kappa_e)\exp\left(-\frac{C}{\Lambda}t\right) \qquad [65]$$

for $\kappa_e \geq 0$ with $\kappa_e = \kappa_e(\dot{\gamma})$

where $\kappa = \kappa_0$ for $t = 0$ for Eqs. [64] and [65]

Assuming that the function ψ may be approximated by a straight line, i.e.

$$\psi = -(a_1 + b\dot{\gamma}) \qquad [66]$$

with a_1 and $b > 0$, and averaging the function $C(\dot{\gamma})$ in a given range of $\dot{\gamma}$, the following is obtained,

$$\kappa = \kappa_e + (\kappa_0 - \kappa_e) \exp(-(a + b\dot{\gamma})t) \qquad [67]$$
$$\text{for } \kappa_e \leq \kappa_0 \quad \text{with } \kappa_e = \kappa_e(\dot{\gamma})$$

and

$$\kappa = \kappa_e + (\kappa_0 - \kappa_e) \exp(-\bar{C}(a + b\dot{\gamma})t) \qquad [68]$$
$$\text{for } \kappa_e > \kappa_0 \quad \text{with } \kappa_e = \kappa_e(\dot{\gamma})$$

In this model there are nine parameters to be determined: σ_0, n, η, m, s, A, a, b, $\bar{C}$.

Figure 6 illustrates the meaning of the parameters described above. When the sample is placed in the test station, first it is sheared at a given shear rate ($\dot{\gamma}_B$) until an equilibrium shear stress (σ_{Be}) is obtained. At that moment the shear rate is increased or decreased ($\dot{\gamma}_A$) and the shear stress value (σ_A) obtained immediately after the shear rate change is recorded. The sample is continually sheared until equilibrium (σ_{Ae}) is reached at this shear rate. After reaching this point, the shear rate is brought to the initial shear rate ($\dot{\gamma}_B$) until equilibrium shear stress (σ_{Be}) is reached again. The shear rate is changed to a new value ($\dot{\gamma}_C$) and the corresponding initial value of shear stress is recorded (σ_C); the test continues until the equilibrium shear stress (σ_{Ce}) at this shear rate is reached. The points

ABC in Fig. 6 generate a curve corresponding to a constant structural parameter value. The exponent of this curve corresponds to the value m defined in Eq. [58], and the extrapolated value of shear stress when the shear rate is zero corresponds to the yield stress ($\sigma_y(\kappa)$) associated with that value of structural parameter, defined in Eq. [55].

By repeating the procedure outlined above at other initial shear rates, a family of curves of different structural parameter values are generated, and from these, the parameters A and s defined in Eq. [55] may be calculated.

By following the transient shear stresses after a change in shear rate has been performed (i.e. from σ_A to σ_{Ae} at $\dot{\gamma}_A$) during several cycles, the values of the natural time function ψ defined in Eq. [62] can be obtained.

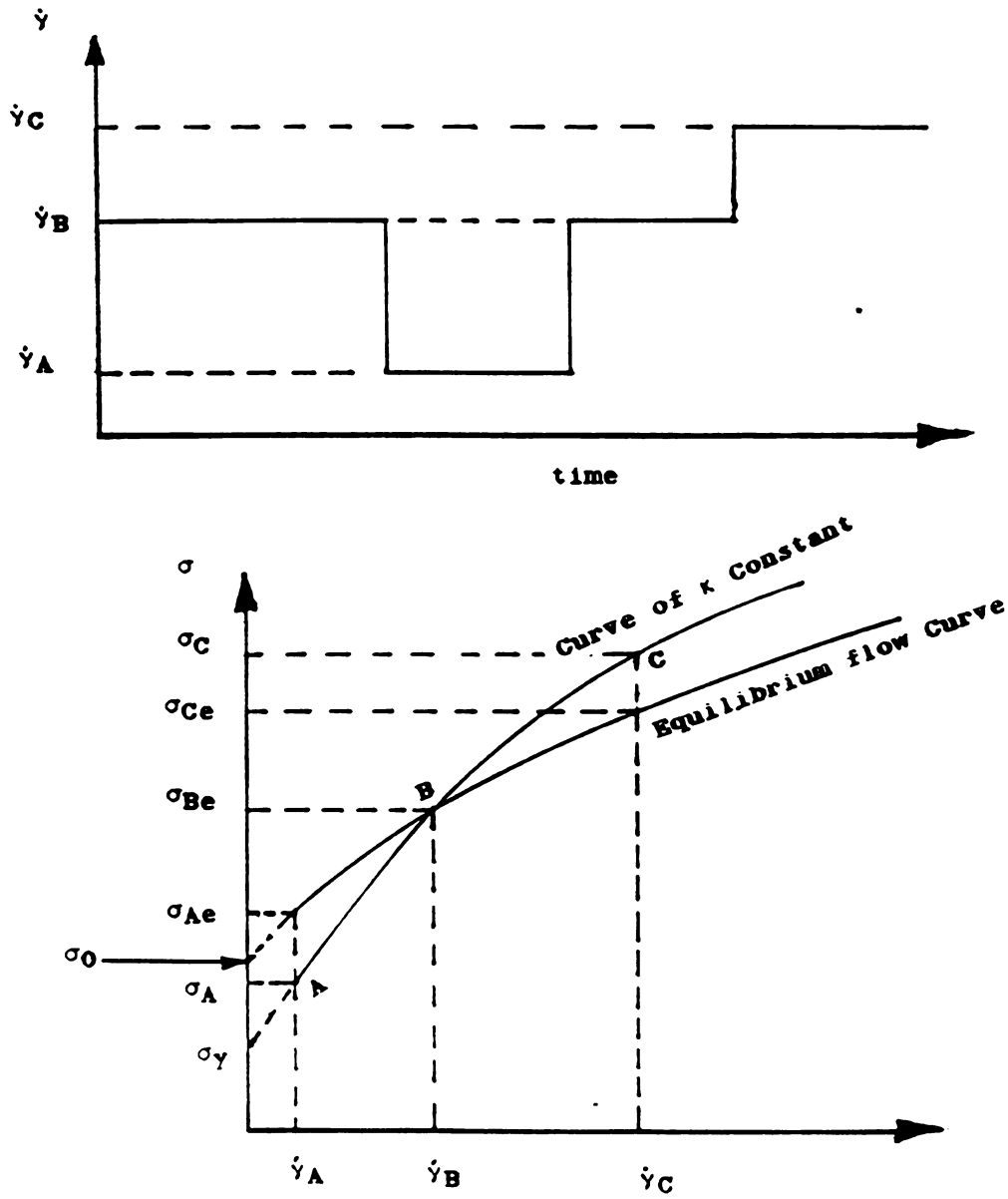

Figure 6. Illustration of the experiment to obtain the parameters of the Kemblowski and Petera model.

3.1.2 Modified Kemblowski and Petera Model

The complete Kemblowski and Petera model gives two different equations (Eqs. [67] and [68]) depending on whether the shear rate is increased or decreased from an original shear rate where the sample has been allowed to reach equilibrium. The only difference between Eq. [67] and Eq. [68] is the function in the exponential term. This difference comes from Eq. [62] where a natural time function ψ is defined. This function, ψ, is assumed to be linear in Eq. [66]. With all this assumptions, it would be necessary to determine nine parameters from Eq. [59].

The approach followed in this study was to replace the parameter $C_\Lambda(\psi)$ defined by Eq. [61] by a parameter Γ, called the inverse time constant. This parameter is the inverse of the natural time function ψ defined in Eq. [62]. With the definition of Γ, only one equation is needed to express the structural parameter κ. Also, Γ is a function of the shear rate, but this definition of Γ allows one to find any type of relationship between Γ and shear rate, and it does not limit this relationship to a linear equation. In this way, this definition generalizes the Kemblowski and Petera model.

Rewriting Eq. [63] in terms of Γ gives,

$$\dot{\kappa} = \Gamma (\kappa_e - \kappa) \qquad [63.a]$$

where:

Γ = $\Gamma(\dot{\gamma})$ = inverse time constant for a thixotropic fluid in a back extrusion device, s^{-1}

Integration for a constant shear rate leads to,

$$\kappa = \kappa_e + (\kappa_0 - \kappa_e) \exp (- \Gamma t) \qquad [67.a]$$

where:

$\kappa = \kappa_0$ at $t = 0$.

An equilibrium value for a thixotropic material is defined as the steady value obtained, at a given shear rate, after a time long enough that there are no variations in the value being measured over time

Considering both Eq. [59] and Eq. [67.a], there are seven parameters determined in the current work: σ_0, n, η, m, s, A, and Γ.

3.2 Use of Back Extrusion Device to Measure Thixotropic Characteristic

In this section, a fluid mechanics study of a time-dependent fluid in a back extrusion device will be conducted. The model of thixotropy developed by Kemblowski and Petera (1979,1980) will be incorporated to the mathematical equations developed by Osorio-Lira (1985) for a Hesrchel Bulkley fluid in a back extrusion device.

In the case of a very long pipe ($L \to \infty$) the structural parameter of a thixotropic fluid changes from κ_0 to the equilibrium values corresponding to the local shear rates at the various points in the pipe cross section. Therefore, the local shear stress at a cross section far away from the pipe entrance will be given by Eq. [56].

It is assumed that the fluid entering the annulus in a back extruder has a uniform structure, characterized by κ_0. It may also be assumed that the entrance region may be neglected, i.e. the fluid effectively enters the annulus with an established velocity profile corresponding to the rheological properties at the entry conditions. This is because, for a fluid of high apparent viscosity, the boundary layer develops quickly (Kemblowski and Petera, 1981).

At a cross section near the annulus entrance, where the velocity profile is fully developed, but where the structural parameter is still approximately equal to κ_0 (a constant), the local shear stress is given by Eq. [60].

Because the flow behavior indexes are unequal ($m \neq n$) Eqs. [60] and [56] describe at the same linear velocity u_z, different distributions of the local axial velocity. The velocity field in the pipe has two velocity components: one axial and the other radial. The radial component arises from the fact that the fluid must move at right angles to the axial direction if the velocity profile is changing (Kemblowski and Petera, 1981).

Eq. [39] for a Herschel Bulkley fluid in a region of the annulus is,

$$\sigma = \frac{P\,R}{2}\left(\rho - \frac{\lambda^2}{\rho}\right)$$

Assuming that the shear stress for a time-dependent fluid in an annulus can be written as,

$$\sigma = (A_1 + B_1)\,R\left(\rho - \frac{\lambda^2}{\rho}\right) \qquad [69]$$

where $A_1 = A_1(z)$, and is a function of the axial coordinate z. In the special case of $A_1(z) = 0$, Eq. [69] describes the flow of a fluid with no memory, for which the axial pressure gradient is constant. Then,

$$B_1 = \frac{1}{2} P\Big|_{\infty} \qquad [70]$$

and the radial pressure gradient is zero, i.e.

$$\frac{\partial P}{\partial r} = 0 \qquad [71]$$

For a thixotropic fluid, conditions [70] and [71] are fulfilled for $z \to \infty$, because then (at V_z = constant) the fluid becomes time independent.

The function $A_1(z)$ has to fulfill the following conditions,

$$A(z) \to 0 \quad \text{for } z \to \infty\,, \qquad [72]$$

$$A(z) \to A \quad \text{for } z \to 0 \qquad [73]$$

Condition [72] assures that for $z \to \infty$ the term $A_1(z)$ vanishes, and, from Eq. [39],

$$\sigma\Big|_{\infty} = P\Big|_{\infty} \frac{R}{2} \left(\rho - \frac{\lambda^2}{\rho} \right) \qquad [74]$$

The relation for $z \to 0$ is

$$\sigma\Big|_{0} = P\Big|_{0} \frac{R}{2} \left(\rho - \frac{\lambda^2}{\rho} \right) \qquad [75]$$

assuming that

$$A_1 = \left[P\Big|_{\infty} - P\Big|_{0} \right] \frac{R}{2} \left(K - \frac{\lambda^2}{K} \right) \qquad [76]$$

where $K = \frac{a}{R}$

It is necessary now to generate a function, $A_1(z)$, which fulfills conditions [72] and [73]. $A_1(z)$ determines the rate of change of the pressure gradient in the axial direction, and depends on the natural time constant of the fluid. As the natural time increases, the pressure gradient will approach the equilibrium value $P\Big|_{\infty}$ more slowly.

The velocity profile in the cross section of the annulus changes from a profile with an exponent m to a profile with an exponent n (where $m > n$). Because the values m and n are not usually much different (Kemblowski and Petera, 1981) it may be assumed that the velocity profiles do not differ significantly. For fluids with high values of the natural time constant (in comparison with the residence time in the annulus) the mean velocity profile will be closer to that for the exponent m. It may be assumed therefore that the velocity distribution in the whole annulus is characterized by the exponent m. Consider a steady

state distribution of the structural parameter in the annulus. This distribution is given by Eq. [63] as

$$\dot{\kappa} = \frac{\partial \kappa}{\partial t} = \frac{\partial \kappa}{\partial z} \frac{\partial z}{\partial t} = \Gamma (\kappa_e - \kappa) \qquad [63]$$

where:

$\Gamma = \Gamma (\dot{\gamma})$ = inverse time constant of the thixotropic material, s^{-1}

and,

$$u_z \frac{\partial \kappa}{\partial z} = \Gamma (\kappa_e - \kappa) \qquad [77]$$

Eq. [77] is obtained by taking into account the fact that the radial velocity component u_r is much smaller than the axial component u_z. For $u_z \neq 0$, Eq. [77] may be considered an ordinary differential equation.

$$d\kappa = \frac{\Gamma}{u_z} (\kappa_e - \kappa)dz = \Gamma (\kappa_e - \kappa)dt \qquad [78]$$

Integration gives, using the following boundary condition:

$\kappa(r,0)=\kappa_0$ at $z=0$,

$$\kappa = \kappa_e - (\kappa_e - \kappa_0) \exp (- \Gamma t) \qquad [79]$$

for $u_z \neq 0$.

For $u_z = 0$, from Eq. [63]

$$u_z \frac{\partial \kappa}{\partial z} = 0 = \Gamma (\kappa_e - \kappa) \qquad [80]$$

meaning that $\kappa = \kappa_e$ [81]

where κ_e is given by Eq. [58].

Placing Eq. [79] into Eq. [60] and simplifying gives,

$$\sigma = \sigma_0 + \eta\ \dot{\gamma}^n + (\kappa_0 \eta\ \dot{\gamma}^m - \eta\ \dot{\gamma}^n)\ \exp (- \Gamma\ t) \qquad [82]$$

For $t = 0$ Eq. [82] yields,

$$\sigma\Big|_0 = \sigma_0 + \kappa_0\ \eta\ \dot{\gamma}^m \qquad [83]$$

and, from Eq. [75]

$$\sigma\Big|_0 = P\Big|_0 \frac{R}{2} \left(\rho - \frac{\lambda^2}{\rho} \right)$$

When $t \to \infty$, Eq. [82] collapses to

$$\sigma\Big|_\infty = \sigma_0 + \eta\ \dot{\gamma}^n \qquad [84]$$

and from Eq. [74]

$$\sigma\Big|_\infty = P\Big|_\infty \frac{R}{2} \left(\rho - \frac{\lambda^2}{\rho} \right)$$

Substituting Eqs. [83] and [84] into Eq. [82] yields,

$$\sigma = \sigma\Big|_\infty + (\sigma\Big|_0 - \sigma\Big|_\infty)\ \exp (- \Gamma\ t) \qquad [85]$$

Incorporating Eqs. [74] and [75] into Eq. [85] gives,

$$\sigma = \left\{ P\Big|_{\infty} + \left(P\Big|_{0} - P\Big|_{\infty} \right) \exp\left(- \Gamma t \right) \right\} \frac{R}{2} \left(\rho - \frac{\lambda^2}{\rho} \right) \qquad [86]$$

Comparison of Eq. [86] to Eq. [69] yields,

$$B_1 = \frac{1}{2} P\Big|_{\infty} \qquad [87]$$

and

$$A_1 = \frac{1}{2} \left(P\Big|_{0} - P\Big|_{\infty} \right) \exp\left(- \Gamma t \right) \qquad [88]$$

Neglecting the dependence of the local pressure on the radial coordinate, and approximating the shear stress by Eq. [39],

$$\sigma = P \frac{R}{2} \left(\rho - \frac{\lambda^2}{\rho} \right)$$

Comparing Eq. [39] to Eq. [86] gives,

$$P = P\Big|_{\infty} + \left(P\Big|_{0} - P\Big|_{\infty} \right) \exp\left(- \Gamma t \right) \qquad [89]$$

Eq. [89] allows measurement of the inverse time constant, Γ, of a thixotropic fluid in a back extrusion device. Knowing the equilibrium values for pressure drop per unit of length, $P\Big|_{0}$ and $P\Big|_{\infty}$ at the initial and final plunger velocity, respectively, and the values of the pressure drop per unit of time, P, during the transient immediately after the change in plunger velocity, the natural time function is readily calculated.

CHAPTER 4

MATERIALS AND METHODS

4.1 Description of the Instruments

To test the thixotropic behavior of the samples in a back extrusion device, laboratory experiments were conducted using 250 ml graduate cylinders as sample holders, and aluminum and plexiglas plunger rods. An Instron Model 4202 Universal Testing Machine (Instron Corp., Canton, Mass.) was used to operate the plunger. The plunger was attached to a compression load cell (50 N) screwed to the cross- head of the Instron. An x-y recorder was used to record force as a function of time (and position).

Other instruments were also used to determine thixotropic properties. A Haake RV-12 viscometer, interfaced to a Hewlett-Packard 85 computer and 3497 data acquisition system, with a M-500 head and the MV cup (radius = $2.1\ 10^{-2}$m) and MVII sensor (radius = $1.84\ 10^{-2}$ m; equivalent length = $57.66\ 10^{-2}$ m) was used to obtain a concentric cylinder configuration. Another instrument used was a Rheometrics Fluid Spectrometer (RFS) Model 8400 (Rheometrics Inc., Piscataway, NJ) equipped with a 100 g-cm torque transducer. Steady and dynamic tests were carried out on the RFS using a parallel plate configuration (0.025 m radius).

4.2 Methodology

4.2.1 Preparation of Samples

4.2.1.1 Preparation of Bentonite

The bentonite used in these experiments was a Wyoming bentonite (American Colloid Company, Skokie, Il.). The moisture content of bentonite powder was determined prior to preparing the suspension. A suspension of 7% (weight/volume) was prepared. The required amount of bentonite was added slowly to the water being stirred in a Hobart mixer; it took 30 minutes to add all the bentonite into 10 liters of deionized water. After the bentonite was added, the suspension was stirred for an additional 30 minute period to get the solids totally dispersed. Then, the bentonite suspension was packed into 250 ml graduate cylinders. Approximately 130 ml of suspension were added to each graduate cylinder. To check the final concentration, samples were oven dried at 104^{o}C until a constant weight was obtained. To allow the suspension to stabilize, the material was allowed to set unused for approximately two months. During this time, experiments were performed to check the presence of time-dependent behavior. The material used during preliminary testing was discarded.

4.2.1.2 Preparation of Iota-Carrageenan

The Iota-Carrageenan used in these experiments was GELCARIN GP 359 obtained from FMC Corporation (Philadelphia). The sample (1 % weight/volume concentration) was prepared by heating deionized water to 90-95^{o}C and while stirring it, iota-carrageenan was added slowly. Once all the solid was added to the hot water, the solution was poured into 250 ml graduate cylinders. Approximately 130 ml of solution was added to each graduate cylinder. The sample was allowed to set for two days prior to performing the tests. Benzoic acid (0.1 %) was added to preserve the sample.

4.2.2 Back Extrusion Testing

Two types of experiments were performed using the back extrusion device. The first was to determine the equilibrium rheological properties, that is, the rheological properties under steady state conditions. The second type of experiment was done to determine the time-dependent properties. To perform all experiments, a graduate cylinder containing approximately 130 ml of sample was aligned with the plunger attached to the 50 N compression load cell of the Instron machine.

4.2.2.1 Equilibrium Rheological Properties

After aligning the cylinder and the plunger, a plunger velocity was selected from the control panel of the Instron. The plunger penetrated into the sample approximately 8 cm from the original level of the undisturbed sample, leaving 2 cm of undisturbed material. At that point the plunger was stopped and the force decay over time recorded. Several plunger velocities were used.

4.2.2.2 Time-Dependent Rheological Properties

In this case, the plunger velocity was changed at a certain point during its travel into the sample. It was found that the time-dependent effect is better observed when the test starts with a high plunger velocity and, at a certain point during downward travel, the plunger velocity is reduced. When the relationship between recorded force and position at the high plunger velocity is a straight line, the equilibrium has been reached, and it is possible to change the plunger velocity to a lower value and record the force decay over time until the relationship between recorded force and position at this lower plunger velocity is a straight line.

4.2.3 Concentric Cylinder

Experiments were conducted using concentric cylinder configuration to validate those results obtained with the back extrusion device. Also this was done to verify the problems reported by some authors when

thixotropic materials are used in concentric cylinders (Van Wazer et al., 1963; Hutton, 1963; Blake and Moran, 1975; Mewis, 1979; Cheng, 1984; Nguyen and Boger, 1985, 1987). It was necessary to use the MV cup and MVII sensor configuration in the Haake viscometer because when the MVI sensor was used, the sample rose in the small gap between the rotor and the gap, and sample material came out of the gap.

A core of sample was withdrawn from a container and placed into the Haake MV cup. In this way the structure was preserved until the sensor was pushed into the sample. Due to the presence of a yield stress, the instrument was first run without the sample in place, so the sensor rotated in the air, this was taken as the zero reading for the initial torque. The sensor was stopped and the cup containing the sample was put in place. Step changes in shear rate were given to each sample. Each sample was sheared to equilibrium before changing to another shear rate.

4.2.4 Parallel Plate Testing

To avoid damage to the structure of the gels prior to the test, a small cylindrical core of material was withdrawn from a container and placed into the sample holder. The upper plate was lowered slowly to make sure the gel is not destroyed while filling the gap with experimental material. The gap between the plates was between 1.5 and 2.5 mm for all the experiments.

4.2.4.1 Steady Tests

Once a sample was in place as described above, several tests were done to different samples of the same batch. First, a thixotropic loop was performed to qualitatively check for time dependency. Second, a series of step changes in shear rate were done to different samples of the same batch. All these experiments were done in triplicate.

4.2.4.2 Oscillatory Tests

With the sample filling the gap between the parallel plates, two experiments were performed in oscillatory mode using the RFS. First, to determine the viscoelastic linear range, a strain sweep was done at two different frequencies. Second, after the linear range was determined, a frequency sweep was done at a constant strain within the linear range.

4.3 Data Analysis Procedure

4.3.1 Back Extrusion Testing

4.3.1.1 Equilibrium Constants

4.3.1.1.1 Determination of the Flow Behavior Index

From the relationship between dimensionless flow rate and plunger velocity given by Osorio-Lira (1985),

$$\Phi = \left[\frac{2\,\eta}{P\,R} \right]^{\frac{1}{n}} \frac{v_p}{R} K^2 \qquad [90]$$

where:

Φ = dimensionless flow rate;

η = consistency coefficient, Pa s^n;

n = flow behavior index, dimensionless;

P = pressure drop per unit of length, Pa/m;

R = radius of outer cylinder of annulus, m;

v_p = velocity of the plunger, m/s;

K = ratio of radius of plunger to that of outer cylinder, dimensionless; a/R.

If a Herschel Bulkley fluid is tested in a back extrusion device at two different plunger velocities, and if the plunger and cylinder are the same in both experiments, then the dimensionless radius K is constant in both tests as is R. Then the above equation can be written as,

$$\frac{\Phi_i}{\Phi_j} = \frac{v_{pi}}{v_{pj}} \left[\frac{Fcb_j}{Fcb_i} \frac{L_i}{L_j} \right]^{\frac{1}{n}} \left[\frac{T_{wi} + K}{T_{wj} + K} \right]^{\frac{1}{n}} \qquad [91]$$

rearranging and taking the logarithm yields,

$$\ln \left[\frac{v_{pi}}{v_{pj}} \right] = \ln \left[\frac{\Phi_i}{\Phi_j} \left[\frac{T_{wi} + K}{T_{wj} + K} \right]^{\frac{1}{n}} \right] + \frac{1}{n} \ln \left[\frac{Fcb_i}{Fcb_j} \frac{L_j}{L_i} \right] \qquad [92]$$

By plotting $\ln(v_{pi}/v_{pj})$ versus $\ln\{Fcb_i L_j / Fcb_j L_i\}$ the flow behavior index n is obtained as the inverse of the slope. Once the flow behavior index is known, it is possible to obtain the equilibrium yield stress and the consistency coefficient.

4.3.1.1.2 Shear Rate Determination. Newtonian Approximation

To facilitate calculations, a trial an error method is used to determine the shear rate. First, a Newtonian approximation for shear rate is used.

The Newtonian shear rate is given by the following expression,

$$\dot{\gamma}_N = v_p \left[\frac{K - K^3}{\Phi R} \right] \qquad [93]$$

where:

$\dot{\gamma}_N$ = Newtonian shear rate, s^{-1}

v_p = plunger velocity, m/s

K = dimensionless plunger radius,

Φ = dimensionless flow rate.

The dimensionless flow rate is given by Eq. [43],

$$\Phi = \phi_p K^2$$

where,

$$\phi_p = \epsilon^2 \ln\left[\frac{\epsilon}{K} \right] + \frac{K^2 - 1}{2} - \epsilon^2 \ln \epsilon \qquad [94]$$

and

$$\epsilon^2 = \frac{K^2 + 1}{2} \qquad [95]$$

4.3.1.1.3 Shear Stress Approximation

The expression $\frac{F_{cb}}{\pi L a R} = P (Tw + K)$ [96]

is obtained by applying a force balance on the plunger, where,

Fcb = force corrected for buoyancy, N

L = length of annulus region, m

a = radius of the plunger, m

R = radius of outer cylinder of annulus, m

Tw = dimensionless shear stress at the plunger wall,

K = dimensionless plunger radius.

The value of (Tw + K) is very close to 1. Therefore it is possible to approximate the expression Fcb/(π L a R) to the value of P with a maximum of 3% error. Using this above approximation, Tw may be obtained as,

$$Tw = 1 - K \qquad [97]$$

The dimensionless shear stress at the plunger wall is obtained from Equ[36]:

$$Tw = \frac{2\ \sigma_w}{P\ R} \qquad [98]$$

where,

σ_w is the actual shear stress at the wall, Pa

Hence, the shear stress at the wall may be obtained from the expression,

$$\sigma_w = \frac{Tw\ Fcb}{2\ \pi\ L\ a} \qquad [99]$$

4.3.1.1.4 Equilibrium Yield Stress and Consistency Coefficient Determination

In a back extrusion test, there is a decay in measured force over time when the plunger is stopped inside a time-dependent sample. It is difficult to obtain the equilibrium yield stress from the plot of force versus time because the plot shows a decrease in force with time and after waiting some time, the residual force starts to increase again. This is due to the fact that the destruction rate and build-up rate are not equal. To obtain the equilibrium yield stress, it is necessary to

generate data of shear stress and shear rate, and the equilibrium yield stress is obtained by curve fitting.

With the approximated values for shear rate and shear stress calculated with Eq. [93] and Eq. [99] respectively; and the flow behavior index calculated with Eq. [92], the equilibrium yield stress and the consistency coefficient are determined by curve fitting.

4.3.1.1.5 Consistency Coefficient Determination Using Back Extrusion

With the flow behavior index obtained with Eq. [92] and the equilibrium yield stress obtained by curve fitting as described above, the consistency coefficient is obtained using back extrusion (Osorio-Lira, 1985). Notice, when using back extrusion the value for pressure drop per unit of length is calculated in each iteration, so there is no need for using the approximation in 4.3.1.1.3.

When the consistency coefficient is obtained, the pressure drop per unit of length (P) at each plunger velocity is obtained, also the dimensionless shear stress at the wall (Tw) is obtained. Therefore, it is now possible to obtain the shear stress at the plunger wall using,

$$\sigma_w = Tw\ R\ P/2 \qquad [100]$$

and the shear rate at the plunger wall is obtained by using Eq. [47].

With the values of flow behavior index, consistency coefficient, and values of shear stress and shear rate, it is possible to determine the equilibrium yield stress.

4.3.1.2 Time-Dependent Constants

The inverse time constant Γ, of a thixotropic fluid in a back extrusion device, is obtained by performing a test at a given plunger velocity and at a certain point after equilibrium conditions have been attained, the plunger velocity is changed to a lower value. The transient pressure drop per unit of length, P, is determined as a function of the time. Γ is evaluated with Eq. [89].

A flow diagram of the calculation steps involved in the determination of time-dependent rheological properties using back extrusion technique is shown in Fig. 7.

Figure 7. Flow diagram for the analysis of back extrusion data

Input Data:	
a, R	Radii of plunger and outer cylinder
l_{ch}, C_{sp}, F_T, F_{Te}	Values from chart-strip recorder
v_{p1}	Plunger velocity when the test starts
v_{p2}	Final velocity of the plunger

1.	$\frac{F_{cb}}{\pi L a R}$	Calculate $\frac{F_{cb}}{\pi L a R}$ from the input data for a given plunger velocity
2.	n	Calculate n from Eq. [92]
3.	$\dot{\gamma}_N$	Calculate $\dot{\gamma}_N$ from Eq. [93]
4.	σ_w	Calculate σ_w from Eq. [99]
5.	σ_0	Calculate σ_0 from a nonlinear regression of $\dot{\gamma}_N$ and σ_w calculated in steps 3. and 4. respectively. Use the Herschel Bulkley model
6.	P	Assume a value for the dimensionless yield stress T_0 and calculate P from Eq. [37]
7.	Φ, λ_+	Calculate Φ and λ_+ from Eqs. [40], [41] and [43]
8.	T_w	Calculate T_w from Eq. [44]
9.	η	Calculate η from Eq. [48.a]
10.	$P(T_w+K)$	Calculate this expression
11.	Assume a new value for T_0 and return to step 6. to obtain at least three values of $P(T_w+K)$ and η	
12.	Draw the line corresponding to the value of $\frac{F_{cb}}{\pi L a R}$ computed in step 1.	
13.	v_p	Use a new plunger velocity and repeat steps 1. to 12. for this new value of v_p

Figure 7 (cont'd.).

14. The equilibrium rheological properties of the fluid are found when the consistency coefficient, η, is the same in the curves corresponding to different plunger velocities

15. $\left.\frac{d\phi}{d\rho}\right|_{\rho=K}$ — Calculate $\left.\frac{d\phi}{d\rho}\right|_{\rho=K}$ from Eq. [46]

16. $\dot{\gamma}_{HB}$ — Calculate $\dot{\gamma}_{HB}$ from Eq. [47]

17. T_w — Calculate T_w from Eq. [44]

18. σ_w — Calculate σ_w from Eq. [36]

19. σ_{0_c} — Calculate σ_{0_c} from a nonlinear regression for the Herschel Bulkley model, with the values of $\dot{\gamma}_{HB}$ and σ_w obtained in steps 16. and 18., respectively

20. σ_0? σ_{0_c} — Compare σ_0 calculated in step 5. to σ_{0_c} calculated in step 19. If they are different, replace σ_0 by σ_{0_c} and repeat all calculations from steps 6. to 20.

Time-Dependent Parameters

21. $\frac{F_{cb}}{\pi\ a\ R}$ — Calculate $\frac{F_{cb}}{\pi\ a\ R}$ from the transient data, corresponding to a given time

22. L — Calculate L for each value of the expression $\frac{F_{cb}}{\pi\ a\ R}$ calculated in step 21.

23. $\frac{F_{cb}}{\pi\ L\ a\ R}$ — Calculate $\frac{F_{cb}}{\pi\ L\ a\ R}$ for the transient data

24. t — Calculate the time elapsed, t, since the plunger changed velocity, for each value of the expression $\frac{F_{cb}}{\pi\ a\ R}$ calculated in step 21.

25. F_b — Calculate F_b corresponding to the transient and the equilibrium curve of the final plunger velocity v_{p2}

Figure 7 (cont'd.).

26.	F_T	Obtain the linear regression between the total equilibrium force F_T corresponding to the final plunger velocity v_{p2} and the position L of the plunger inside the fluid
27.	$\frac{F_{cb}}{\pi L a R}$	Obtain $\frac{F_{cb}}{\pi L a R}$ for the final plunger velocity corresponding to each position of the plunger considered in step 22.
28.	Γ	Calculate Γ from Eq. [89]
29.	m, σ_y	Calculate m and σ_y from Eq. [57] using nonlinear regression. The values of σ_w are those corresponding to the value of the shear stress immediately after the plunger velocity is changed from v_{p1} to v_{p2}
30.	κ	Calculate κ from Eq. [58]
31.	A, s	Calculate A, s from Eq. [55]

4.3.2 Concentric Cylinder Testing

Tests were performed using concentric cylinders geometry. The Haake MV cup and MVI and MVII sensors were used to evaluate equilibrium and time-dependent constants.

4.3.2.1 Equilibrium Constants

4.3.2.1.1 Shear Rate Determination

The shear rate was evaluated using the method developed by Krieger (1968). Krieger showed that the shear rate at the wall of the sensor for any fluid is,

$$\dot{\gamma}_{R_b} = \frac{2\,\Omega}{s}\left[\frac{1}{1 - \alpha^{2/n}}\right]\left[1 + s^2 s' f\left[\frac{2}{s}\ln\left(\frac{1}{\alpha}\right)\right]\right] \qquad [101]$$

where:

$$\alpha = \frac{R_b}{R_c} \qquad [102]$$

$$s = \frac{d(\ln \sigma_b)}{d(\ln \Omega)} \qquad [103]$$

$$s' = \frac{d(1/s)}{d(\ln \sigma_b)} \qquad [104]$$

$$f(t) = \frac{t[\, e^{t}\,(t - 2) + t + 2\,]}{2\,(\, e^{t} - 1\,)^{2}} \qquad [105]$$

Ω = angular velocity, rad/s

$$\sigma_b = \frac{M}{2\,\pi\,h\,R_b^{\,2}} \qquad [106]$$

σ_b = shear stress at the bob, Pa

R_b = radius of the sensor, m

R_c = radius of the outer cylinder, m

M = external torque, N m

h = level of the fluid in contact with the sensor, m

4.3.2.1.2 Rheological Parameters Determination

After obtaining values of shear rate with the method developed by Krieger (1968), a rheogram is plotted with the equilibrium shear stress as a function of shear rate. Nonlinear regression was applied to determine the rheological parameters of the Herschel Bulkley model.

4.3.2.2 Time-Dependent Constants

The method used to determine the time-dependent constants from concentric cylinder viscometer data was developed by Kemblowski and Petera (1979,1980,1981). An outline is presented below.

- From the equilibrium conditions, the equilibrium yield stress is found, corresponding to σ_o. Also the consistency coefficient η and the flow behavior index n are obtained from this equilibrium conditions.

- A step shear rate test is performed where the sample is sheared to equilibrium at a constant shear rate before a step change to another shear rate is done (refer to Fig. 6). The value of shear stress immediately after the step change in shear rate is recorded. The sample is brought to the initial shear rate, and left to reach equilibrium again. After equilibrium is reached, a step change to another shear rate is made, and the value of the shear stress immediately after this change is recorded. At this point there are three values of shear rate

with three corresponding values of shear stress. These points define a curve whose characteristic is to have a constant value of the structural parameter κ. By fitting a curve through these points, the exponent defined by Eq. [57] is determined as it is the value for the yield stress σ_y, defined by Eq. [55], corresponding to that structural parameter.

- Starting from other initial equilibrium values for the shear rate, different values for the structural parameter are obtained. In this way, for each structural parameter there is a corresponding value for yield stress.

- With the values of the structural parameter and its corresponding yield stress, the parameters A and s, defined in Eq. [55], are calculated.

- Finally, using the values of shear stress during the transient to reach equilibrium after a shear rate change, the natural time constant defined in Eq. [68] is obtained.

4.3.3 Parallel Plate Testing

4.3.3.1 Steady Tests

4.3.3.1.1 Shear Rate Determination

The shear rate at the rim of the plate for a parallel plate geometry (torsional flow) is given by,

$$\dot{\gamma} = \frac{\Omega R}{h} \qquad [107]$$

where:

$\dot{\gamma}$ - shear rate at the rim of the plate, s^{-1}

Ω - angular velocity, rad/s

R - Radius of the plate, m

h - gap width between the plates, m

4.3.3.1.2 Shear Stress Determination

The shear stress at the rim of the plate for a parallel plate geometry (torsional flow) is given by,

$$\sigma_R = \frac{3\,M}{2\,\pi\,R^3}\left[1+\frac{1}{3}\,\frac{d\{\ln M\}}{d\{\ln \dot{\gamma}\}}\right] \qquad [108]$$

where:

σ_R = shear stress at the rim of the plate, Pa

M = torque, N

R = radius of the plate, m

$\dot{\gamma}$ = shear rate at the rim of the plate, s^{-1}

4.3.3.1.3 Rheological Parameters Determination

A rheogram is plotted with the equilibrium shear stress, determined with Eq [108], as a function of shear rate, determined with Eq. [107]. Nonlinear regression was applied to determine the rheological parameters of the Herschel Bulkley model.

4.3.3.2 Time-Dependent Constants

The method used to determine the natural time constant of a thixotropic fluid in a parallel plates geometry is the same as that described when using concentric cylinders, section 4.3.2.2.

4.3.3.3 Dynamic Tests

Dynamic tests were performed to characterize the sample fluid, and to help understand the behavior of bentonite when creeps out of the concentric cylinder gap.

When performing dynamic tests, the stress and/or strain vary harmonically with time. The following expression gives the relationship between shear stress and the strain and the rate of strain,

$$\sigma = G'\gamma + \frac{G''}{\omega}\dot{\gamma} \qquad [109]$$

where:

σ = shear rate, Pa

G' =storage modulus or dynamic rigidity, Pa

G" = loss modulus, Pa

ω = frequency, rad/s

γ = strain, dimensionless

$\dot{\gamma}$ = rate of strain, s^{-1}

When an oscillatory test is performed on a Hookean solid, the stress and stress are in phase, therefore G" is equal to zero, meaning that there is no lost of energy. If an oscillatory test is done on a Newtonian fluid, stress and strain are 90^{o} out of phase and G' is equal to zero, indicating that there is no storage of energy.

For viscoelastic materials, G' and G"are non-zero.

A dynamic viscosity is defined in oscillatory test as,

$$\eta' = \frac{G''}{\omega} \qquad [110]$$

where:

η' = dynamic viscosity, Pa s^{-1}

G" = loss modulus, Pa

ω = frequency, rad/s

4.4 Selection of Experimental Fluids

4.4.1 Bentonite

Bentonite suspension was chosen as a thixotropic fluid model for the following reasons:

i- Researchers have used bentonite-water suspensions to simulate a variety of heat transfer applications, primarily because of its low cost and chemical stability relatively to food (Unklesbay, 1982). Jackson and Olson (1953) used a 1, 3.25 and 5% bentonite suspension in water to simulate canned food. Yamano et al. (1975) found in a retort study that the thermal diffusivity of a 40% bentonite suspension was similar to published values for fish and meat; these researchers recommended use of these suspensions because of their stable physiochemical properties and because they accommodate a wide range of water contents. Peterson and Adams (1983) performed research on retort pouches containing a 10% bentonite suspension. Darsch et al. (1979) used a 5% bentonite, 47.5% glycerin and 47.5% water suspension to simulate solid foods; and a 1% bentonite, 49.5% glycerin and 49.5% water suspension to simulate soup and beverages when testing a food service tray system. Similar heat retention characteristics among the suspensions and many foods were noted. In these studies, suspensions were used to

avoid compositional variations inherent in foods. When Unklesbay et al. (1980) used bentonite-water suspensions to simulate steaks during infrared heat processing, no significant differences in energy usage were found between the bentonite models and steaks; these researchers also modeled sausage patties and found no significant differences between sausage patties and the bentonite model. Niekamp et al. (1983) modeled a heterogeneous food with a bentonite-water suspension, and found no significant differences in energy consumption with meat products during convective heat treatment. Niekamp et al. (1984) used bentonite- water suspensions to determine thermal properties of bentonite suspensions as a way of facilitating mathematical modeling of foods.

ii) By changing the solids concentration, different types of rheological properties can be obtained. As the concentration increases from zero, the suspension shows increasing departure from Newtonian behavior and also exhibits thixotropic properties. At higher concentration a yield stress makes its appearance (Cheng, 1965). No references were found with respect to the effect of temperature on the rheological properties of bentonite suspensions.

Most of the material that follows was obtained from the book by Grim and Güven (1978). The name bentonite was suggested in 1898 for a peculiar clay-like material with soapy properties from its occurrence in the Fort Benton unit of Cretaceous age formations in Wyoming (U.S.A.) (Grim and Güven, 1978). Bentonite is a rock composed essentially of a crystalline clay- like mineral formed by the devitrification and the accompanying chemical alteration of a glassy igneous material, usually

a tuff or volcanic ash. The unique physical properties of the Wyoming clay quickly gave it high commercial value.

A distinctive feature of the sodium Wyoming bentonite is that it disperses in water into relatively large and extremely thin flakes. As a consequence of this feature, the bentonite has important colloidal, plastic, and bonding properties. The morphological features, modes of aggregation, and crystal structure of bentonite are related to the rheological behavior and other properties of these clays. Various applications of this material in industry, technology, and science are directly related to the above characteristics.

Members of the montmorillonite-beidellite (Montmorillonite is the name of a clay mineral first found near Montmorillon in France in 1874) series form the smectites commonly occurring in bentonites. The properties of bentonites are contingent upon the fact that they are composed of smectite clay minerals, and the properties of the smectite in turn are contingent upon its chemical composition, atomic structure, and morphology. Smectite is composed of silica and alumina sheet-like units arranged in such a way that smectites are essentially books of sheets or laths, or bundles of needles. The individual skeets or laths or needles are loosely tied together-in fact water can enter between the sheets, laths or needles separating them. As a consequence, smectite clays are readily dispersed in water into extremely small particles.

Bentonite particles are flat, plate-like particles, approximately 7000 Å x 7000 Å x 20 Å (Mercer, 1973). Montmorillonite is composed of

units made of two silica tetrahedral sheets with a central alumina octahedral sheet. All the tips of the tetrahedrons point in the same direction and toward the center of the unit. The tetrahedral and octahedral sheets are combined so that the tips of the tetrahedrons of each silica sheet and one of the hydroxyl layers of the tetrahedral and octahedral layer became oxygens instead of hydroxyls. The layers are continuous in the x and y directions and are stacked one above the other in the z direction (Grim, 1962).

In the stacking of the silica-alumina-silica units, oxygen layers of each unit are adjacent to oxygens of the neighboring units with a consequence that there is very weak bond and an excellent cleavage between them. The outstanding feature of the montmorillonite structure is that water and other polar molecules, such as certain organic molecules, can enter between the units layers causing the lattice to expand in the z direction. The z direction is not fixed but varies from 9.6 Å when no polar molecules are between the unit layers, to substantially complete separation in some cases. Fig. [8] is a diagrammatic sketch of the structure of montmorillonite.

Exchangeable cations occur between the silicate layers, and the z axis spacing of completely dehydrated montmorillonite depends somewhat on the size of the interlayer cations, being greater the larger the cation. The thickness of the water layers between the silicate units also depends on the nature of the exchangeable cations at a given water vapor pressure. Under ordinary conditions, a montmorillonite with sodium as the exchangeable ion frequently has one molecular water layer

and a z axis spacing of about 12.5 Å. The expansion properties are reversible unless the structure is completely collapsed by the removal of all the interlayer polar molecules, in which case it may be difficult or impossible to expand the structure. The theoretical formula for the montmorillonite is $\{OH_4Si_8Al_4O_{20}$ n (interlayer) $H_2O\}$, and the theoretical composition without the interlayer material is,

SiO_2 - 66.6 %,

Al_2O_3 - 28.3 %, and

H_2O - 5 %

Montmorillonite always differs from the above theoretical formula because of substitutions within the lattice of aluminum and possibly phosphores for silicon in tetrahedral coordination and/or magnesium, iron, zinc, nickel, lithium, etc., for aluminum in the octahedral sheet (Grim, 1962). An atom of lower valence often replaces one of higher valence, resulting in an excess of negative charge, which is compensated by absorption of cations on the layer surfaces which are too large to be accommodated in the interior of the lattice. In the presence of water, these cations have a tendency to diffuse away from the layer surface. The result of this diffusion is the formation of an atmospheric distribution of the cations in the diffuse electric double layer on the exterior flat surfaces of the clay particle (Mercer, 1973).

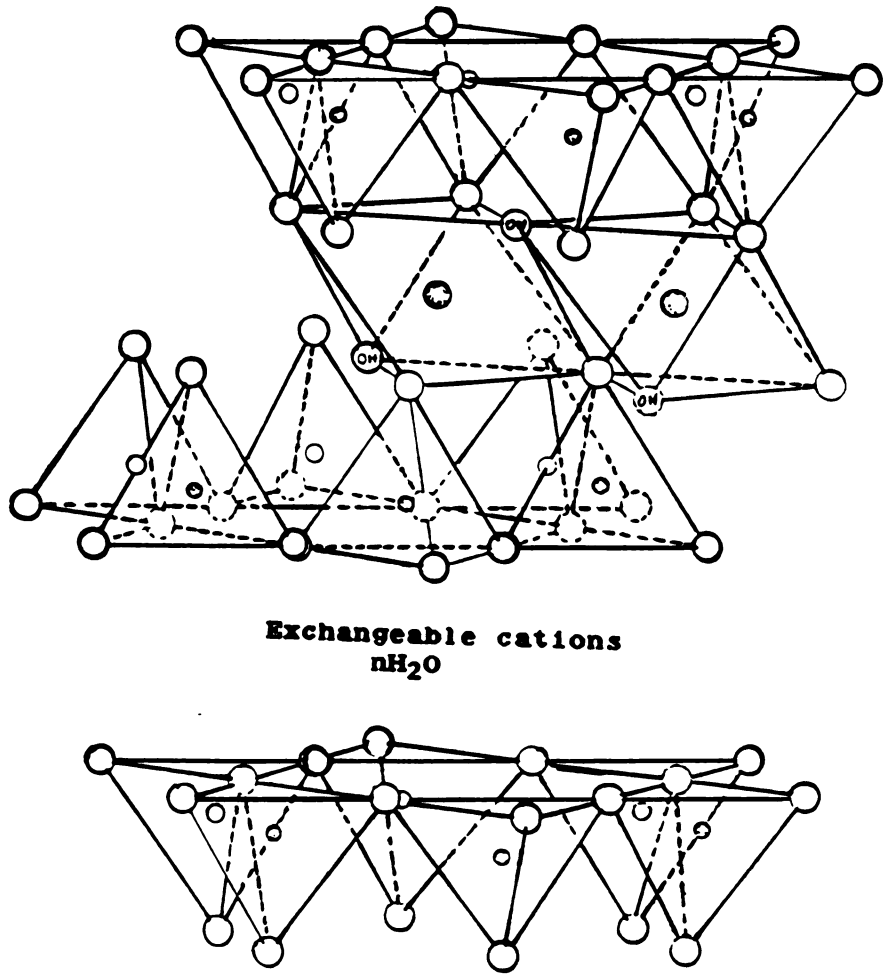

Figure 8. Diagrammatic sketch of the structure of montmorillonite. (From Grim, 1962)

Detailed mineralogical studies have been carried out on bentonite samples from Wyoming (Grim and Güven, 1978). The X-ray diffraction data indicate that the Wyoming samples contain a predominantly Na-montmorillonite as its main interlayer cation (Grim and Güven, 1978). Because of the impurities even in 1 μm fraction, a structural formula was calculated only for one sample from eight samples for Wyoming type bentonite (Grim and Güven, 1978):

$$\left[(Si_{3.86}Al_{0.14})(Al_{1.58}Fe^{3+}_{0.17}Mg_{0.24})\ O_{10}(OH)_2\ \right] M^{+}_{0.38}$$

Ross (1970) gives the following chemical composition for Volclay Wyoming bentonite (American Colloid Company, Skokie, Illinois):

SiO_2 = 64.00 %,

Al_2O_3 = 20.00 %,

Fe_2O_3 = 3.03 %,

and 10% of Feldspar, Gypsum, Talc, Carbonate, Quartz, and other impurities. Mercer (1973) gives the following chemical composition for Wyoming bentonite: SiO_2 = 49.4 %, Al_2O_3 = 20.4 %, TiO_2 = 0.4 %, Fe_2O_3 = 3.7 %, MgO = 2.55%, CaO = 1.8 %, Na_2O = 0.34%, K_2O = 1.12%, H_2O = 20.15%

Because of the electrostatic charge associated with the bentonite particles, and also because of the Van der Waals attractive force between particles, they tend to associate and become stuck together. It is generally recognized that an undisturbed bentonite suspension consists of a loose cluster of aggregates formed by the bentonite particles, in which the dispersible phase is trapped and immobilized. Upon the application of shear, the aggregate structure is partially

broken down. The degree and characteristics of this structural change governs the rheological behavior of bentonite suspensions. It is found that as the shear rate increases, the aggregate structure of the suspension is further destroyed and more of the dispersible phase is released and so the apparent viscosity decreases. At very high shear rates, the structure is totally destroyed so that all the particles present will be singlets. When the shear rate is held constant there exits an equilibrium aggregate size distribution.

The flat surfaces of bentonite particles carry a net negative charge. In addition to the flat layer surfaces, there are also edge surfaces exposed on the particles. These edge surfaces are very likely to carry a positive charge.

There are three different modes of particle association: face to face (FF), edge to edge (EE), and edge to face (EF). Each type of association is governed by a different electrical interaction energy for the combination of the two double layers. Also the Van der Waals interaction energy and therefore the total potential curve, will be different for each type of association. In addition, the rate at which particles approach each other are different for each type of association, so the three types of association may not occur simultaneously or to the same degree.

The physical results of the three types of association will also be different. FF association merely leads to thicker flakes, whereas EE and EF association will lead to large house-of-cards type of structure

in which the dispersible phase is immobilized. The rheology of the suspension is very sensitive to the type of association which takes place. The apparent viscosity of the suspension will increase when EE and EF takes place but will decrease if FF association takes place. Further, if FF association takes place simultaneously with EF and EE association for a given suspension, the yield stress will decrease.

Fig. 9 shows the rate of water adsorption for sodium montmorillonite, which begins slowly and then after 10 min increases very rapidly.

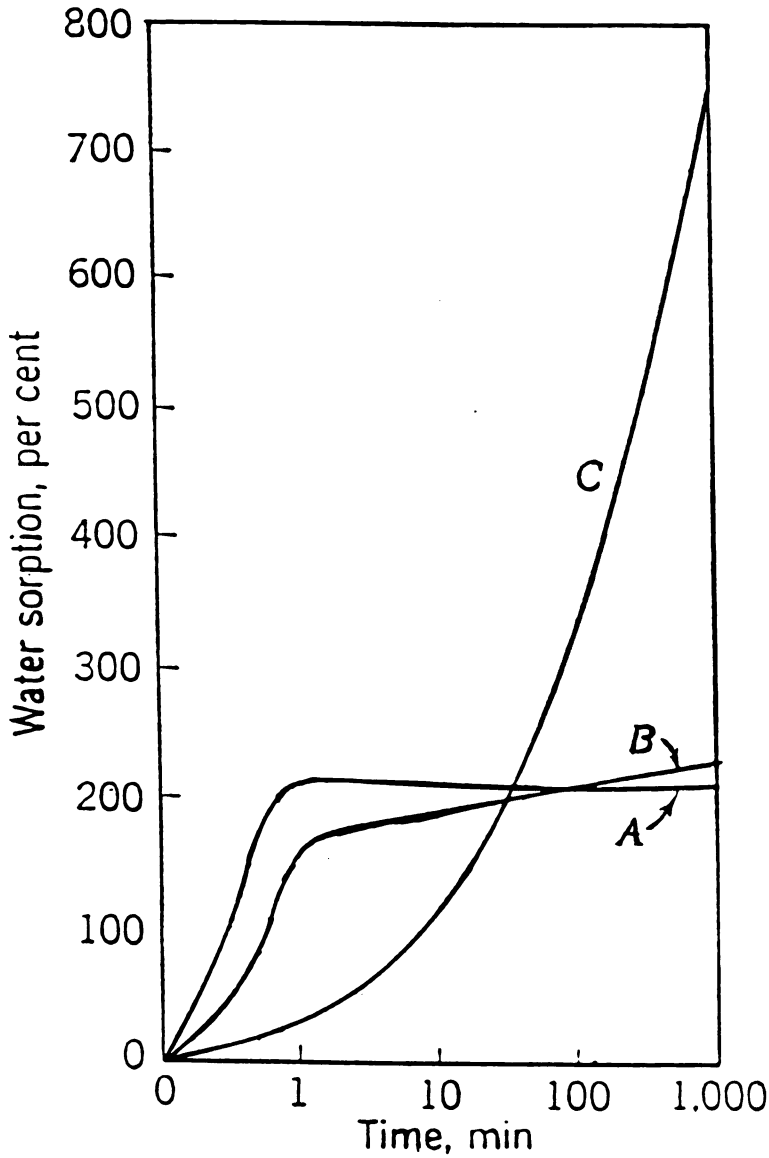

Figure 9. Water-sorption curves for attapulgite (A), calcium montmorillonite (B), and sodium montmotillonite (C). (From Grim, 1962)

4.4.2 Iota-Carrageenan

The use of gelling agents in foods is a "technological need" (Pederson, 1980). Macromolecular hydrocolloids or gums are used in the food industry as texture modifying agents. Carrageenan are capable of forming viscous solutions at low concentrations in cold water, with the apparent viscosity dependent on temperature, pH, concentration, type of carrageenan molecules and solutes present.

Above the gel melting point, Iota-Carrageenan has shear thinning flow characteristics. At low concentrations below the gelation temperature Iota-Carrageenan gels have thixotropic properties.

The primary function of a gel in foods is to bind/solidify the free water in the food. Only a few polysaccharides (for example, agar, alginates, guar gum, locust bean gum, gum arabic, methylcellulose, sodium carboxymethylcellulose, microcrystalline cellulose, carrageenan and starches) and a few proteins (for example, gelatin, soya and whey) are used to form food gels.

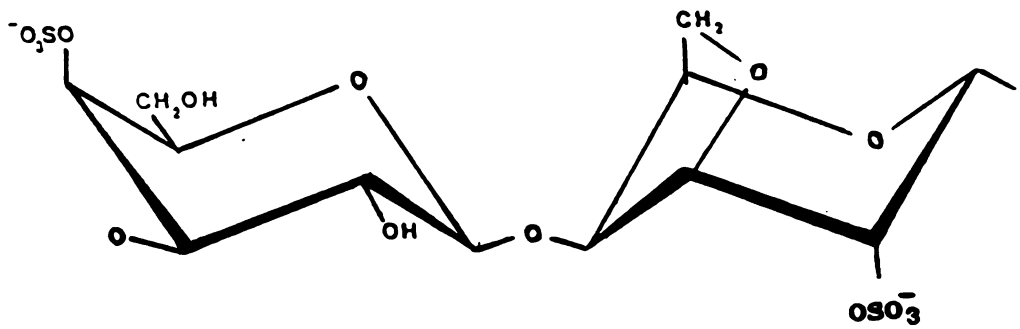

D-galactose-4-sulphate

3, 6-anhydro-D-galactose-2-sulphate

Figure 10. Iota - Carrageenan Structure.

Carrageenan is not a well defined substance, but rather a designation for a group of salts of sulphated galactans. Five families of red seaweeds are listed as carrageenan raw materials. Various types or fractions of carrageenan are defined according to idealized structures and designated by greek letters (lambda, kappa, iota, etc). By selection of seaweeds it is possible to obtain carrageenan which are predominantly, for example, the iota type.

Carrageenan is a high molecular weight linear polysaccharide made up of repeating galactose units, and 3,6 anhydrogalactos (3,6-A-G), both sulphated and nonsulphated, joined by alternating α 1-3, β 1-4 glycosidic linkages (see Fig. 10). Iota-carrageenan is 32 % ester sulphate and 30 % 3,6-A-G. Table 2 gives the physical properties of iota-carrageenan.

The largest single use of carrageenan in foods is probably as a gelling agent in gelled milk desserts: puddings, flans, ice cream, yoghurts. Others uses are in meat gels, fish gels, whipped toppings, pizza sauces,etc. Iota-carrageenan forms a thixotropic gel, recovery after pumping gives sufficient support for a topping to be placed on products after filling.

The internal structure that causes the thixotropic behavior of Iota-carrageenan can be explained in terms of hydrogen bonding forces existing between molecules. The nonionic mechanism that explains thixotropy for Iota-carrageenan is quite different than the electrical double layer theory for bentonite.

TABLE 2 . Properties of Iota-Carrageenan.

Solvent	Temperature (^{o}C)	Solubility Presence of Salts	Comments
water	20	Na^{+}	soluble
water	20	Ca^{+2}	swells to form thixotropic dispersion
water	80		soluble
milk	20		insoluble
milk	80		soluble
10% salt solution	90		soluble
50% sugar solution			insoluble
GELATION			
strongest gel		with Ca^{+2} ion	
gel texture		elastic	
regelation after shear		YES	
syneresis		NO	
freeze/thaw stability		YES	

CHAPTER 5

RESULTS AND DISCUSSION

5.1 Bentonite

The bentonite used during the tests had a concentration of 7% (weight/volume) with a standard deviation of 0.12. The density of the sample was 1035.0 kg/m^3 with a standard deviation of 13.2 kg/m^3 (sample size = 9).

5.1.1 Equilibrium Rheological Properties

5.1.1.1 Back Extrusion Tests

5.1.1.1.1 Yield Stress

The final equilibrium force recorded after the plunger is stopped inside the sample is used to calculate the yield stress value in back extrusion experiments.

Figures 11 to 13 show typical curves obtained during a back extrusion test. When the plunger reaches position A, the plunger velocity is changed, and this velocity is kept until the plunger reaches position B. At position B the plunger is stopped while the residual force is continuously recorded. After the plunger is stopped, the force decays until it reaches a minimum, and afterwards, increases its value until a plateau (equilibrium) is reached. This type of behavior could be explained in terms of structural kinetics. When the suspension is being sheared by the plunger movement in the sample, the weak physical bonds forming the internal structure are ruptured, so that the network breaks down. After the plunger is stopped, the process mentioned above continues, but the weak physical bonds between the particles begin to reform, and the particle aggregates start forming a spatial network and the suspension rebuilds an internal structure. When the rate of rebuilding the internal structure overcomes the destruction rate initiated by the movement of the plunger, the recorded force reaches a minimum, and thereafter the rate of rebuilding dominates until the final internal equilibrium structure is reached and the recorded force is constant indicating equilibrium state.

Therefore, when measuring the yield stress of thixotropic materials when using the back extrusion technique, it is important to follow the changes in the recorded force over time, to make sure that the final internal equilibrium structure has been reached, and use that value, corresponding to the plateau, to calculate the yield stress corresponding to undisturbed conditions.

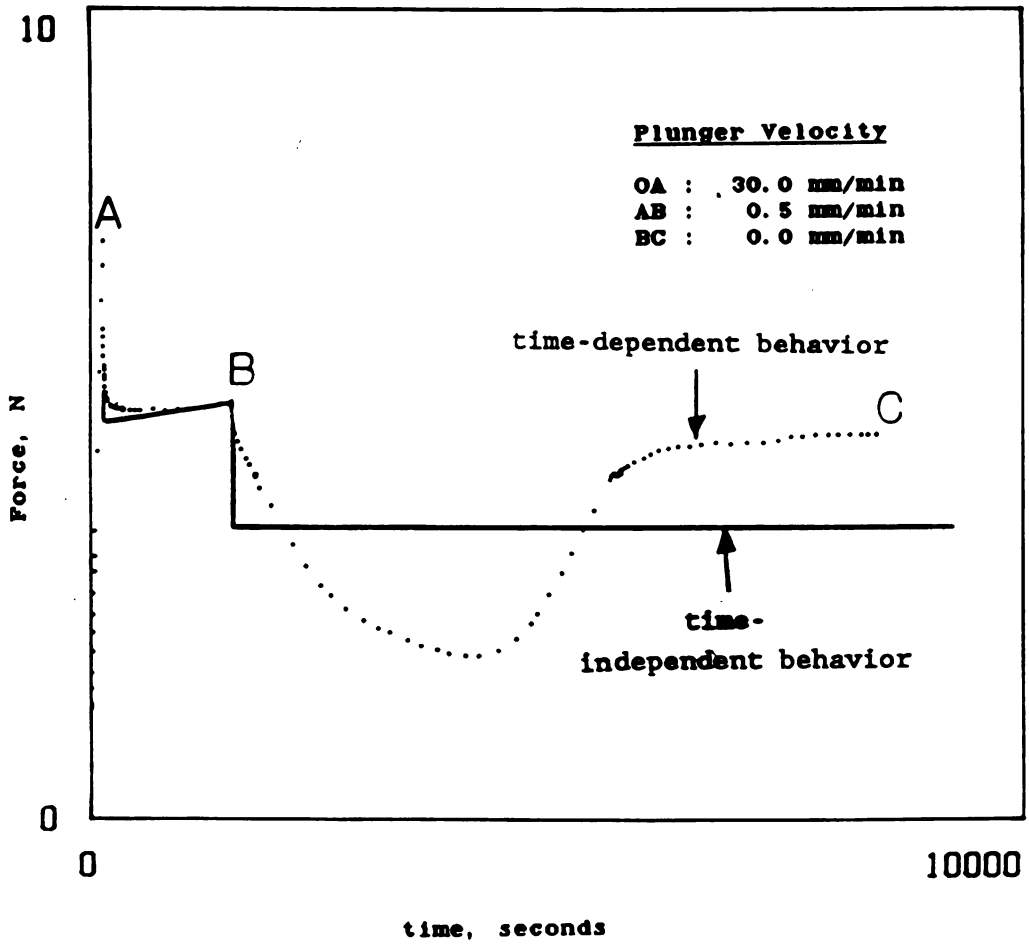

Figure 11. Back extrusion data for plunger velocities of 30mm/min, 0.5 mm/min and 0.0 mm/min. 7% bentonite.

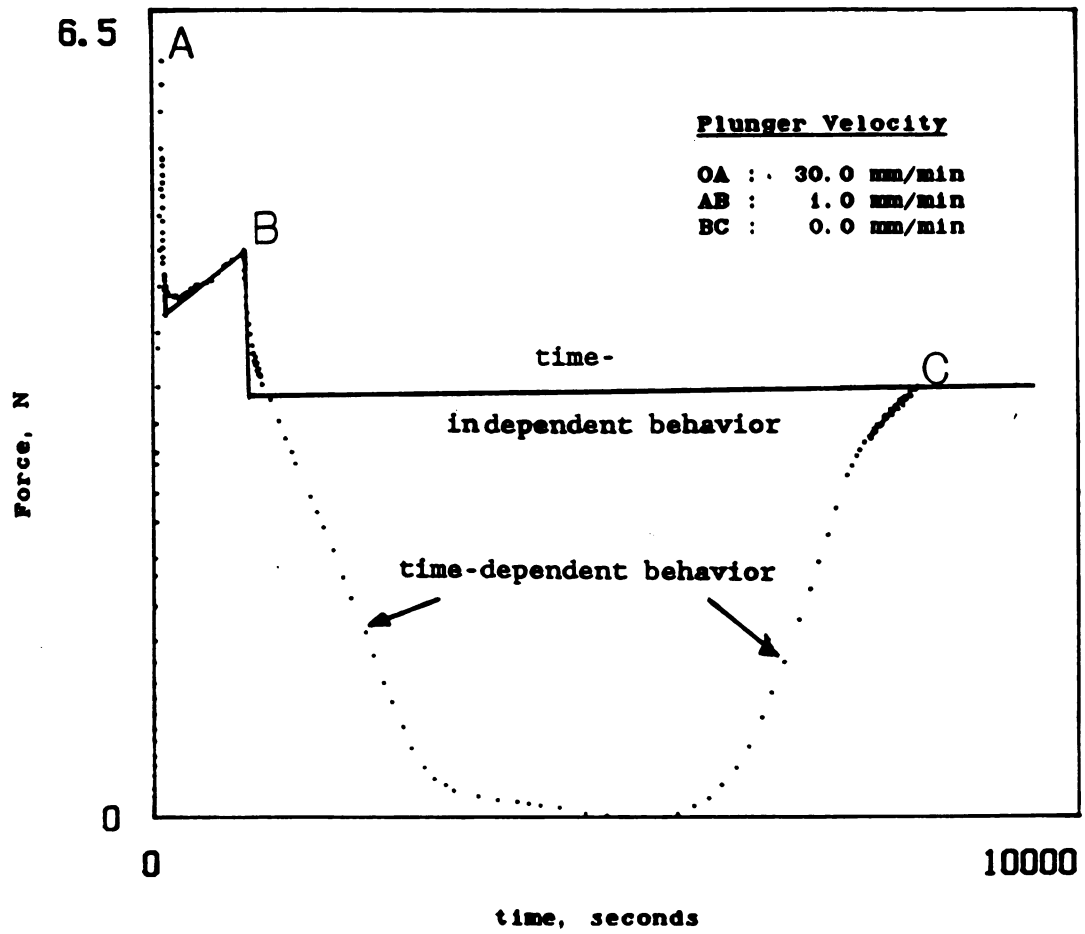

Figure 12. Back extrusion data for plunger velocities of 30mm/min, 1.0 mm/min and 0.0 mm/min. 7% bentonite.

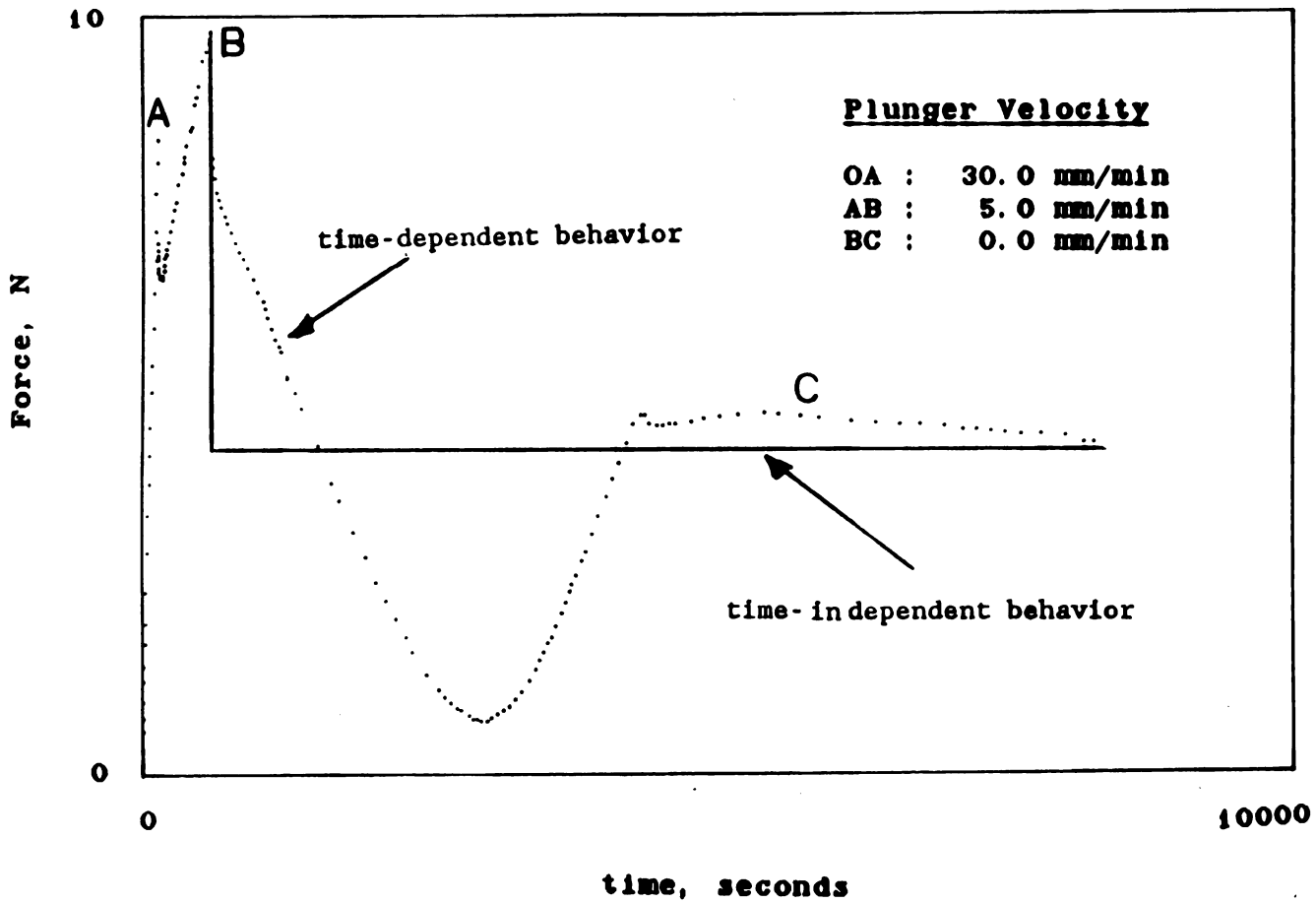

Figure 13. Back extrusion data for plunger velocities of 30mm/min, 5.0 mm/min and 0.0 mm/min. 7% bentonite.

When measuring the yield stress of the final internal equilibrium structure of a 7% bentonite suspension, a value of 184.6 Pa was obtained, with a standard deviation (32 tests) of 25.6 Pa. This value should be considered as the value corresponding to undisturbed conditions, although it is not necessarily the value of the undisturbed sample prior to the penetration of the plunger. It would be the same if the process were totally reversible.

For a thixotropic material under flow conditions, at each shear rate there is a corresponding equilibrium shear stress. If the shear rate decreases to zero, an equilibrium shear stress, known as yield stress, is obtained. This yield stress is calculated, in practice, by extrapolating the rheogram curve to a zero shear rate value. When plotting the values of shear stress versus shear rate and extrapolating to zero shear rate, a value of 30.1 Pa is obtained for the yield stress calculated in this way. This value is six times higher than the value obtained for undistubed conditions (184.6 Pa); this means that if the sample is allowed to rest in a pipe, the pump will need more energy to re-start the flow of this material than the energy needed under steady conditions.

5.1.1.1.2 Flow Behavior Index

Eq. [92] is used to obtain the flow behavior index. Fig. 14 shows the experimental values obtained for the expression $F_{cb}/(\pi LaR)$ versus plunger velocity. By using nonlinear regression, the value for the flow behavior index was found to be 0.295, and the mean square error

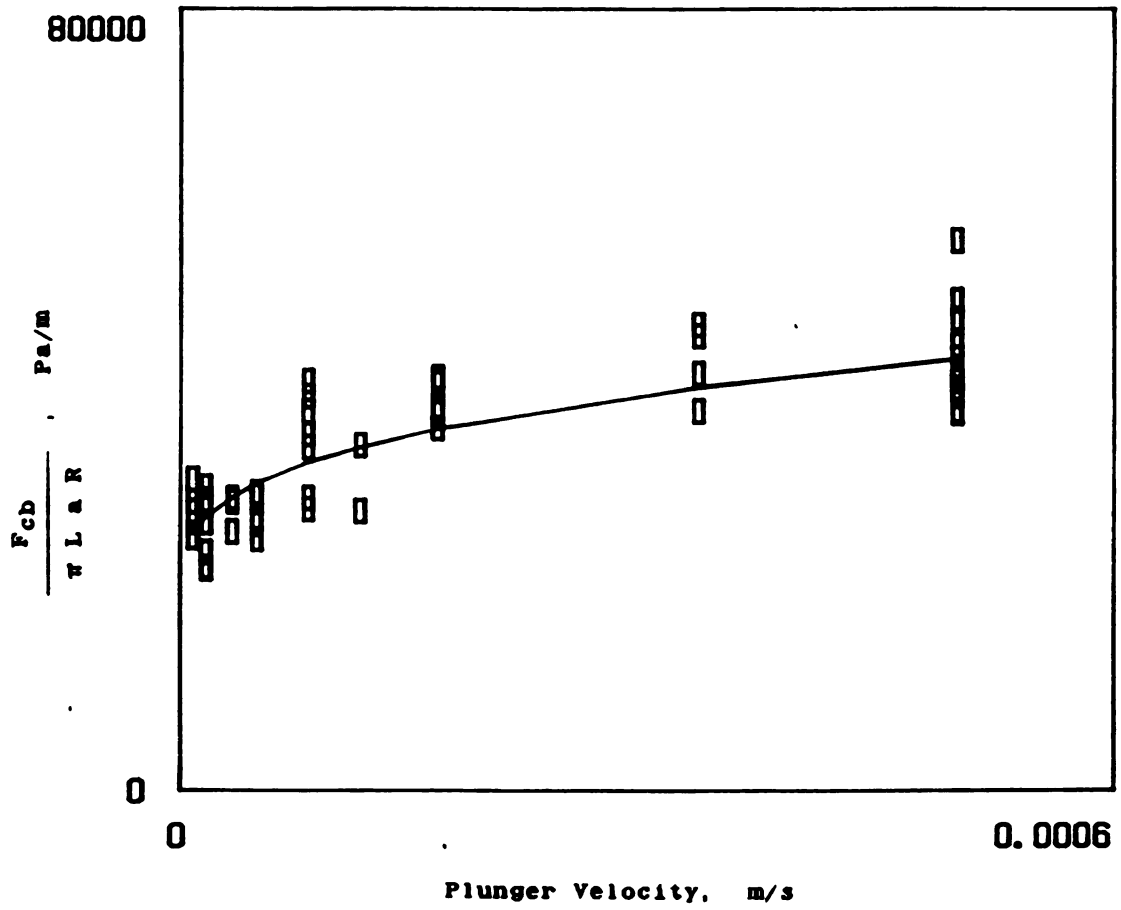

Figure 14. Values of $F_{cb}/(\pi LaR)$ versus plunger velocity when using back extrusion technique for determining rheological properties of 7% bentonite suspension samples.

was 1.8 10^7 for 50 tests, using the least square method.

5.1.1.1.3 Consistency Coefficient

Figures 15 and 16 illustrate the procedure described in section 4.3.1.1 that was followed when using back extrusion technique to determine the consistency coefficient. The value for this parameter was 22.5 Pa s^n, with a standard deviation of 0.5 Pa s^n.

5.1.1.2 Concentric Cylinders

Table 3 shows the rheological properties of 7% bentonite obtained by using concentric cylinders, both smooth and serrated. When using smooth and serrated cylinders with a very narrow gap (MV1 bob and MV cup), the sample creeps out of the cup. This could be due to the effect of an auger that the serrated bob creates for a material of very high apparent viscosity. Also, it could be due to a viscoelastic behavior of the bentonite, and a small Weissenberg effect could be present in the sample. Therefore, for each shear rate it was necessary to change the sample. The measurements for smooth cylinders were carried out using a larger gap (MVII bob); this helped keep the sample from creeping out of the cup. The Krieger method was used to find the shear rate values. Nonlinear estimation of the parameters was used with the Quasi-Newton method.

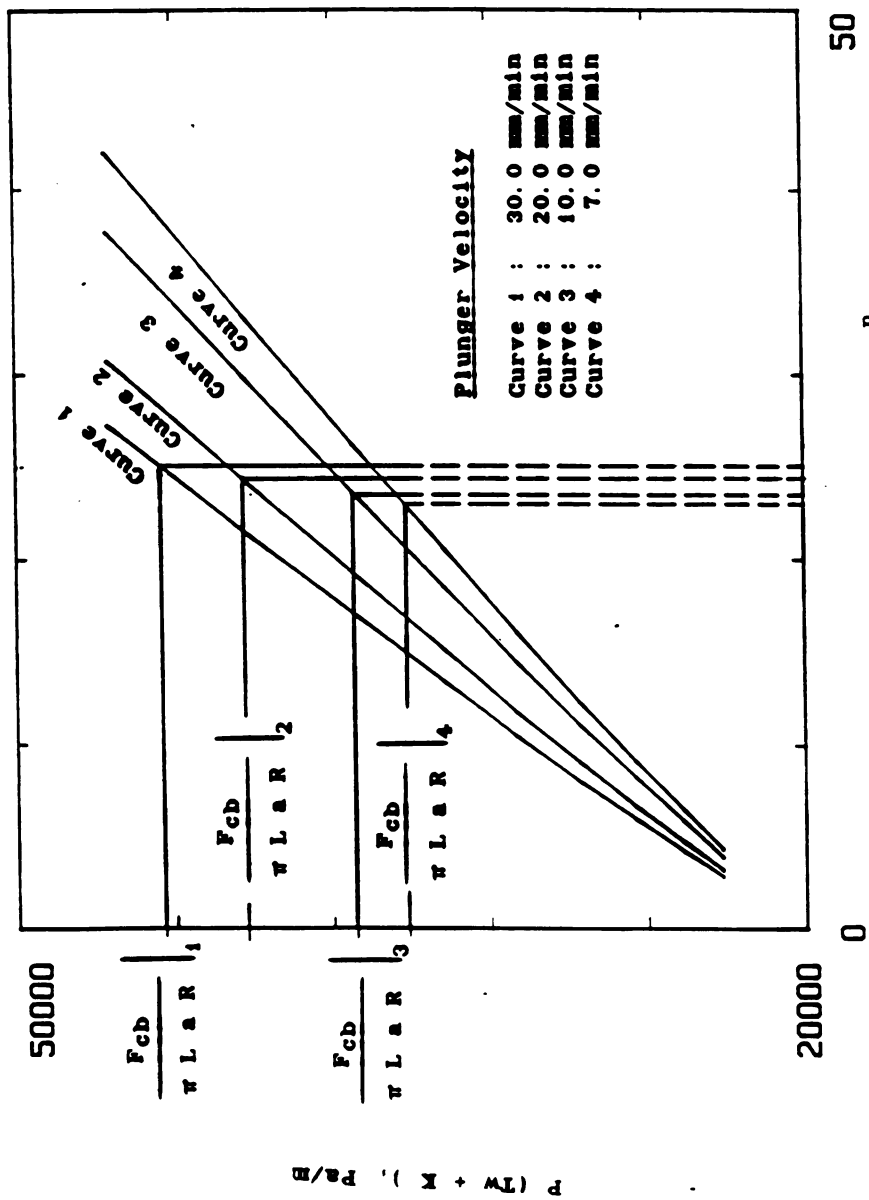

Figure 15. Determination of the rheological properties of 7% bentonite suspension with the back extrusion technique.

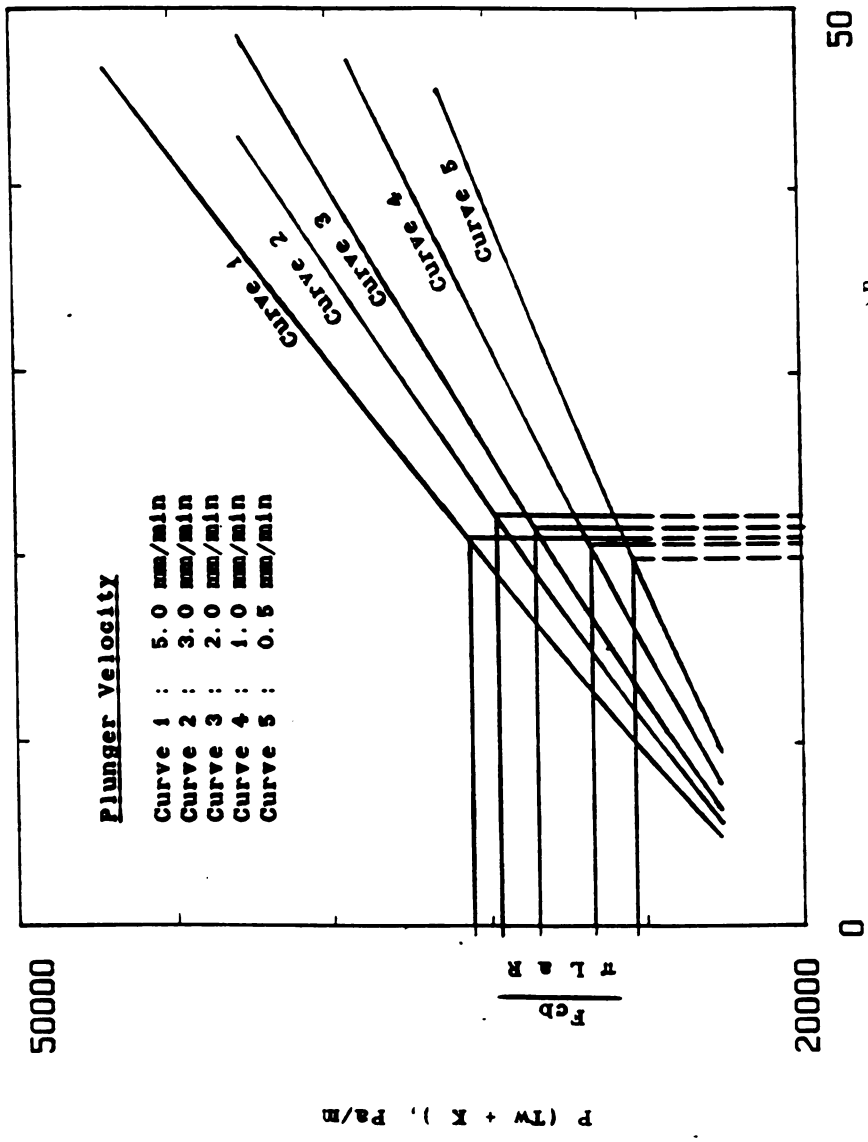

Figure 16. Determination of the rheological properties of 7% bentonite suspension with the back extrusion technique.

Table 3. Rheological Properties of 7% bentonite obtained with concentric cylinders geometry, using both smooth and serrated sensors.

Concentric Cylinder Type	Yield Stress (Pa)	Consistency Coefficient (Pa s^n)	Mean Square Error
Smooth (MVII/MVcup)	30.0	36.0	685.
Serrated (MVI/MVcup)	30.0	52.1	130.4

The sample is highly disturbed when transferred from the sample container into the cup. Although a lot of care is taken when transferring the sample, disruption is inevitable when the bob is inserted in place. The bob is forced down into the sample contained in the cup, and in this way the internal network that provides structure is disrupted.

Therefore, the structure is severely damaged before doing any experiment. If the sample exhibits thixotropy, or it has a long recovery time constant, it will be very difficult to get any measurement of thixotropic behavior.

Figure 17 shows the rheogram obtained for a 7% bentonite suspension when using smooth concentric cylinders. Also shown is the fitted curve. Figure 18 shows the rheogram obtained for the same material when using serrated bob sensor.

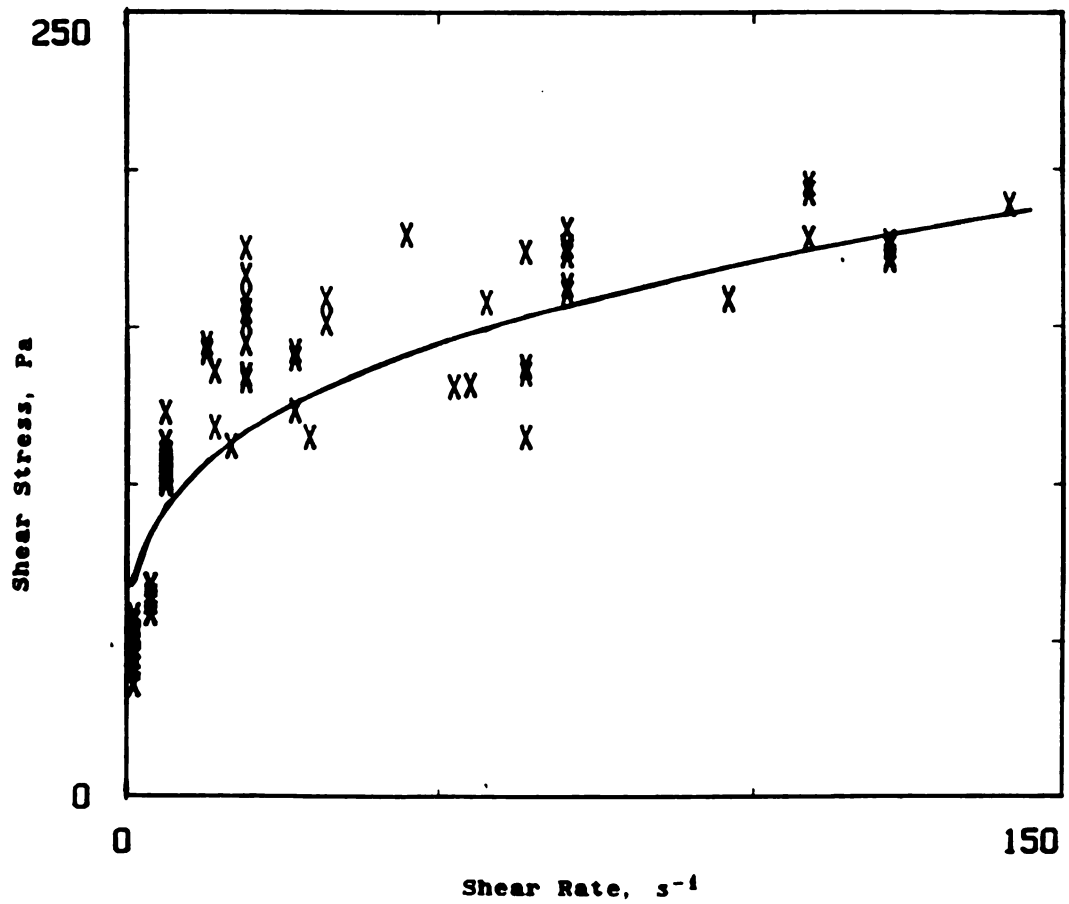

Figure 17. Rheogram of 7% bentonite suspension when using smooth concentric cylinders.

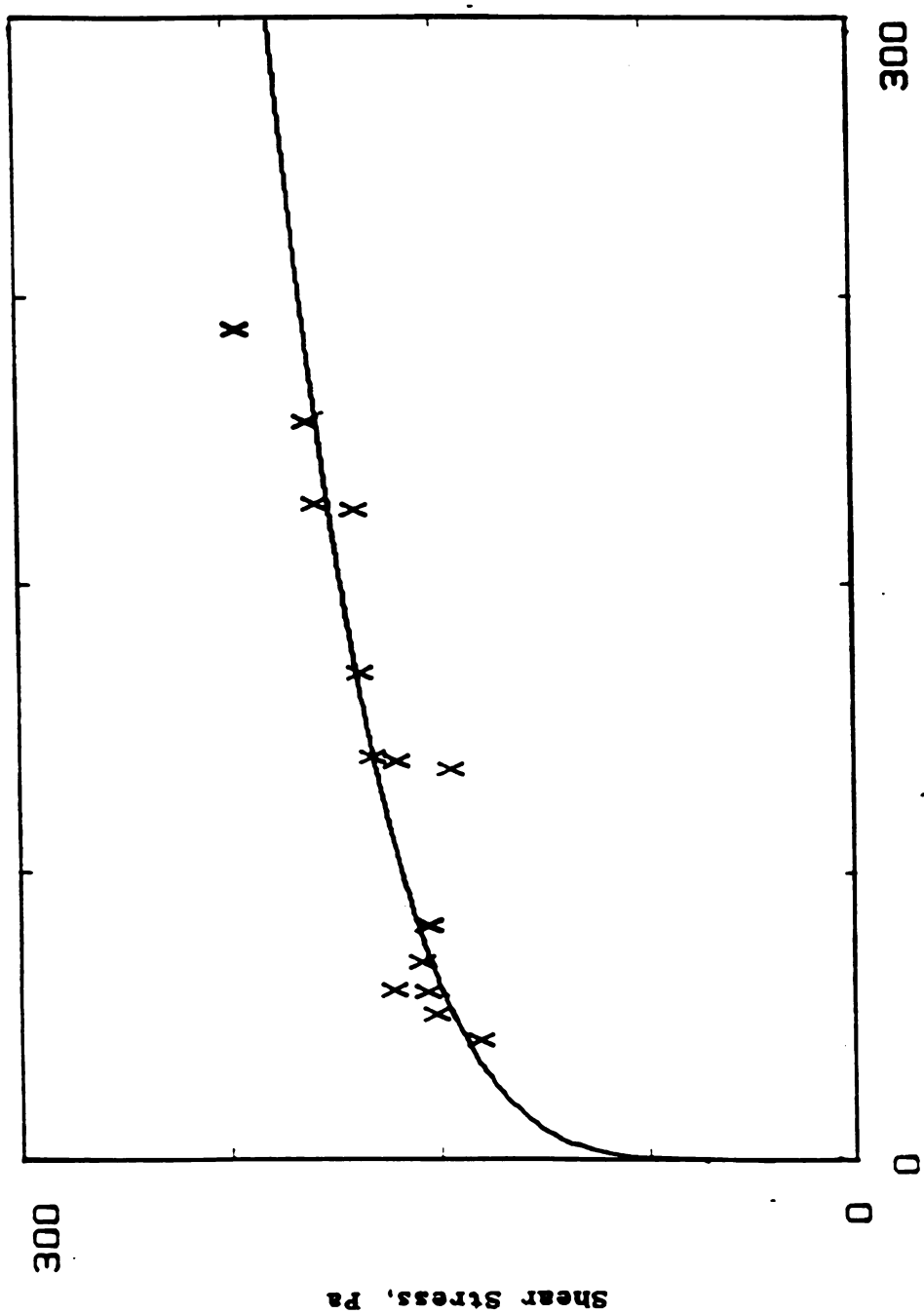

Figure 18. Rheogram of 7% bentonite suspension when using serrated concentric cylinders.

5.1.1.3 Parallel Plate Tests

5.1.1.3.1 Steady Tests

Steady tests using the parallel plate geometry (1.5 mm to 2.5 mm gaps) of the Rheometrics Fluid Spectrometer were conducted. To check for thixotropy, two thixotropic loops at 26.4°C were performed on the samples. A loop consisted of an increasing shear rate from zero to five s^{-1} in five minutes followed by an immediate decrease in shear rate from five to zero s^{-1} in five minutes. Fig. 19 shows the thixotropic loop. A problem arose when performing this type of loop. After the first loop was completed, it was observed that the sample was creeping out of the gap between the parallel plates. A new sample was placed between the plates and a shear rate sweep from zero to two s^{-1} was done on the sample. Fig. 20 shows the shear rate sweep.

By comparing Figs. 19 and 20 it can be seen that the values of shear stress for the shear rate sweep are lower than the values of shear stress of the first branch of the first loop of the thixotropic loop, but they are higher than the values of the second branch of the thixotropic loop. This means that when doing the shear rate sweep, the sample does not have time to reach its equilibrium shear stress at a given shear rate.

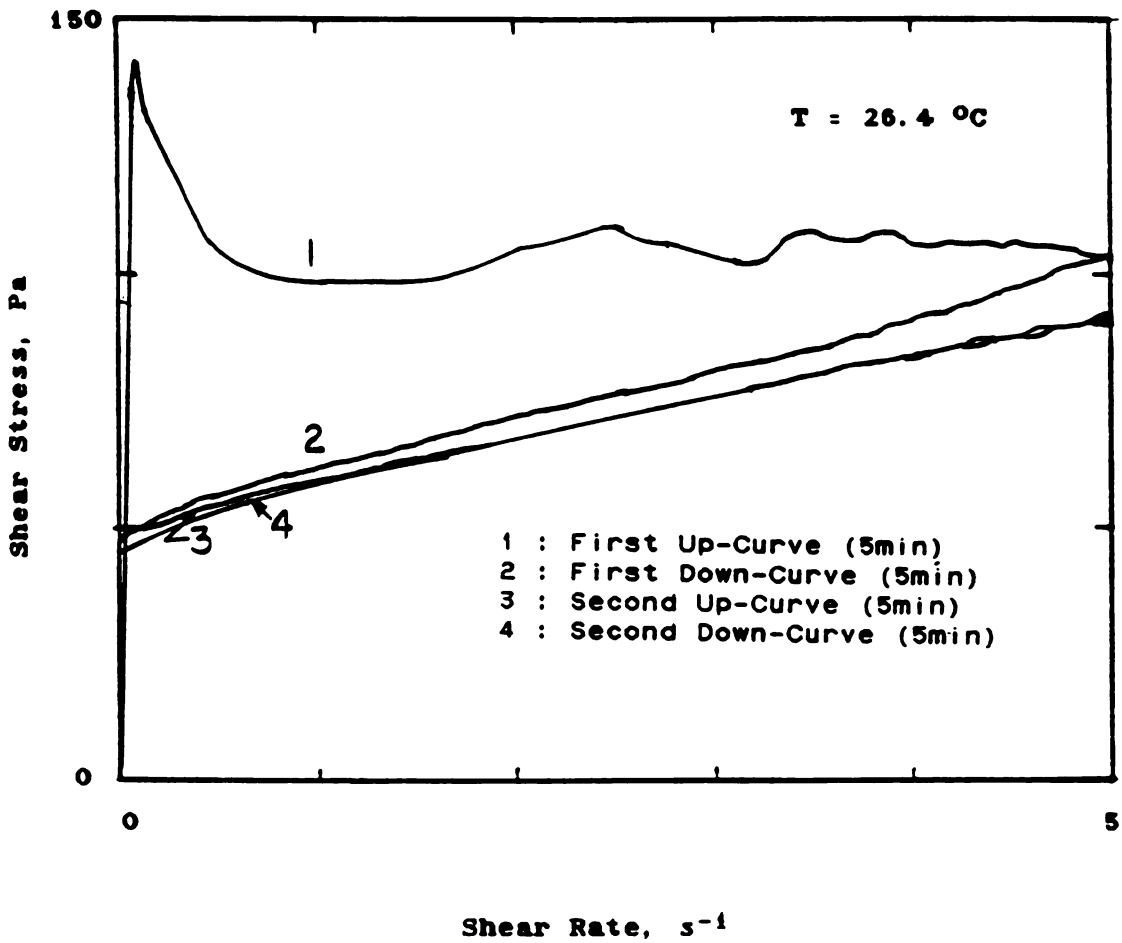

Figure 19. Thixotropic loop of a 7% bentonite suspension. Parallel plates geometry.

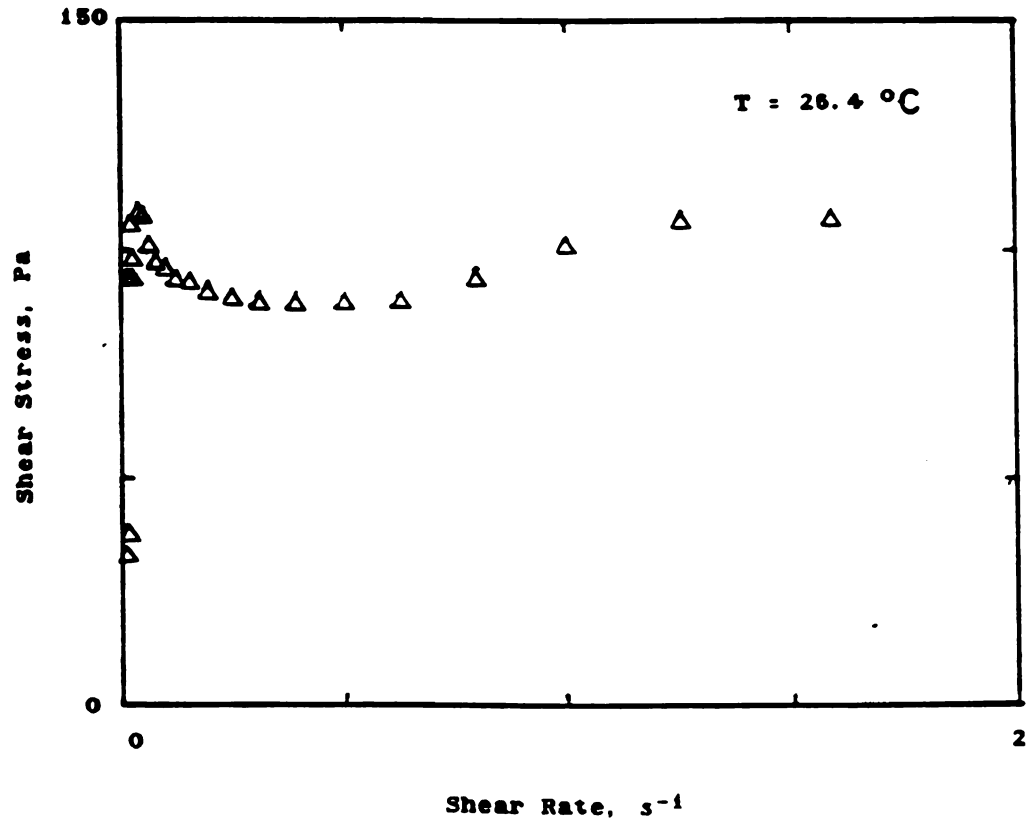

Figure 20. Shear stress as a function of shear rate for 7% bentonite suspension. Parallel plates geometry.

Another type of test was tried when using parallel plates. The idea was to set a given shear rate and obtain the equilibrium shear stress, and then either increase or decrease the shear rate and obtain the new equilibrium shear stress. In this way, the previous history of the thixotropic material should not influence the equilibrium shear stress. Figure 21 shows some results obtained from this type of experiment. It was observed that the sample creeps out of the gap, meaning this data could not be analyzed for thixotropy.

To avoid possible problems due to slip at the plates walls, serrated parallel plates were also used, but the results were similar to those observed with smooth parallel plates. The sample also creeps out of the gap.

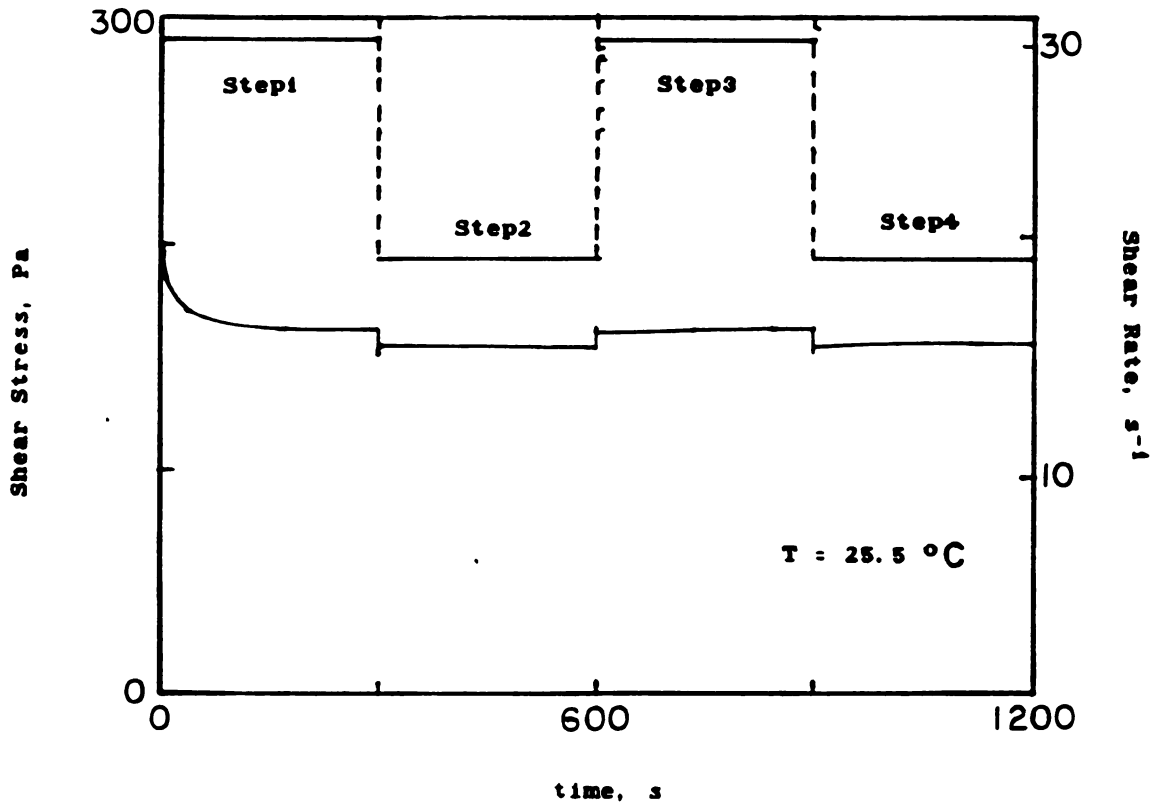

Figure 21. Shear stress history of 7% bentonite suspension when shear rate is changed from 30 s^{-1} (step 1) to 20 s^{-1} (step 2), then back to 30 s^{-1} (step 3), and finally 20 s^{-1} (step 4). Parallel plates geometry.

5.1.1.3.2 Dynamic Tests

Dynamic tests were performed with bentonite samples to verify the presence of viscoelastic properties.

To check the linear viscoelastic range, a strain sweep from 0.2 to 40% at a frequency of 3.0 rad/s was performed at 25°C using the Rheometrics Fluid Spectrometer. Results (Figure 22) show the storage modulus (G') had a constant value up to 2% strain and then decreased continuously. The loss modulus (G'') increased slowly up to 1% strain, then increased considerably up to a maximum value when the strain was 15%, and after that it decreased. The loss modulus and storage modulus curves intersected when the strain was 20%. Therefore, when the strain is below 20%, the elastic behavior is dominant, but when the strain is above 20% the viscous behavior is dominant.

Strain sweeps at higher frequencies show the same behavior. The only difference is that the maximum value for G'' occurs at a lower strain. For a frequency of 20 rad/s the maximum G'' occurs at 10% and the G' and G'' curves intersect at 15% strain (Figure 23). A frequency sweep is shown in Figure 24.

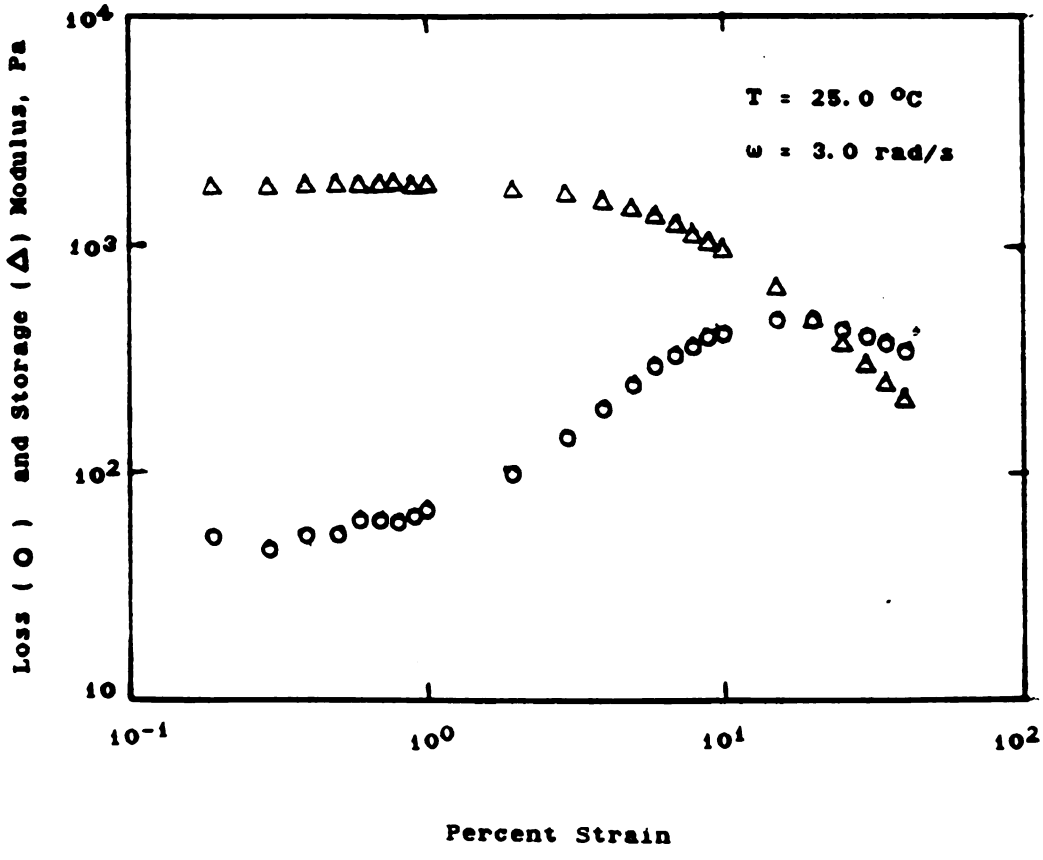

Figure 22. Values of G′ and G" as a function of strain for a 7% bentonite suspension. Parallel plates geometry.

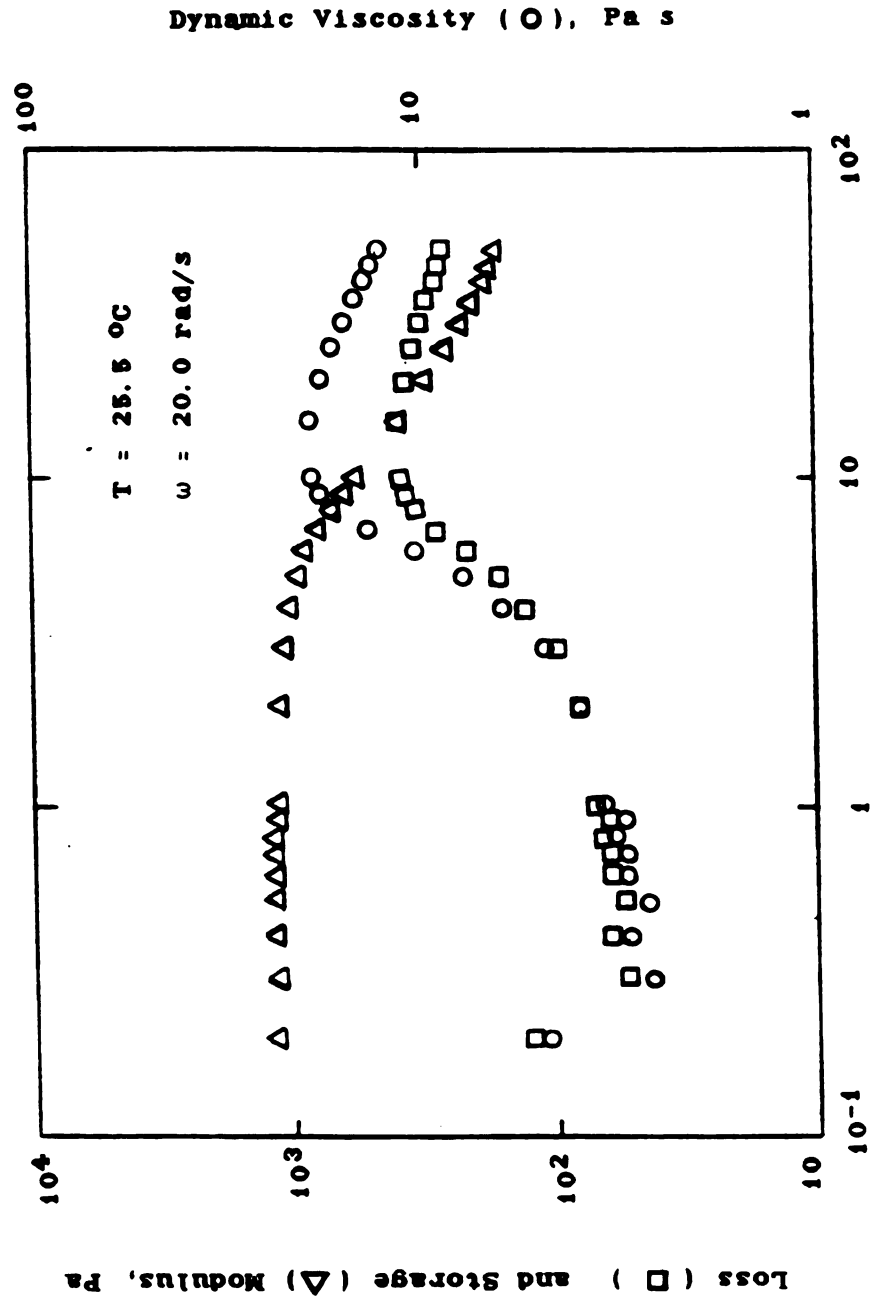

Figure 23. Values of G', G" and dynamic viscosity as a function of strain for a 7% bentonite suspension. Parallel plates geometry.

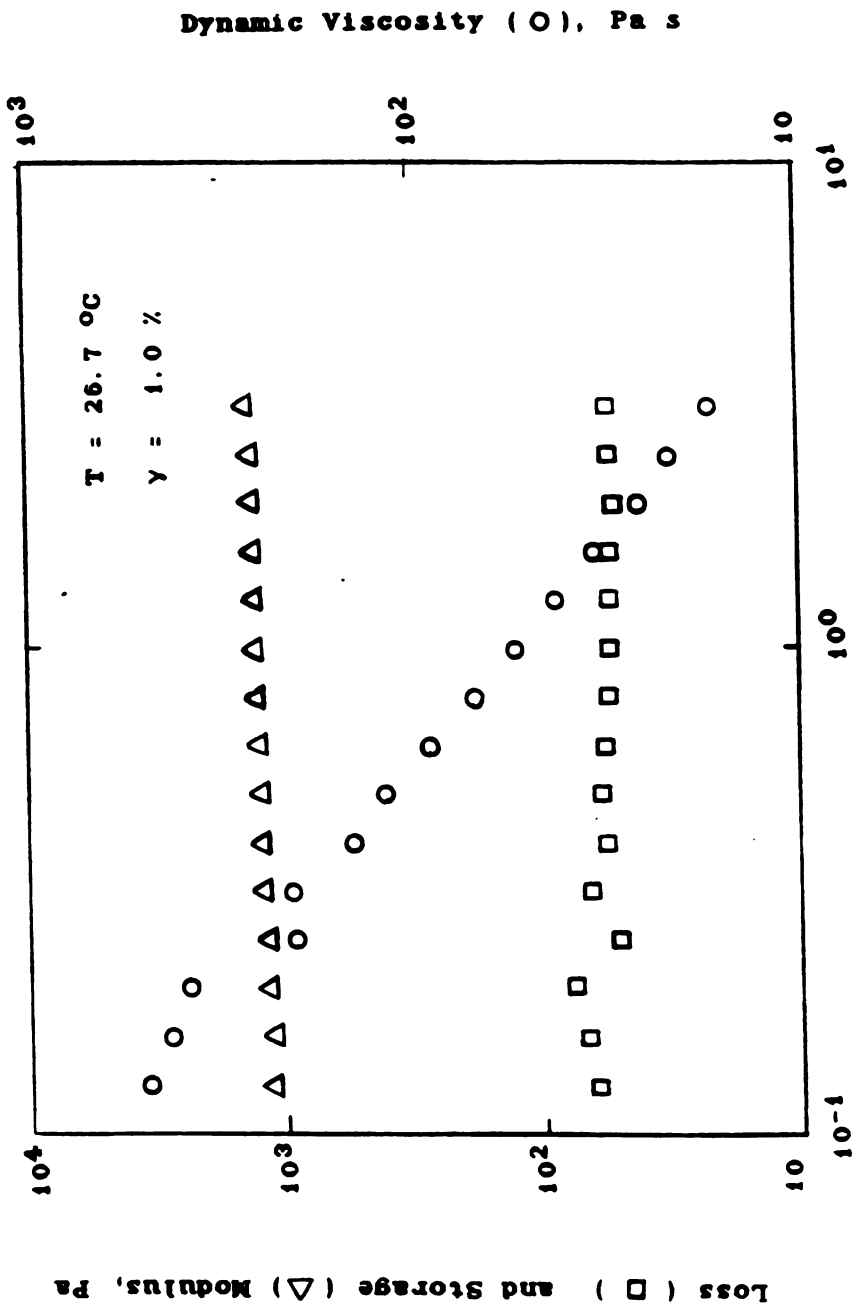

Figure 24. Values of G', G" and dynamic viscosity as a function of frequency for a 7% bentonite suspension. Parallel plates geometry.

Figures 25 and 26 show the variation , at 25°C, of the dynamic viscosity (η') and the complex viscosity (η^*) versus frequency at a 1% strain. As the frequency increases the decrease in value is higher for the dynamic viscosity than for the complex viscosity.

Figure 27 shows the apparent viscosity (η) obtained from Figure 20. When comparing the values of apparent viscosity versus shear rate with the values of dynamic viscosity versus frequency, the values of η and η' are very close, especially for values of shear rate below 0.3 s^{-1}, and for shear rate values above 1.0 s^{-1} the values of η are higher than those of η'.

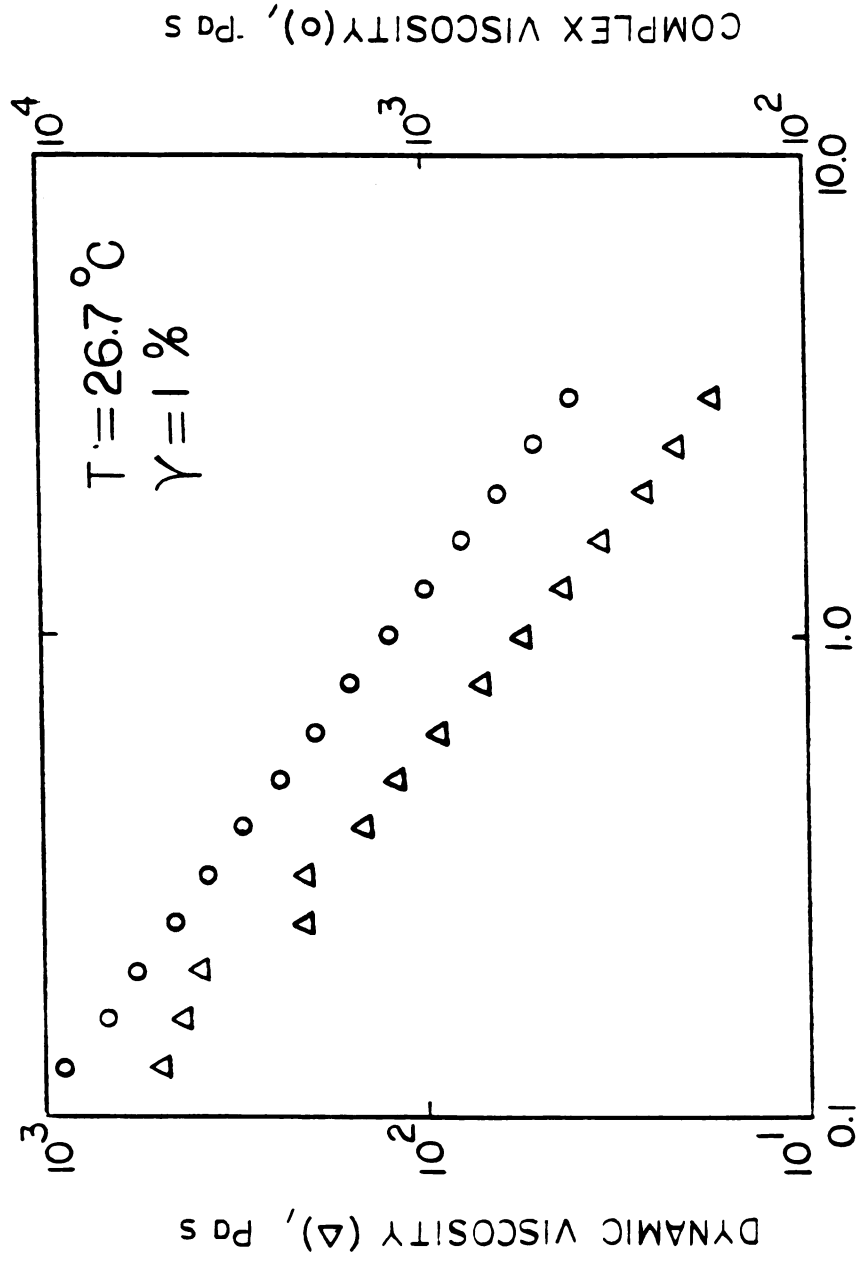

Figure 25. Dynamic and complex viscosities as a function of frequency for a 7% bentonite suspension. Parallel plates geometry.

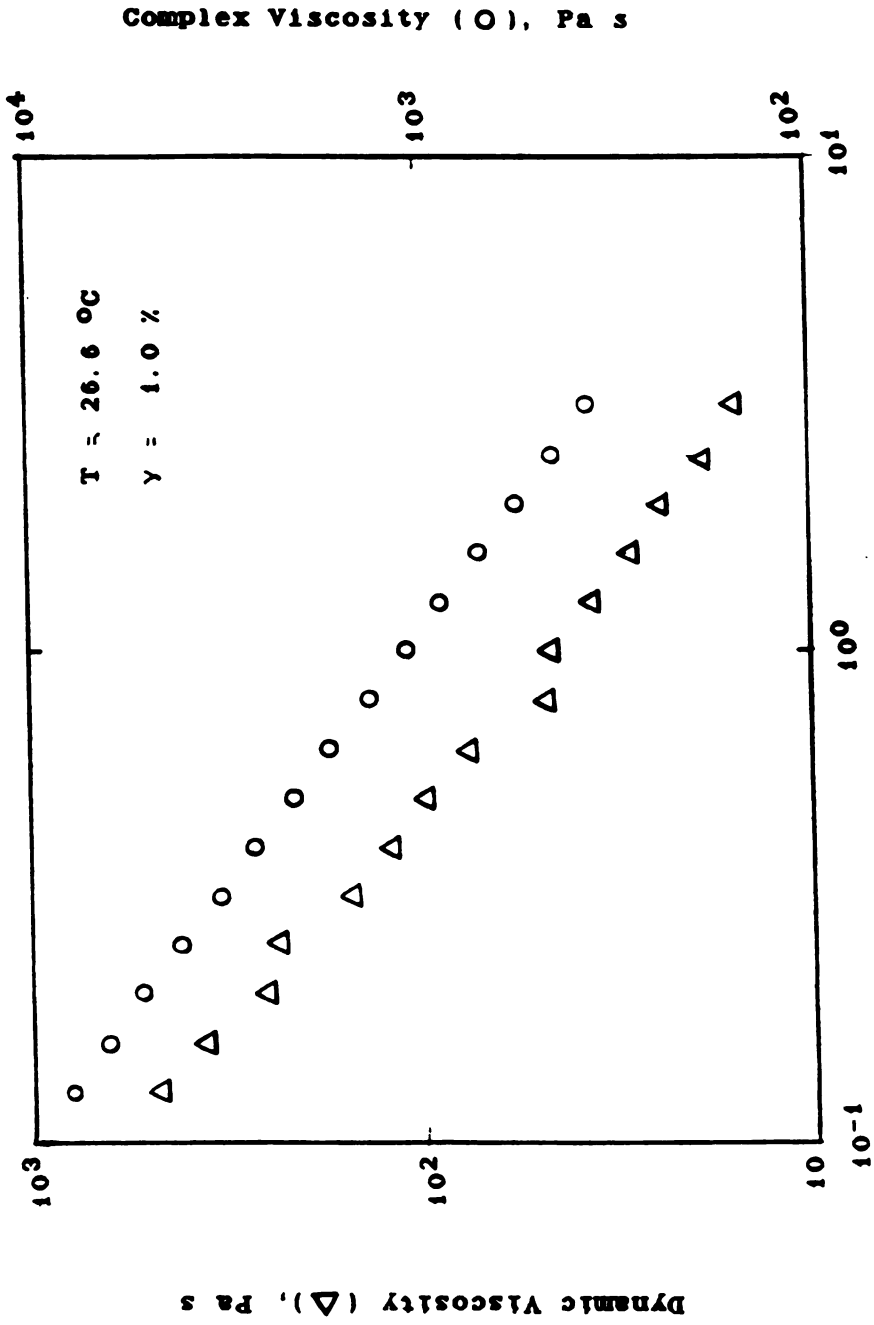

Figure 26. Dynamic and complex viscosities as a function of frequency for a 7% bentonite suspension. Second run after the sample was rested for 10 min. Parallel plates geometry.

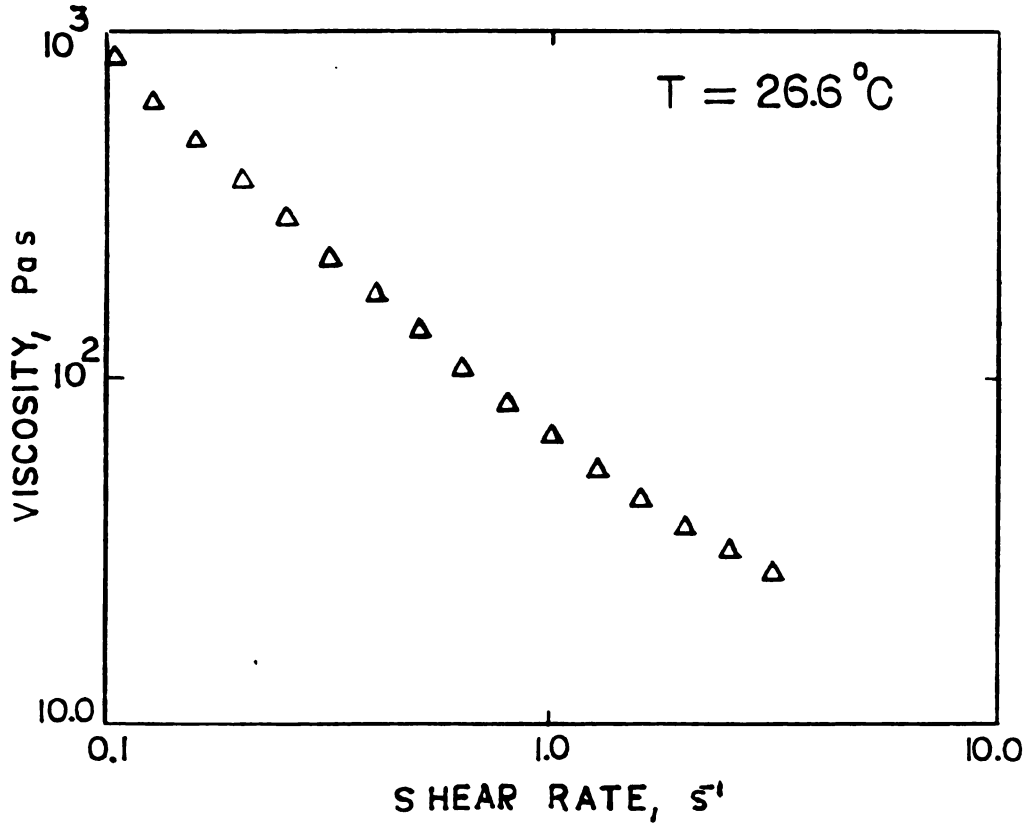

Figure 27. Viscosity as a function of shear rate for a 7% bentonite suspension. Parallel plates geometry.

5.1.3 Comparison of Test Methods to Determine Equilibrium Rheological Properties

When comparing the values of the rheological parameters obtained using back extrusion and other techniques, the following can be said:

-The back extrusion technique allows to follow the development of yield stress over time after a sample is disturbed and then allowed it to rest.

-The parameters of the Herschel Bulkley model are usually correlated. When the flow behavior index was determined using the back extrusion technique, the consistency coefficient and yield stress values where found by the method described in section 4.3.

-The values of consistency coefficient obtained with concentric cylinder data were higher than those obtained with back extrusion data, especially the value obtained with serrated bob sensor.

-The value of the flow behavior index was the same for the smooth bob sensor and back extrusion testing. The value of the flow behavior index obtained with the serrated bob sensor was smaller than that obtained with back extrusion. One explanation for this differences in values obtained with different geometries is the type of flow involved, and therefore the boundary conditions are different in each case. The

type of disturbance applied on the fluid is also different. In concentric cylinders there is a centrifugal force acting on an element of fluid, and the fluid is moving in circles as the centrifugal force is pulling the element of fluid. There is no pressure driven flow in concentric cylinders geometry. In back extrusion, on the other hand, the fluid is moving upwards while the gravity is pulling an element of fluid down. This is a pressure driven flow.

-In a concentric cylinder viscometer, when the sensor is stopped, there is no more force acting on an element of fluid, there is no spring-like behavior in the fluid. In a back extrusion device, after the plunger is stopped, the fluid is still disturbed by the plunger.

5.1.3. Time-Dependent Properties

5.1.3.1 Back Extrusion

Following the modified technique developed by Kemblowsky and Petera (1980, 1981), the dependence of the yield stress on the structural parameter κ was studied. To do this, the first value of shear stress obtained inmediately after the plunger velocity was changed during the test, was used to determine the exponent m defined by Eq. [58]. The values of the initial shear stress calculated after different initial and final shear rates are shown in Table 4. From the data (Table 4) the value for the exponent m was 0.111. This value of m equal

Table 4. Values of shear stress immediately after a change of shear rate when performing back extrusion testing of a 7% bentonite suspension.

Initial Shear Rate (s^{-1})	Final Shear Rate (s^{-1})	Shear Stress (Pa)
9.52	0.21	80.1
9.52	0.37	63.2
9.52	0.37	60.1
9.52	0.37	55.1
9.52	1.00	58.4
9.52	1.00	67.0
9.52	1.00	64.1
9.52	1.00	61.5
9.52	1.00	76.8
9.52	1.64	62.7
9.52	1.64	71.6
9.52	2.25	75.8
9.52	2.25	63.9
6.37	0.21	66.0
6.37	0.37	71.8
6.37	0.69	59.4
6.37	1.64	77.5
3.21	0.21	60.4
3.21	0.37	67.2
3.21	0.37	62.9
3.21	0.69	60.7
3.21	1.64	71.9
1.63	0.21	66.0
1.63	0.37	67.9
1.63	0.69	65.8

to 0.111 means that when the plunger velocity is decreased, the value for the shear stress immediately after the velocity has been decreased will be higher than the corresponding equilibrium value. Under this condition, the structure of the bentonite will continue to be destroyed at this lower plunger velocity until the build-up rate equals the destruction rate. Also, the extrapolated values of yield stress obtained from the curves of equal value of structural parameter are shown in Table 5. By using the values shown in Table 5 in Eq. [55], the Equation governing the yield stress variation of 7% bentonite is given by,

Table 5. Yield stress values corresponding to a given structural parameter for a 7% bentonite suspension when using the back extrusion technique.

Structural Parameter, κ (dimensionless)	Yield Stress σ_y (Pa)	Shear Rate $\dot{\gamma}$ (s^{-1})
1.242	23.0	3.19
1.404	20.0	6.13
1.512	15.0	9.12

$$\sigma_y = 30.1 \left(1 - \exp \left(-1.197 \, \kappa^{-3.62} \right) \right)$$

Eq. [89] was used to determine the inverse time constant Γ. Figure 28 shows the values obtained for 7% bentonite suspension when the plunger velocity is decreased during a test. To try to generalize the results, the time constant is plotted against the ratio of the initial to the final shear rate. From the plot it can be seen that there is a maximum value for the time constant at a given shear rate ratio. The maximum value of Γ is higher when the initial plunger velocity is higher.

From Figure 28 it can also be seen that, to observe time dependency for this sample of bentonite 7% using the back extrusion technique, it is necessary to use the range of shear rate ratios covered in this study. For higher initial shear rates, the values for Γ would be much higher than 0.1 s^{-1}, and therefore the velocity of destruction of the network would be too fast to detect with this technique. This type of plot is very important because it gives the region where the relationships between initial and final shear rate that should be used when working with back extrusion technique to determine time dependency or thixotropy.

The reason for this behavior can be explained taking into account the structure of bentonite. When the ratio of the initial shear rate to the final shear rate is too big (i.e. the final shear rate is very small

when compared to the initial shear rate) the water trapped and immobilized in the house-of-cards type of structure formed by the edge to edge (EE) and edge to face (EF) particle association is released; so, there is no appreciable time-dependent effects at the lower shear rate. As the relative value of the shear rate ratio decreases, the inverse time function constant Γ increases, meaning that the EE and EF type of structures are not totally destroyed and at the lower shear rate there are time-dependent effects.

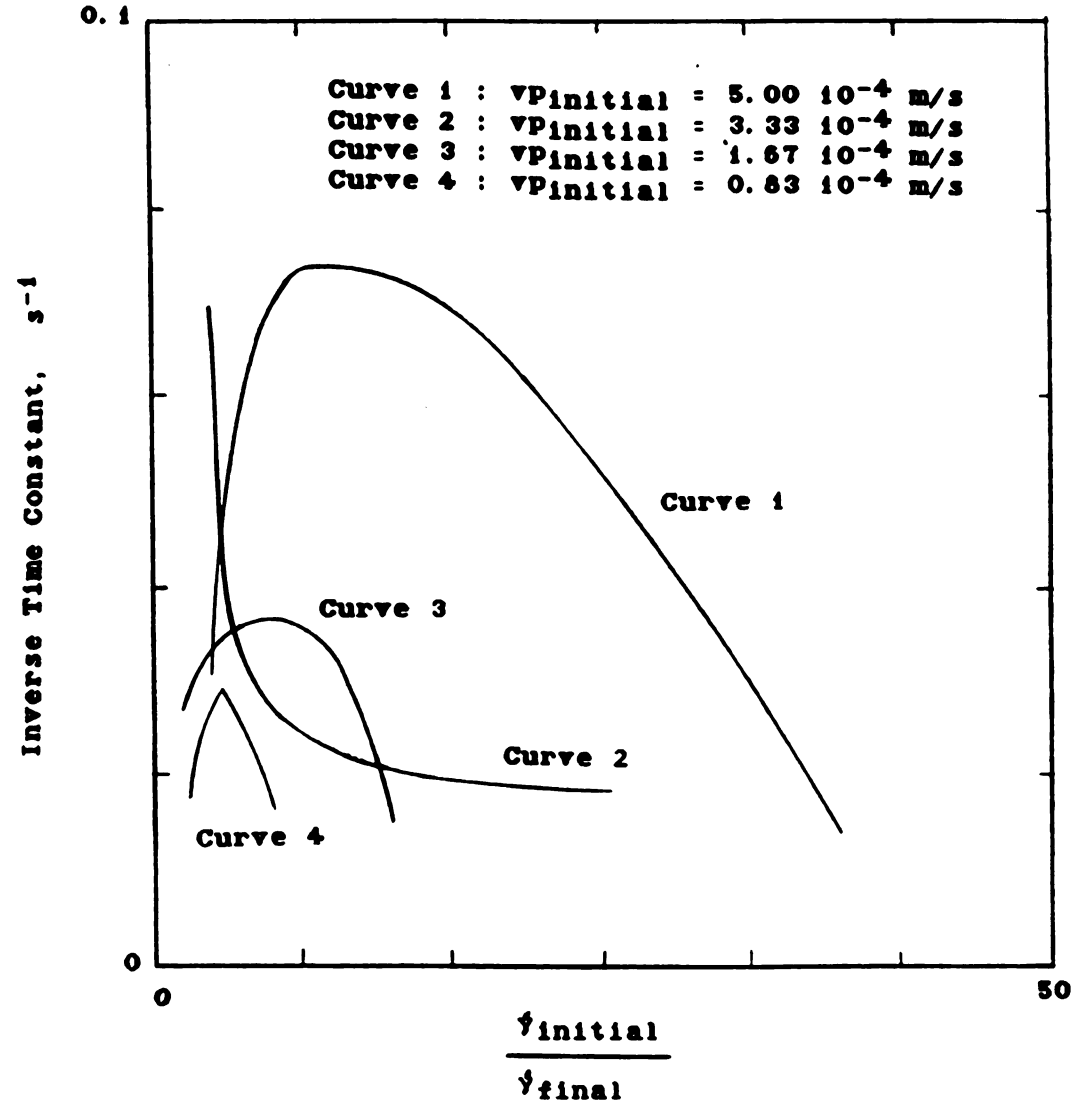

Figure 28. Inverse time constant, Γ, as a function of the ratio initial shear rate /(final shear rate) for a 7% bentonite suspension. Back extrusion technique.

5.1.3.2 Concentric Cylinders

5.1.3.2.1 Smooth Sensor

It was not possible to obtain time-dependent properties of 7% bentonite with the use of smooth concentric cylinders. The sample did not show measurable transient response when the angular velocity was either increased or decreased. The reason for this can be explained by the fact that a lot of disruption is done to the internal structure of the sample when placing the sample in the measuring unit, and when the sensor is pushed down into the sample. Adequate resting of the sample did not guarantee a rebuilding of the structure. The water entrapped in the house-of-cards type of structure could have been displaced irreversibly, and a face to face (FF) particle association may have occurred, with no time-dependent effects.

5.1.3.2.2 Serrated Cylinder

In this case, besides having the same problems mentioned above (5.1.3.2.1) the sample kept creeping out of the viscometer. This could have happened because the serrated bob (MV1) acted like an auger for the solid-like material. Also a Weissenberg effect could have been present in the material causing this climbing out of the cup.

5.1.3.3 Parallel Plates

5.1.3.3.1 Steady Tests

Figures 29 and 30 show the type of response obtained with the parallel geometry. The sample showed a very short transient at high shear rates. At lower shear rates the sample showed high inestability (Figure 29); therefore, it was not possible to measure the transient.

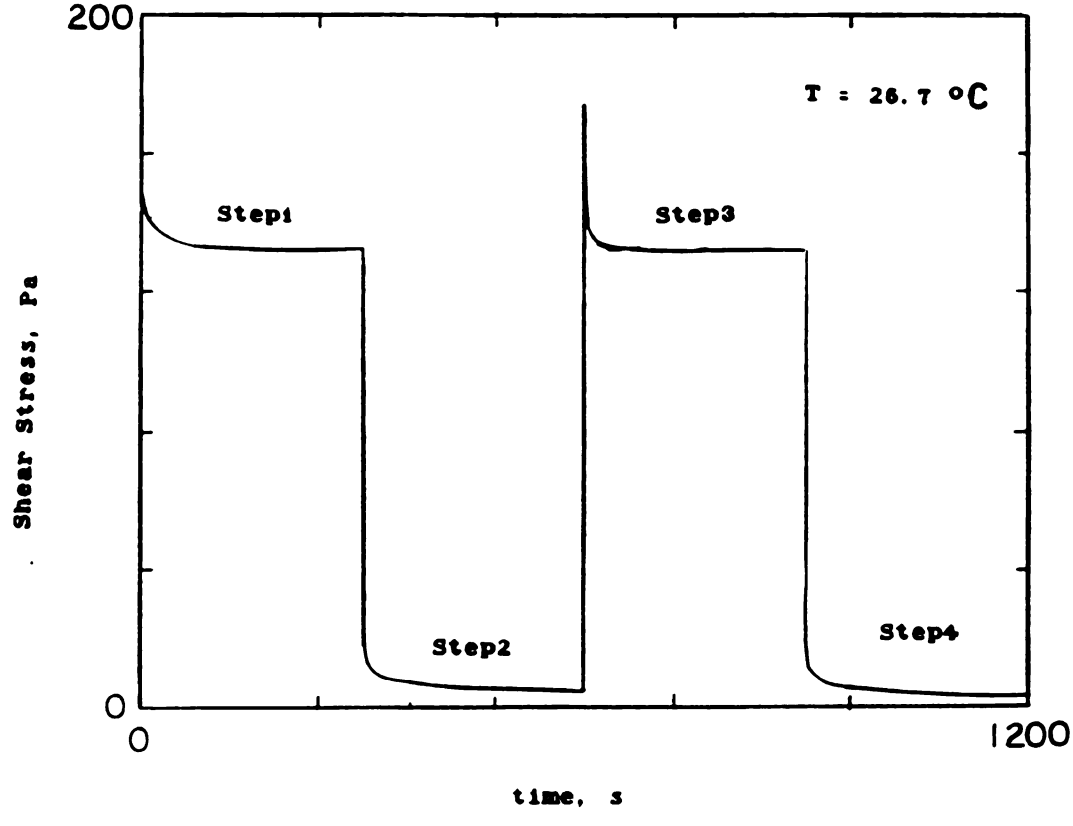

Figure 29. Shear stress history of 7% bentonite suspension when shear rate is changed from 20 s^{-1} (step 1) to 0 s^{-1} (step 2), then back to 20 s^{-1} (step 3), and finally 0 s^{-1} (step 4). Parallel plates geometry.

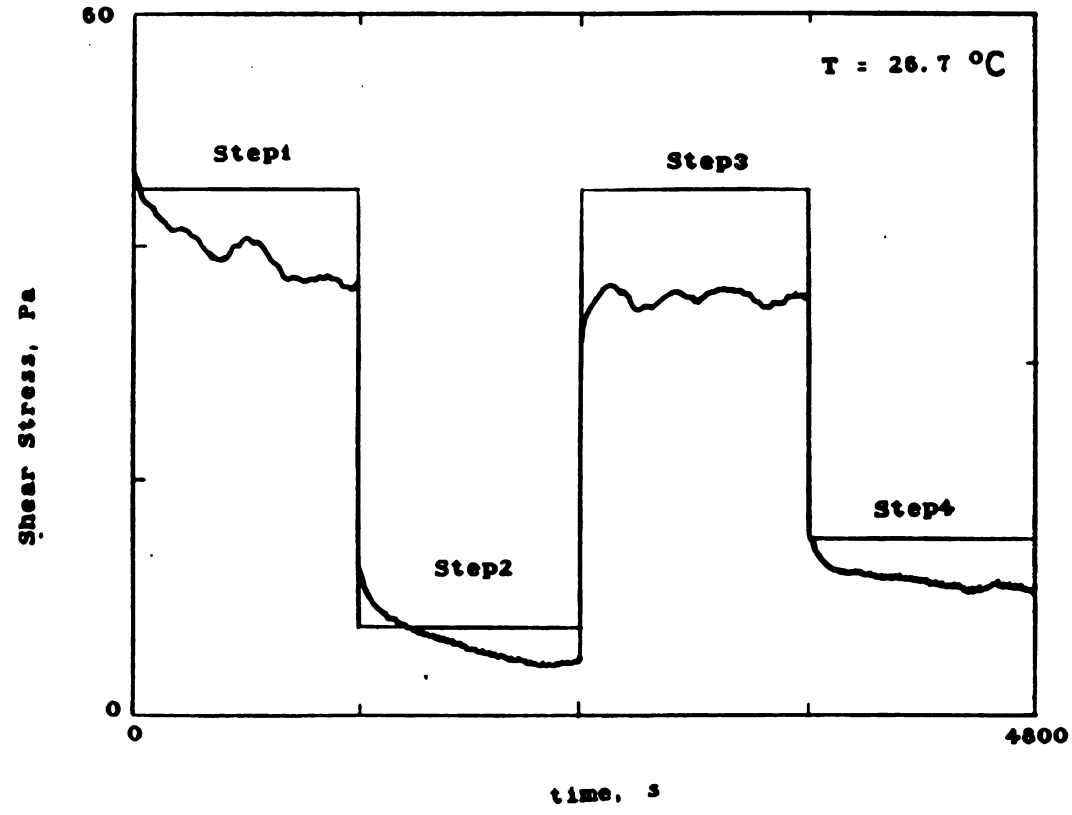

Figure 30. Shear stress history of 7% bentonite suspension when shear rate is changed from 3 s^{-1} (step 1) to 0.5 s^{-1} (step 2), then back to 3 s^{-1} (step 3), and finally 1 s^{-1} (step 4). Parallel plates geometry.

5.1.3.3.2 Dynamic Tests

Experiments were performed to study the changes in viscoelastic properties over time. Figures 31 to 36 show the variation of loss and storage modulus with time at a frequency of 3 s^{-1} for strain rates from zero to 30%. Over a period of five minutes there was not a significant change in either G' or G'' over time. As the strain increased, G' and G'' curves approached each other and, at a 30% strain, the curves reversed with the G'' curve going above the G' curve. Therefore, if the strain is above 30%, the sample will behave as a liquid, and below 30% solid behavior dominates.

It can be concluded from this test that the sample behavior was more sensitive to strain than changes due to time dependency.

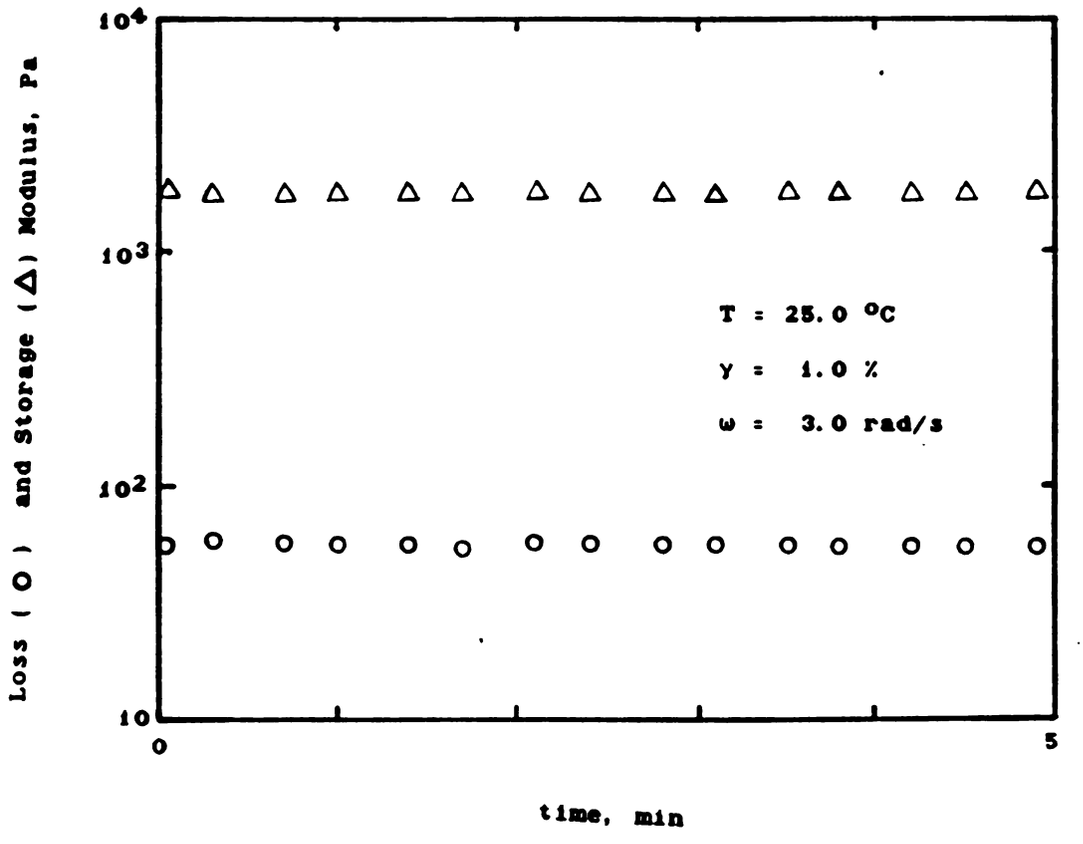

Figure 31. Dependency of G', G" with time for a 7% bentonite suspension. Parallel plates geometry.

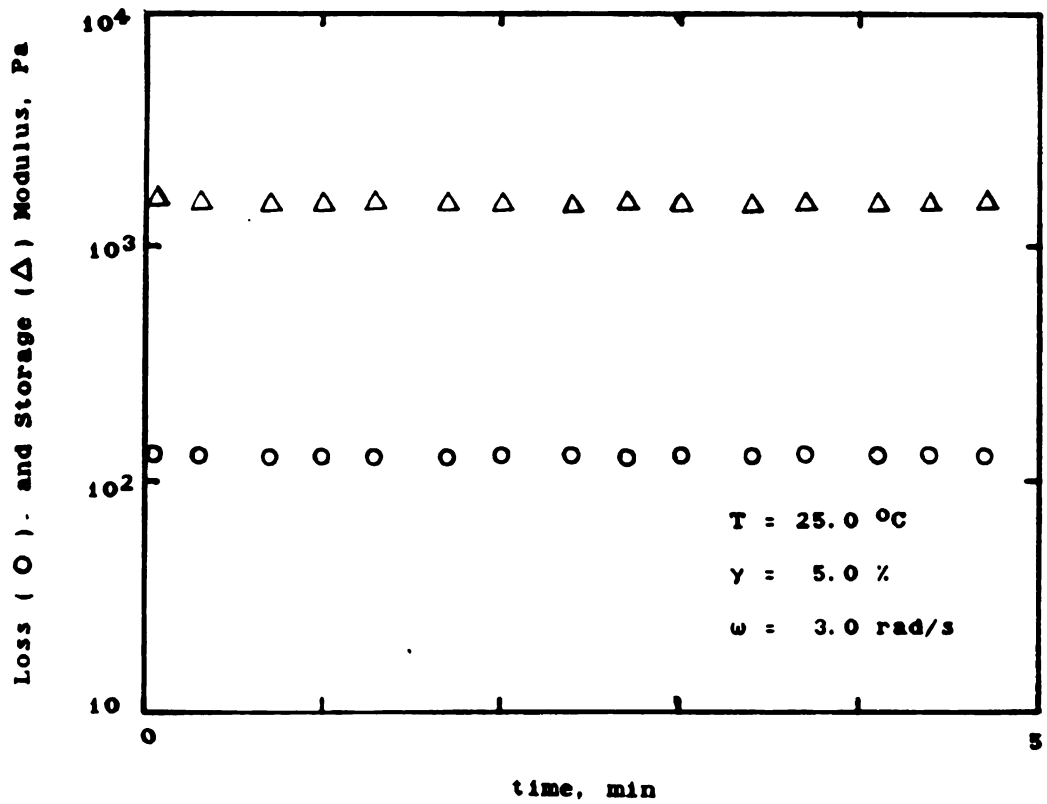

Figure 32. Dependency of G', G" with time for a 7% bentonite suspension. Parallel plates geometry.

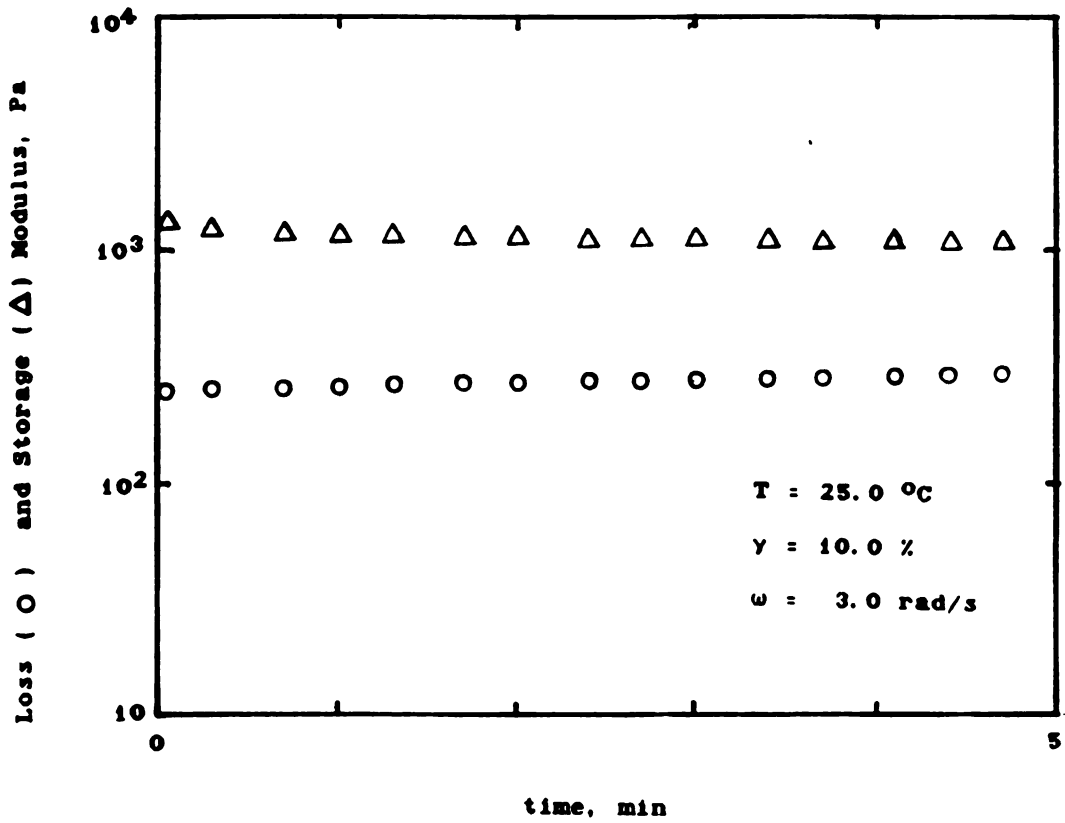

Figure 33. Dependency of G', G" with time for a 7% bentonite suspension. Parallel plate geometry.

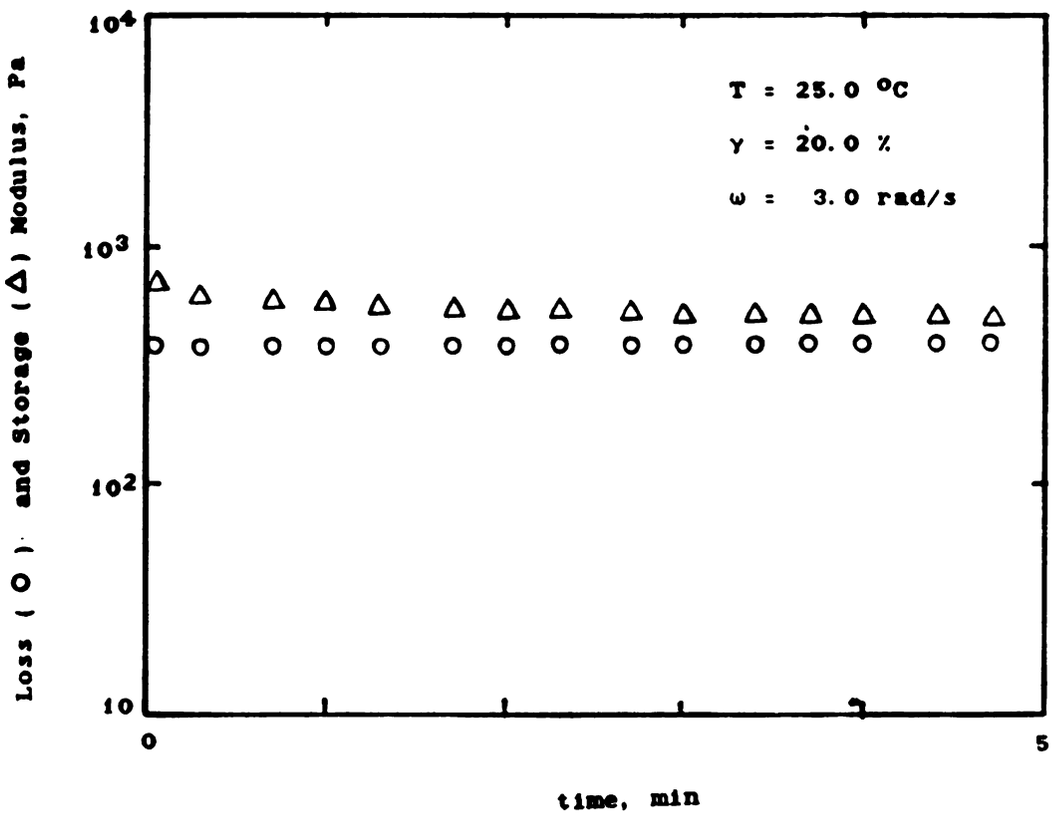

Figure 34. Dependency of G', G" with time for a 7% bentonite suspension. Parallel plates geometry.

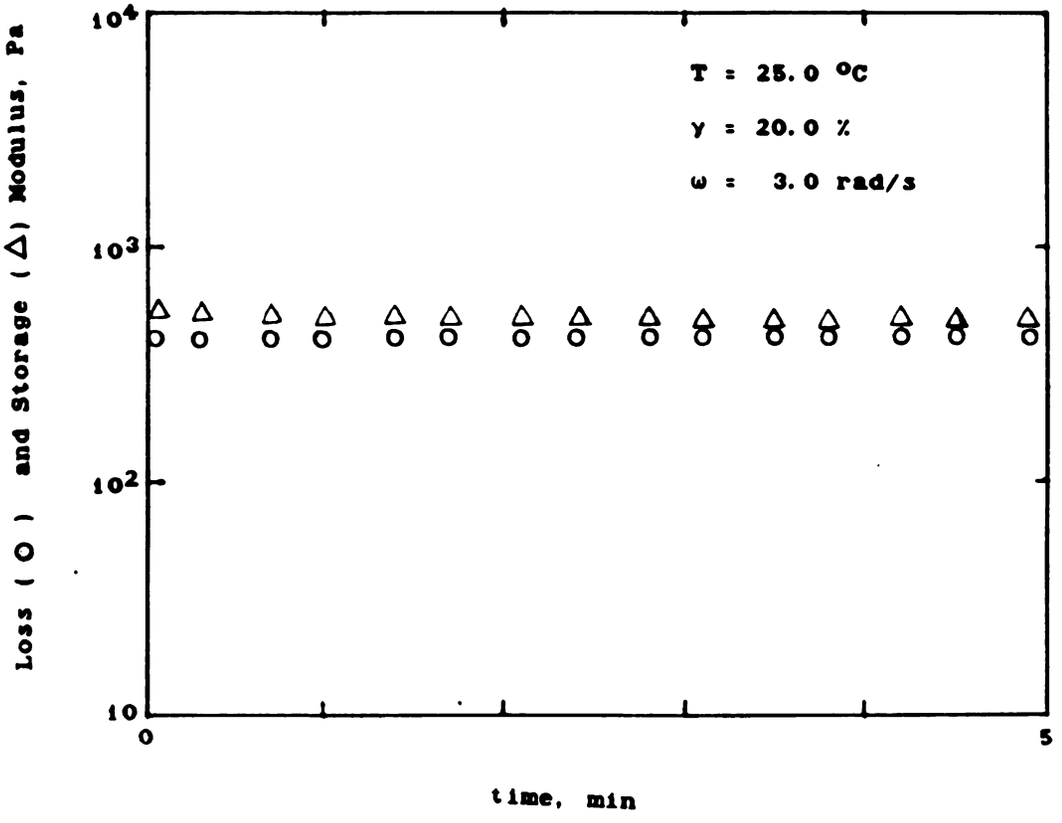

Figure 35. Dependency of G', G" with time for a 7% bentonite suspension. Sample rested 10 minutes after first run. Parallel plates geometry.

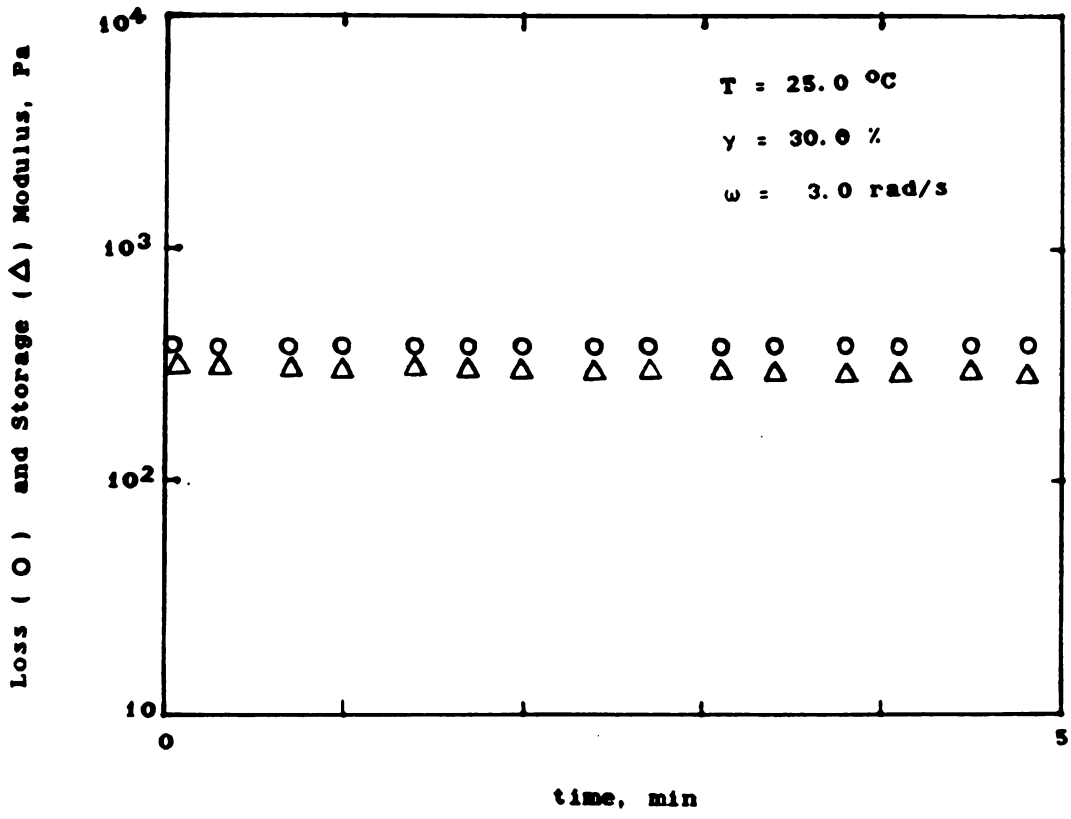

Figure 36. Dependency of G', G" with time for a 7% bentonite suspension. Parallel plates geometry.

5.2 Iota-Carrageenan

The 1% (weight/volume) sample of Iota-Carrageenan had a density of 1008.0 kg/m^3, with a standard deviation of 9.9 kg/m^3.

5.2.1 Equilibrium Rheological Properties

5.2.1.1 Back Extrusion Tests

Figure 37 shows the experimental values of $F_{cb}/(\pi LaR)$ as a function of plunger velocity for 1% Iota-Carrageenan. By using nonlinear regression, the flow behavior index was calculated with Eq. [92] and found to be 0.793, with a standard deviation of 0.15. The mean square error was $5.8\ 10^7$.

By using the method described in Section 4.3 (Data Analysis Procedure), the rheological properties of 1% Iota-Carrageenan were obtained (Table 6).

Figure 38 shows the pressure drop per unit of length, P, as a function of consistency coefficient with plunger velocity as parameter. From this plot, by knowing the experimental values of the expression $F_{cb}/(\pi LaR)$ (which is equal to pressure drop per unit of length P for a given plunger velocity) the consistency coefficient is obtained, and for this case is equal to 52 Pa s^n.

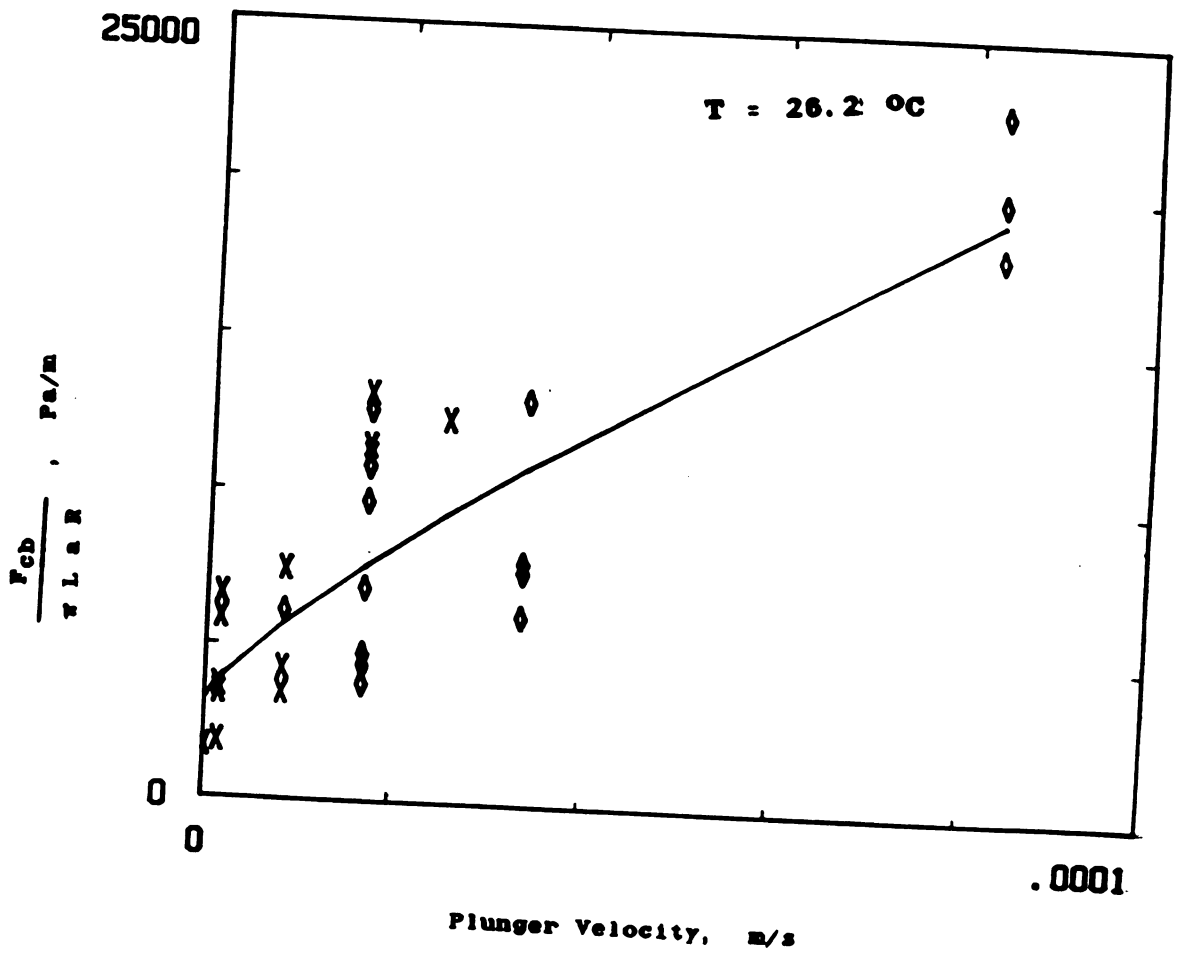

Figure 37. Values of the expression $F_{cb}/(\pi$ LaR) as a function of plunger velocity for Iota-Carrageenan. Back extrusion technique

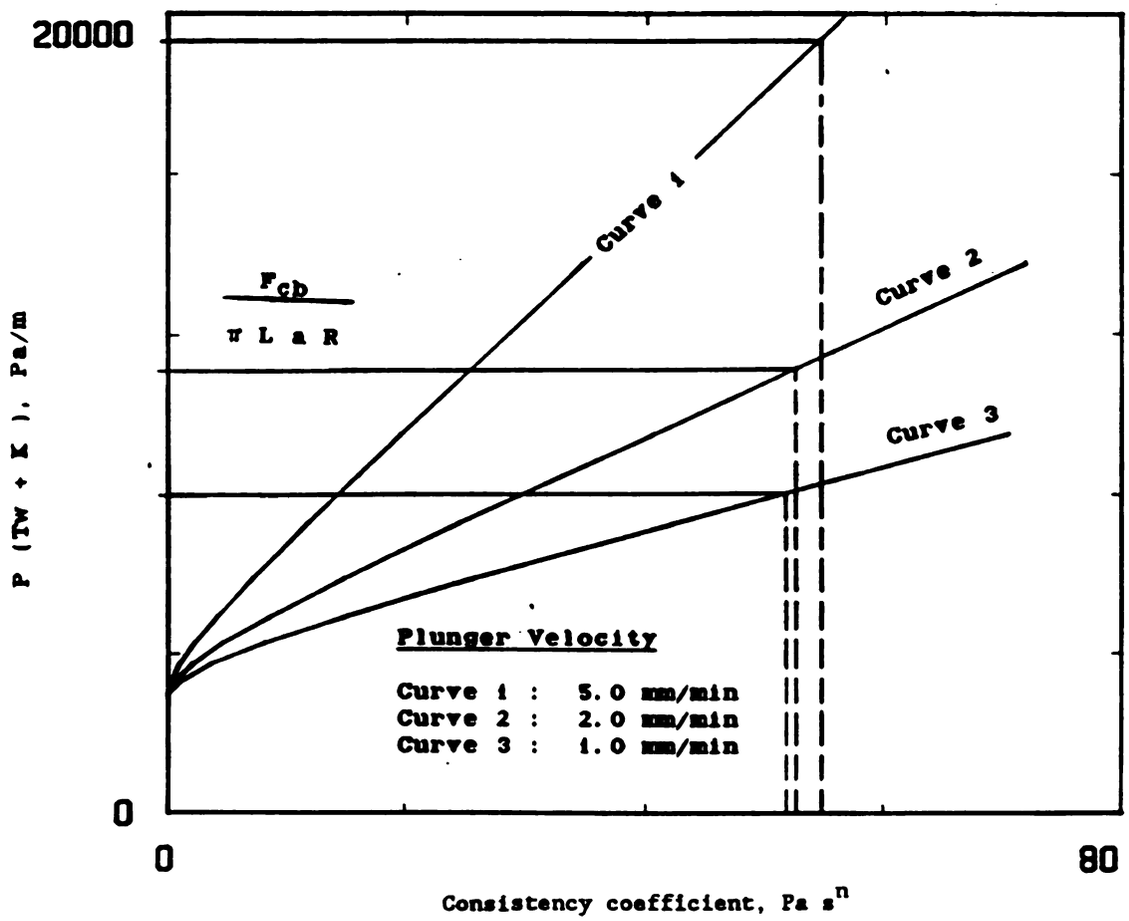

Figure 38. Determination of the rheological properties of Iota-Carrageenan with the back extrusion technique.

Table 6. Equilibrium rheological properties of 1% Iota-Carrageenan using back extrusion technique.

Herschel Bulkley Parameter	Value	Units
Yield Stress	5.0	Pa
Consistency Coefficient	52.0	Pa s^n
Flow Behavior Index	0.793*	dimensionless

*) Mean square error when determining flow behavior index was $5.8\ 10^7$.

Yield Stress

When the residual force recorded (after the plunger is stopped inside the sample) has reached the plateau or equilibrium value is used to calculate the yield stress, it gives a value of 12.16 Pa with a standard deviation of 6.4 Pa.

When the values of force recorded while the plunger is moving down the sample are used to determine the yield stress, a value of 5.0 Pa is obtained.

5.2.1.2 Parallel Plates

The structure formed by 1% Iota-Carrageenan is easily destroyed when transferring from the sample container to the sample holder in the test station of the Rheometrics Fluid Spectrometer. When adjusting the parallel plates configuration to the desired gap between the plates, further destruction is done. The gap between the parallel plates varied for the different tests from 1.5 to 2.0 mm.

Two types of experiments were performed. The first type was a rate sweep from zero to 10 s^{-1}. Higher values of shear rate caused the sample to flow out of the gap. Figs. 39 and 40 show replicates of the test.

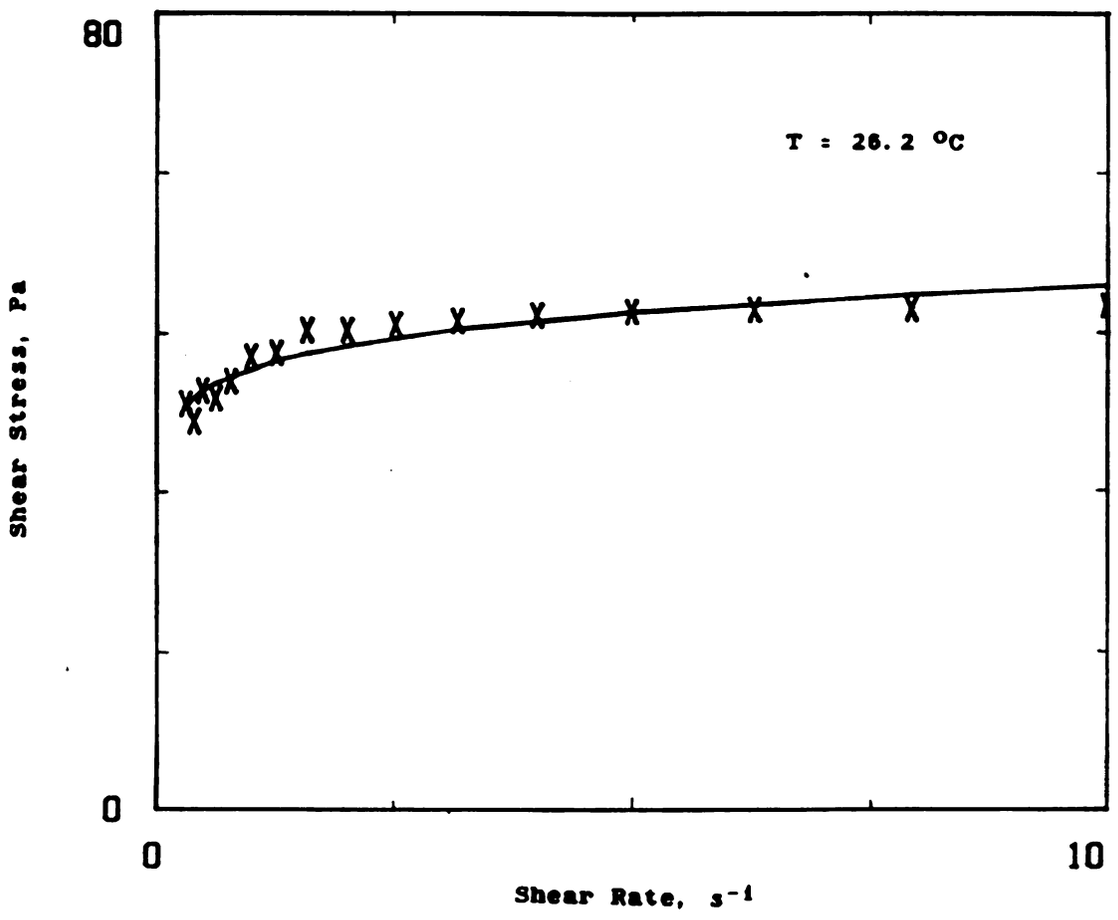

Figure 39. Rheogram of Iota-Carrageenan obtained by a rate sweep using the Rheometrics Fluid Spectrometer using parallel plates with a 1.5 mm gap.

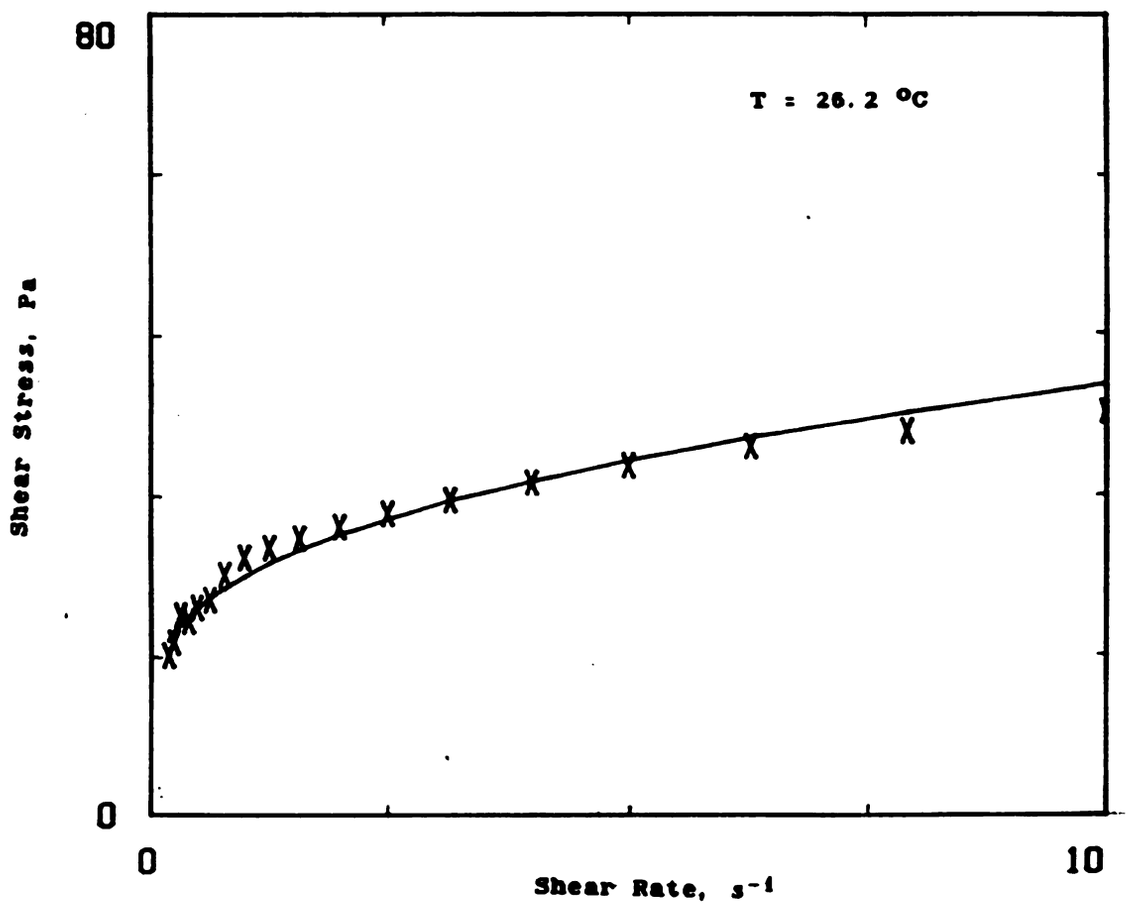

Figure 40. Rheogram of Iota-Carrageenan obtained by a rate sweep using the Rheometrics Fluid Spectrometer using parallel plates with a 1.5 mm gap.
Second run after resting the sample for 10 minutes.

The second type of test was done by setting a constant shear rate until the resultant shear stress reached an equilibrium value; at that moment the shear rate was either increased or decreased and the resultant equilibrium shear stress corresponding to the fixed shear rate was used to plot a rheogram. Fig. 41 shows a rheogram of the equilibrium shear stresses versus the corresponding shear rates. It can be seen that there is a big variation in values of shear stress for a given shear rate. This fact suggests that the sample is showing its response to a previous shear history, although the principle underlying the model developed by Kemblowski and Petera is that after the sample is sheared to equilibrium at a given shear rate, it will erase any previous shear history.

Table 7 shows the value of the rheological parameters of a Herschel Bulkley model when fitting the experimental data from Figs. 39, 40 and 41. The values obtained using equilibrium shear stress at a fixed shear rate will be used in further calculations.

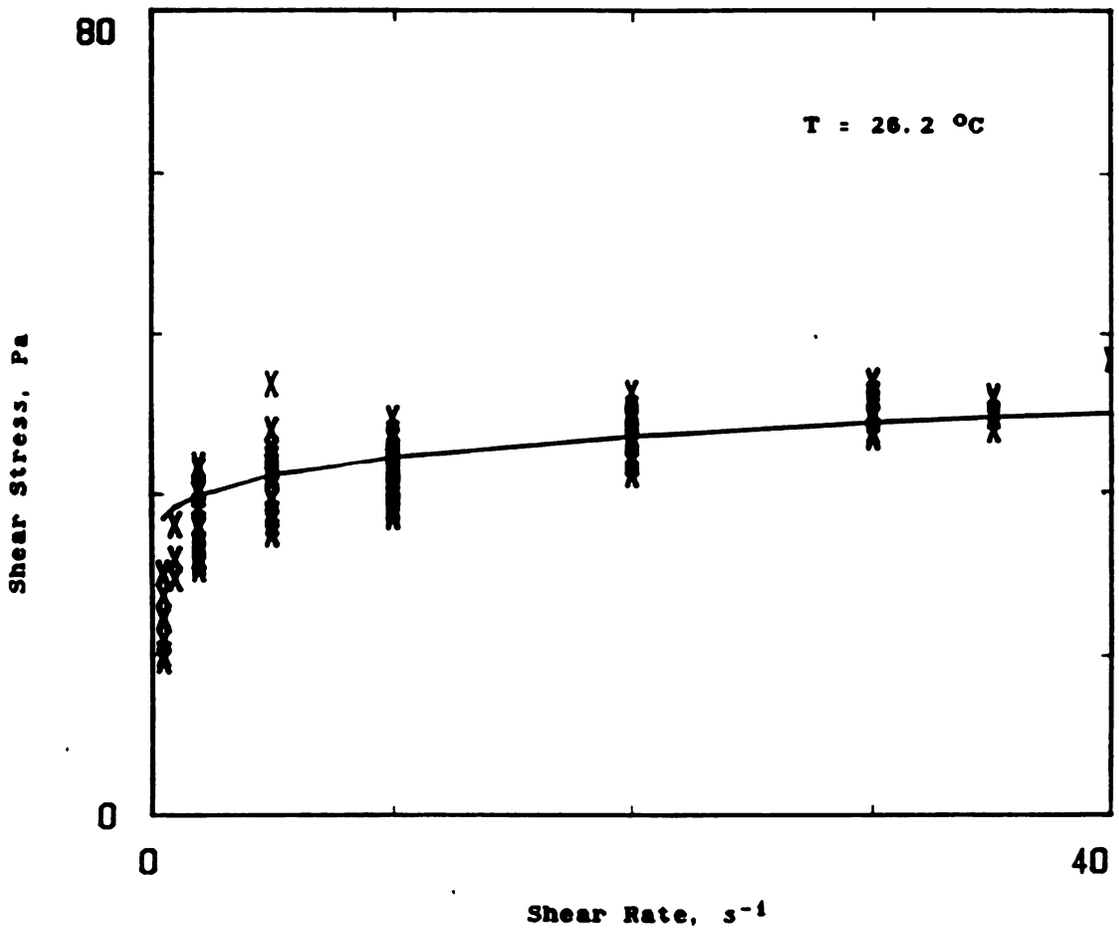

Figure 41. Rheogram of Iota-Carrageenan obtained after reaching an equilibrium value for shear stress at a fixed shear rate. Parallel plates geometry.

Table 7 . Equilibrium Parameters of the Herschel Bulkley model for 1% Iota-Carrageenan when using parallel plate geometry.

Experiment	Flow Behavior Index (dimensionless)	Consistency Coefficient (Pa s^n)	Yield Stress (Pa)	Mean Square Error
Rate Sweep 1	0.097	34.2	10.	2.09
Rate Sweep 2	0.377	13.9	10.	1.75
Equilibrium shear stress at fixed shear rate	0.221	7.5	23.	11.9

5.2.2 Time-Dependent Properties

5.2.2.1 Back Extrusion

When determining time dependency of 1% Iota-Carrageenan with a back extrusion device,it was not possible to observe a measurable transient when the plunger velocity was changed during a run from a high plunger velocity to a lower one. However, when the plunger is stopped inside the sample and the force continues to be recorded, it is observed that the residual force decays over time and then recovers until a plateau is reached. This inability to obtain a measurable transient is due to the sensitivity of the instrument. When comparing Figs. 16 and 38, it can be seen that the values of the term $F_{cb}/(\pi LaR)$ obtained experimentally for Iota-Carrageenan at a high plunger velocity are much lower than those values obtained for 7% bentonite suspension when the plunger velocity used is the lowest.

5.2.2.2 Parallel Plates

Fig. 42 shows the shear stress history of 1% Iota-Carrageenan when the shear rate is kept constant until an equilibrium shear stress is obtained. After the equilibrium is obtained, the shear rate is changed, and the variation of shear stress with time is recorded until equilibrium is reached at the new shear rate. After this, the shear rate is changed to the initial shear rate value. After obtaining equilibrium at this shear rate, the shear rate is again changed to another value and the variation of stress with time is recorded. The idea is to obtain a set of data for a given value of the structural parameter, κ. Cycles of this type are repeated for other values of the initial shear rate. Table 8 shows values of the equilibrium and initial shear stress for the initial, and final shear rates.

With the data given in Table 8, a curve fitting procedure was used to determine the shear stress-shear rate relationship for a constant value of the structural parameter. The value of the exponent m defined by Eq. [58] was 0.263 (st. dev. = 0.02). Table 9 shows the values for yield stress corresponding at a given value of the structural parameter κ.

The equation governing the yield stress variation of a 1% Iota-Carrageenan is obtained from Eq. [55]:

$$\sigma_y = 23 \left(1 - \exp \left(-0.218\, \kappa^{16.203} \right) \right)$$

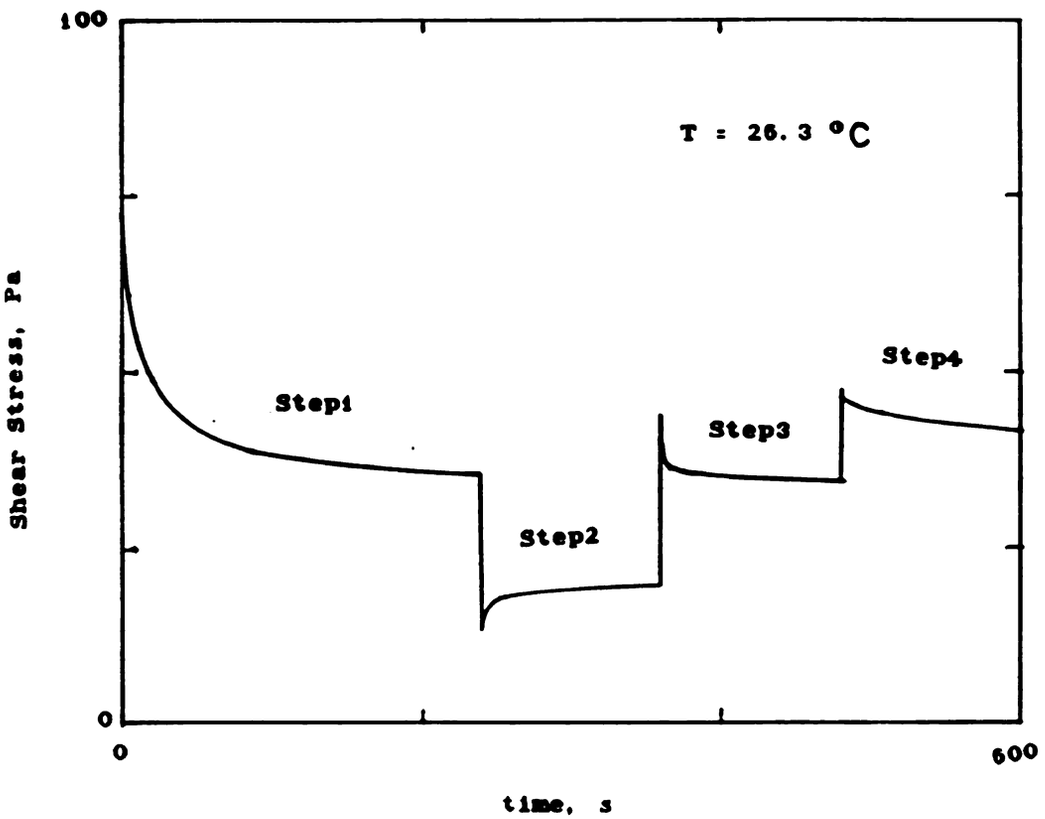

Figure 42. Shear stress history of Iota-Carrageenan when shear rate is changed from 10 s^{-1} (step 1) to 0.5 s^{-1} (step 2), then back to 10 s^{-1} (step 3), and finally 35 s^{-1} (step 4). Parallel plates geometry.

Table 8. Values of the shear stress immediately after the shear rate has been changed to a new value, and values of the equilibrium shear stress at a given shear rate.

Type of value	First Shear Rate 1/s I	Second Shear Rate 1/s II	Third Shear Rate 1/s III
Shear rate	2	0.5	5
Initial shear stress		23.02	37.21
Equil. shear stress	31.9	23.92	34.56
Shear rate	2	10	1
Initial shear stress		44.5	22.8
Equil. shear stress	31.9	37.8	22.35
Shear rate	5	0.5	30
Initial shear stress		19.7	48.8
Equil. shear stress	34.3	21.8	42.6
Shear rate	5	0.5	30
Initial shear stress		14.8	42.0
Equil. shear stress	28.0	17.3	40.0
Shear rate	5	20	0.5
Initial shear stress		45.37	16.51
Equil. shear stress	33.87	40.22	19.23
Shear rate	5	30	10
Initial shear stress		48.74	33.07
Equil. shear stress	33.5	41.72	32.43
Shear rate	10	20	30
Initial shear stress		41.2	43.2
Equil. shear stress	35.2	39.4	41.5
Shear rate	10	20	30
Initial shear stress		40.35	41.3
Equil. shear stress	34.5	37.7	39.15
Shear rate	10	20	30
Initial shear stress		35.87	38.9
Equil. shear stress	30.4	35.15	38.0

Table 8 (cont'd.).

Shear rate	10	0.5	35
Initial shear stress		16.2	45.39
Equil. shear stress	35.28	19.55	41.5
Shear rate	10	0.5	35
Initial shear stress		13.1	41.2
Equil. shear stress	30.7	15.9	39.5
Shear rate	20	30	35
Initial shear stress		41.26	40.6
Equil. shear stress	37.6	39.44	39.5
Shear rate	20	30	35
Initial shear stress		38.48	38.7
Equil. shear stress	35	37.5	38.2
Shear rate	20	0.5	10
Initial shear stress		14.7	31.4
Equil. shear stress	39	19.8	31.5
Shear rate	20	0.5	10
Initial shear stress		12.26	29.47
Equil. shear stress	35.5	15.3	29.61

Table 9. Yield stress values corresponding to a given structural parameter κ for a 1% Iota-Carrageenan solution.

Structural parameter κ (dimensionless)	Yield Stress σ_y (Pa)	Shear Rate $\dot{\gamma}$ (s^{-1})
0.97	2.6	2.0
0.94	2.0	5.0
0.91	1.0	10.0
0.88	0.6	20.0

The time dependency factor is calculated from Eq. [68]. Fig. 43 shows a plot of the structural parameter over time when the shear rate changes from 5 to 0.5 s^{-1}, and Fig. 44 shows the changes of structural parameter over time when the shear rate changes from 5 to 30 s^{-1}.

The values of the inverse time constant Γ parameter are shown in Table 10. It can be seen that the time constant parameter is a function of the shear rate; as the shear rate increases, the time constant decreases. Therefore, the thixotropy effects are better observed at low shear rates.

When comparing the values of the Herschel Bulkley parameters obtained with the back extrusion technique to those obtained with parallel plates, the back extrusion technique gives lower values for the yield stress and higher values for the consistency coefficient and flow behavior index. The range of shear rates reached with back extrusion was from $4.8\ 10^{-3}$ to 0.5 s^{-1}, and the range of shear stresses varied from 5.5 to 35.8 Pa.

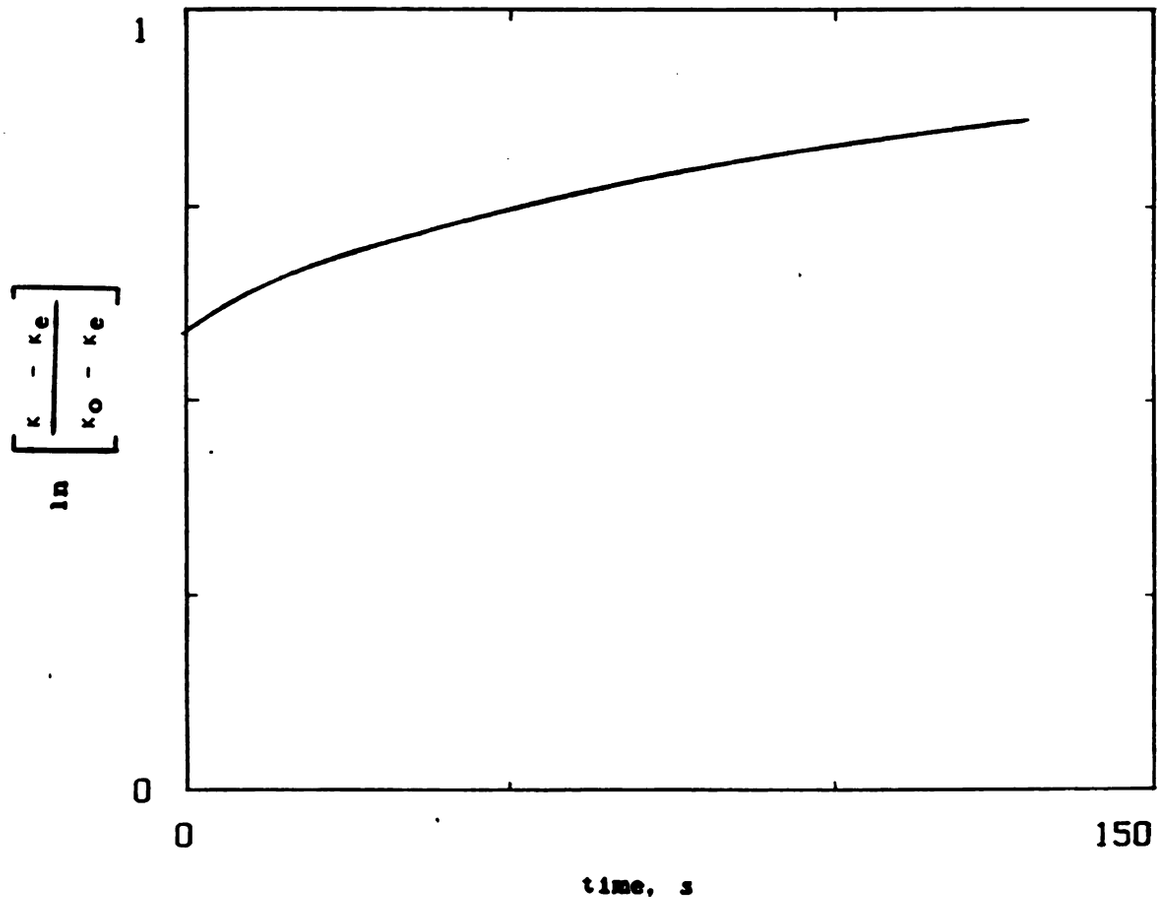

Figure 43. Changes of the structural parameter over time of a 1% Iota-Carrageenan sample when the shear rate changes from 5 to 30 s^{-1}.

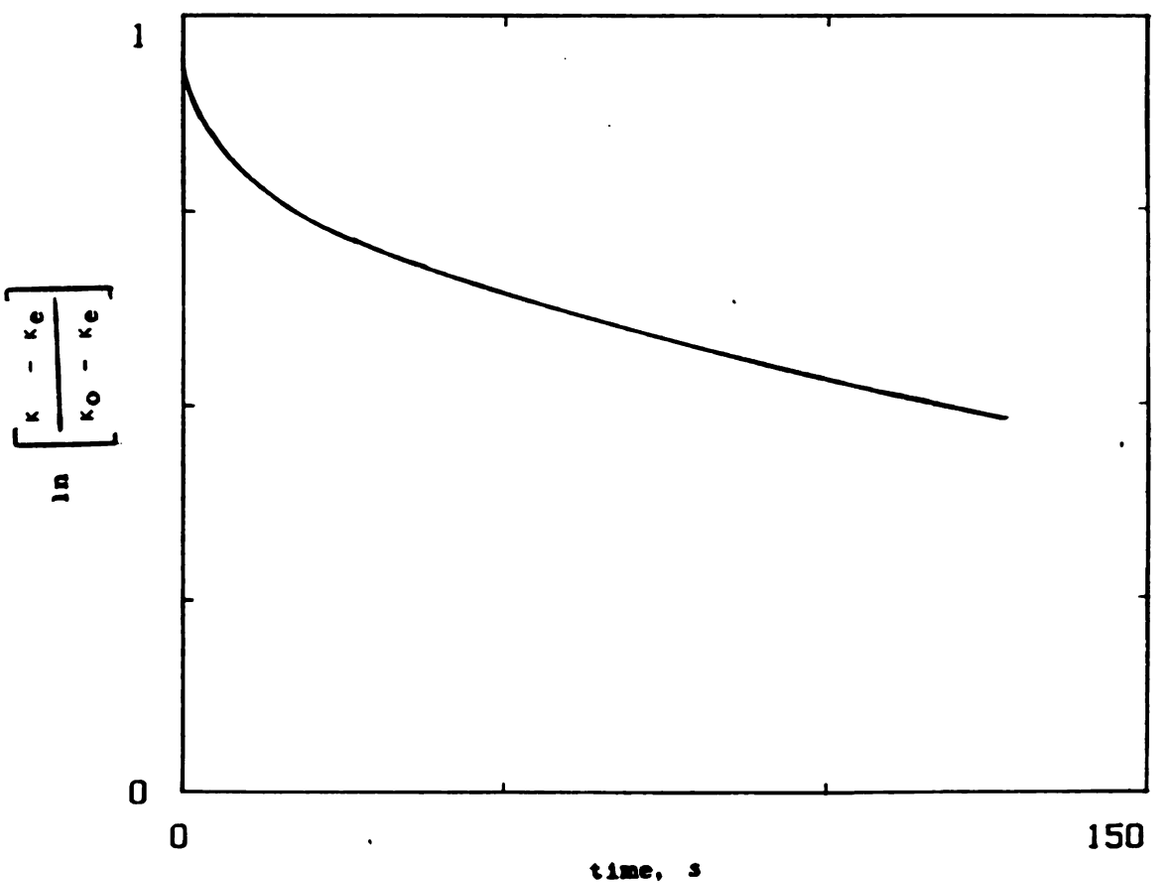

Figure 44. Changes of the structural parameter over time of a 1% Iota-Carrageenan sample when the shear rate changes from 5 to 0.5 s^{-1}.

Table 10. Values of the inverse time constant, Γ, for 1% Iota-Carrageenan obtained with a parallel plate geometry.

Shear Rate (s^{-1})	Inverse Time Constant, Γ (s^{-1})	Standard Deviation (s^{-1})
0.5	$3.35 * 10^{-3}$	$0.47 * 10^{-3}$
30.0	$1.93 * 10^{-3}$	$0.18 * 10^{-3}$
35.0	$1.27 * 10^{-3}$	$0.20 * 10^{-3}$

5.3 Advantages and Disadvantages of Using Back Extrusion to Evaluate Time-Dependent Rheological Properties

Use of the back extrusion technique to evaluate time-dependent rheological properties presents several **advantages**:

-The fluid in the annular gap is always sheared, even if the plunger velocity is very low.

-Very thick fluids can be tested in this device. Very high forces can be applied on the plunger; therefore, it is always possible to generate flow in the annulus.

-If the sample contains suspended particles, the annular gap can be increased.

-The back extrusion technique allows one to follow the development of yield stress over time after a sample is disturbed and then allowed to rest.

-The sample does not need to be disturbed when loading it into the testing vessel

-It is possible to obtain very low shear rates when using the back extrusion device.

-In back extrusion testing, the rheological properties are determined under pressure driven flow, in a similar way as flow in a tube.

Some of the **disadvantages** when using back extrusion to evaluate time-dependent rheological properties are:

-Perfect alignment between the plunger and the graduate cylinder containing the sample is difficult to obtain.

-The evaluation procedure is very elaborate, requiring the use of computer programs for the calculations.

-The shear rate calculation is especially elaborate, and requires several iterations.

-The calculation relies too heavily on non-linear parameter estimation.

-The modified Kemblowski and Petera model is still very complex.

-It is necessary to have compression cells (to use in the Instron Universal Testing Machine) of different capacity ranges. This allows one to accomodate for a wide range of apparent viscosity by increasing the sensitivity of the instrument.

Overall, it can be said that the potential for the use of the back extrusion technique to determine time-dependent rheological properties is excellent.

5.4 Practical Applications

The knowledge of the recovery of the internal structure of a fluid with a yield stress after it has undergone shearing has technological implications. If such a fluid has been pumped through a pipe and for some reason it needs to be held temporarily in a surge tank, after a while this fluid will develod its internal structure. If the pump being used to transport this fluid was designed without considering the increase in yield stress of this fluid, that pump will not be able to move the fluid. Or, if gravity is being used to move the fluid, then the outlet port of the tank has to be properly designed to overcome the higher yield stress developed during the resting of the fluid.

CHAPTER 6

CONCLUSIONS

The conclusions of this study are:

1. Mathematical expressions to describe the behavior of thixotropic fluids in a back extrusion device using the model developed by Kemblowski and Petera for a thixotropic fluid, combined with the expressions developed for back extrusion testing of Herschel Bulkley fluids were developed.

2. The values of the time dependent parameters of a thixotropic fluid from back extrusion data were determined.

3. Using back extrusion methods, the changes in yield stress with respect to time, after the sample has been sheared and brought to rest may be followed.

4. The back extrusion technique is very adequated to perform studies of both totally reversible and totally irreversible structure breakdown.

CHAPTER 7

FUTURE RESEARCH

It would be useful to find a correlation between the shear rate history (strain history) and the inverse time constant of a thixotropic fluid in a back extrusion device. For doing the above, different plunger radii should be used in conjunction with different plunger velocities.

Materials with standard yield stress should be developed, so that the above relationship between shear rate history and natural time function could be verified with other geometries such as capillary tubes.

BIBLIOGRAPHY

BIBLIOGRAPHY

Bauer, W. H. and Collins, E.A. 1967. In "Rheology. Theory and Applications", F.R. Eirich (Ed.), V 4, p 423. Academic Press, New York.

Blake, J.A., and Moran, J.J. 1975. A new approach to capillary extrusion rheometry. J. Texture Studies 6:227-239.

Camina, M., and Roffey, C.G. 1971. Time dependent power law behaviour at low shear rates for paint systems. Rhel. Acta 10:606-607.

Chavan, V.V., Deysarkar, A.K., and Ulbrecht, J. 1975. On phenomenological characterization of thixotropic behaviour. Chem. Eng. J. 10:205-214.

Cheng, D.C.-H.,Ray, D.J., Valentin, F.H.H. 1965. The flow of thixotropic bentonite suspensions through pipes and pipe fittings. Trans. I. Chem. E. 43:176-186.

Cheng, D.C.-H. and Evans, F. 1965. Phenomenological characterization of the rheological behaviour of inelastic reversible thixotropic and antithixotropic fluids. Brit. J. Appl. Phys. 16:1599-1617.

Cheng, D.C.-H. 1973. A differential form of constitutive relation for thixotropy. Rheol. Acta 12:228-233.

Cheng, D. C.-H. 1980. Measurement of Thixotropic Properties. Lecture to Royal Society of Chemistry. Residential School "Rheology of Fluids". 15-19 September. University College of Wales, Aberystwyth.

Cheng, D.C.-H. 1984. Further observations on the rheological behaviour of dense suspensions. Powder Technol. 37:255-273.

Cheng, D.C.-H. 1987. Thixotropy. Int. J. Cosmetic Soc. 9:151-191.

Darsch, G.A., Shaw, C.P., and Tuomy, J.M. 1979. Examination of patient tray food service equipment/an evaluation of the Sweetheart food service cart. Technical Report Natick/TR-79/016. Food Engineering Laboratory, U.S. Army Natick Research & Development Command, Natick, MA.

De Kee, D., Code, R.K., and Turcotte, G. 1983. Flow properties of time-dependent foodstuffs. J. Rheol., 27(6):581-604.

Dziubinski,M. and Petera J. 1984. Laminar flow of some inelastic time-dependent fluids in pipes. Rheol. Acta 23:261-165.

Firth, B.A., Hunter, R.J. 1976. Flow properties of coagulated colloidal suspensions. III. The elastic floc model. J. Coll. Interf. Sci. 57:266-275.

Ford, E.W., and Steffe, J.F. 1986. Quantifying thixotropy in starch-thickened, strained apricots using mixer viscometry techniques. J. Texture Studies 17:71-85.

Fredrickson, A.G. 1970. A model for the thixotropy of suspensions. AIChe J. 16: 436-441.

Gillespie, T. 1960. An extension of Goodeve's impulse theory of viscosity to pseudoplastic systems. J. Coll. Sci. 15: 219-231.

Godfrey, J.C. 1973. Steady shear measurement of thixotropic fluid properties. Rheol. Acta 12:540-545.

Grim, R.E. 1962. "Applied Clay Mineralogy". Mc Graw-Hill Book Co., Inc. New York, Toronto, London. p:16-20, 224-251.

Grim, R.E., and Güven, N. 1978. "Bentonites. Geology, Mineralogy, Properties and Uses ". Elesevier Scientific Publishing Co. Amsterdam, Oxford, New York . p:1,9,19,217.

Hahn, S.J. Ree, T. and Eyring, H. 1959. Flow mechanism of thixotropic substances. Ind. Eng. Chem. 51:856-857.

Harris, J. 1967. A continuum theory of time-dependent inelastic flow. Rheol. Acta, 6:6-12.

Hutton, J.F. 1963. Fracture of liquids in shear. Nature 200:646-648.

Jackson, J.M., and Olson, F.C.W. 1953. Thermal processing of canned foods in tin containers. 4. Studies of the machanisms of heat transfer within the container. In "Sterilization of Canned Foods, Theoretical Considerations in the Sterilization of Canned Foods," p. 35. American Can Co., Barrington, IL.

Kemblowski, Z. and Petera J. 1979. Rheological characterization of thixotropic fluids. Rheol. Acta 18:702-710.

Kemblowski, Z. and Petera J. 1980. A generalized rheological model of thixotropic materials. Rheol. Acta 19:529-538.

Kemblowski, Z. and Petera J. 1981. Memory effects during flow of thixotropic fluids in pipes. Rheol. Acta 20:311-323.

Krieger, I.M. 1968. Shear rate in the Couette viscometer. Trans. Soc. Rheology 12:5-11.

Mercer, H.A. 1973. Time-dependent viscosity of thixotropic bentonite-water suspensions. Ph.D. Dissertation. The University of Rochester, New York.

Mercer, H.A. and Weymann, H.D. 1974a. Structure of thixotropic suspensions in shear flow. III. Time-dependent behavior. Trans. Soc. Rheol. 18:199-218.

Mercer, H.A. and Weyman, H.D. 1974b. Time-dependent behavior of thixotropic suspensions. Rheol. Acta. 13:413-417.

Mewis, J. 1979. Thixotropy-A general Review. J. of Non-newtonian Fluid Mechanics. 6:1-20.

Mewis, J. Rheology of Suspensions. 1980. In "Rheology" Vol 1: Principles. Edited by Astarita, G., Marrucci, G., and Nicolais. Plenum Press-New York and London p:149-167.

Michaels, A.S., Bolger, J.C. 1962. The plastic flow behavior of flocculated kaolin suspensions. Ind. Eng. Chem. Fundam. 1: 153-162.

Nguyen, Q.D., and Boger, D.V. 1985. Thixotropic behaviour of concentrated bauxite residue suspensions. Rheol. Acta 24:427-437.

Nguyen, Q.D., and Boger, D.V. 1987. Characterization of yield stress fluids with concentric cylinder viscometers. Rheol. Acta 26:508-515.

Niekamp, A., Unklesbay, K., Unklesbay, N., and Ellersieck, M. 1984. Thermal properties of bentonite-water dispersions used for modeling foods. J. Food Sci. 49:28-31.

Noll, W., 1958. A mathematical theory of the mechanical behavior of continuous media. Arch. Rational Mech. Anal. 2:197-226.

Noll, W., 1972. A new mathematical theory of simple materials. Arch. Rational Mech. Anal. 48:1-50.

Osorio-Lira, F.A. 1985. Back extrusion of Power Law, Bingham plastic and Herschel-Bulkley fluids. M.S. Thesis. Michigan State University. East Lansing.

Osorio, F.A., and Steffe, J.F. 1987. Back extrusion of power law fluids. J. Texture Studies 18:43-63.

Osorio, F.A., Steffe, J.F., and Ofoli, R.Y. 1989. Back extrusion of Bingham plastic fluids. Presented at the Fifth International Congress of Engineering anf Food. ICEF-5. Cologne, Federal Republic of Germany. May 28 - June 3.

Pedersen, J.K. 1980. Carrageenan, pectin and xanthan/locust bean gum gels. Trends in their food use. Fd. Chem. 6:77-88.

Peterson, W.R., and Adams, J.P. 1983. Water velocity effect on heat penetration parameters during institutional size retort pouch processing. J. Food Sci. 48:457-459,464.

Petrellis, N.C., and Flumerfelt, R.W. 1973. Rheological behavior of shear degradable oils: kinetic and equilibrium properties. Can. J. Chem. Eng. 51:291-301.

Reiner, M. and Scott Blair, G.W. 1967. In " Rheology. Theory and Applications", F.R. Eirich (Ed.), V 4, p 461. Academic Press, New York.

Ritter, R.A., and Govier, G.W. 1970. The development and evaluation of a theory of thixotropic behavior. Can. J. Chem. Eng., 48:505-513.

Ross, R.A. 1970. On the structure of bentonite suspensions. Ph.D. Dissertation, University of Rochester.

Ross, R.A., Weymann, H.D., and Chuang, M.C. 1973. On the structure of thixotropic suspensions in the shear flow. Phys. Fluids 16:784- .

Sestak, J., Houska, M., and Zitny, R. 1982. Mixing of Thixotropic Fluids. J. of Rheology 26(5):459-475.

Skelland, J.G. 1958. "Non-Newtonian Flow and Heat Transfer." John Wiley and Sons, Inc., New York.

Slibar, A. and Paslay, P.R. 1964. In "Proc. Int. Symp. on Second-Order Effects in Elasticity, Plasticity and Fluid Dynamics". Editors: Reiner, M. and Abir, D. Pergamon Press, Oxford, 1964. p:314.

Steffe, J.F., and Ford, E.W. 1985. Rheological techniques to evaluate the shelf-stability of starch-thickened, strained apricots. J. Texture Studies 16:179-192.

Steffe, J.F., and Osorio, F.A. 1987. Back extrusion of non-Newtonian fluids. Food Technol. 41(3):72-77.

Steffe, J.F., Castell-Perez, M.E., Rose, K.J., and Zabik, M.E. 1989. Rapid testing method for characterizing the rheological behavior of gelatinizing corn starch slurries. Cereal Chem. 66(1):65-68.

Storey, B.T., and Merrill, E. W. 1958. The rheology of aqueous solutions of amylose and amylopectin with reference to molecular configuration and intermolecular association. J. Polym. Sci. 23:361-375.

Tiu, C., and Boger, D.V. 1974. Complete rheological characterization of time-dependent food products. J. Texture Studies 5:329-338.

Tung, M.A., Richards, J.F. Morrison, B.C., and Watson, E.L. 1970. Rheology of fresh, aged and gamma-irradiated egg white. J. Food Sci. 35:872-874.

Unklesbay, N., Unklesbay, K., and Henderson, J. 1980. Simulation of energy used by foodservice infrared heating equipment with bentonite models of menu items. J. Food Protect. 43:789-794.

Unklesbay, N. 1982. Overview of foodservice energy research: Heat processing. J. Food Protect. 45:984-992.

Van de Ven, T.G.M., Hunter, R.J. 1977. The energy dissipation in sheared coagulated sols. Rheol. Acta. 16, 534-543.

Van Wazer, J.R., Lyons, J.W., Kim, K.Y., and Colwell, R.E. 1963. "Viscosity and Flow Measurement. A Laboratory Handbook of Rheology." Interscience Publishers, New York.

Whorlow, R.W. 1980. "Rheological Techniques." Halstead Press, New York.

Wilson, K.C. 1986. Modelling the effects of non-Newtonian and time-dependent slurry behaviour. In Proceedings of the 10th International Conference on the Hydraulic Transport of Solids in Pipes (Hydrotransport 10). October 29-31. Paper J1, p283-289. Innsbruck, Austria. BHRA Fluid Engineering, Cranfield, Bedford, England.

Yamano, Y., Ejiri, K., Endo, T., and Senda, M. 1975. Heat processing into flexible packages with food-simulated materials. Japanese J. Food Sci. Technol. 22:199-204.

Zitny, R., Rieger, F. Houska, M., and Sestak, J. 1978. Rheological characterization of thixotropic fluids with respest to equipment design procedures. In Proceedings of the International Congress CHISA. August 1978. Prague, Czechoslovakia.

APPENDIX A: RAW DATA

Bentonite 7% :

density : 1050.8 kg/m3

plunger radius : 0.01425 m

cylinder radius : 0.01765 m

PLUNGER VELOCITY (mm/min) vp1	vp2	FORCE SCALE (N)	TIME SCALE (min)
3	0.1	10	20
3	0.1	10	20
3	0.7	10	20
3	0.5	10	20
3	0.3	10	20
3	0.05	10	20
3	0.3	10	20
3	0.3	10	20
3	0.3	10	20
3	0.1	10	20
3	0.5	10	20
3	0.7	10	20
3	0.3	10	20
2	0.5	5	30
2	0.2	10	30
2	0.05	10	30
2	0.1	10	30
1	0.2	10	30
1	0.1	10	30
1	0.5	10	30
1	0.05	10	30

1	0.1	10	30
0.5	0.2	5	30
0.5	0.05	5	30
0.5	0.1	5	30

CHART LENGTH (cm)		MAXIMUM LENGTH CORRESPONDING TO FORCE (cm)		INITIAL LENGTH IN y-DIRECTION FOR SECOND PLUNGER VELOCITY (cm)
c11	c12	ym1	ym2	
4.1	27.9	18.4	14.8	13.1
4.1	26.8	18.2	13.9	13.25
3.5	10.8	15.7	19.9	12.9
3.7	14.2	16.8	20.2	13.4
4	20.2	18.8	21	14.55
3.1	29	17.9	12.9	12.2
4	12.1	17.6	16.6	14.25
3.7	10.4	16.1	14.5	12.7
4	15.2	20.9	19	16.2
4.3	21.8	18.1	14	13.2
3.5	13.2	16.9	19.6	13.8
3.3	7.2	16.7	19.5	14.2
4.1	18.5	17.2	19.3	14.1
1.5	5.6	15	22.6	13
3.4	10.9	14.4	14	11.6
4.1	23.7	18.7	15.5	13.7
3.4	22.8	16.7	15.5	12.7
7.2	16.8	14.6	17.9	12.8
6.8	18	15.2	15.2	13.1
6	9.3	13.6	21.4	12.6
5.6	20.7	11.9	10.2	9.45
5.8	19.3	12.2	12.4	10.35
6.7	11.7	14.1	19.5	13.1
8.3	17.2	18.1	17	15.4
5.8	20	13	16.5	11.4

CONCENTRIC CYLINDER DATA

SMOOTH SENSORS:

BOB RADIUS = 0.0184 m
CUP RADIUS = 0.021 m

RPM	Shear Stress (Pa)
1	51.5
1	55.8
1	52.2
1	50.5
1	47.8
1	52.3
1	44.5
1	57.6
1	41.13
1	36.1
3	67.4
3	63.7
3	58.5
3	61.9
5	113
5	105.6
5	104.8
5	105
5	106.8
5	108.4
5	99.4
5	104.2
5	100.1
5	122.5
5	109.1
5	102
5	101.4
5	104.1
10	144.3
10	142.1
10	141.4
11	135.3
11	117.5
13	111.5
15	174.8
15	165.7
15	158.4
15	154.8

15	151.6
15	144.3
15	134.1
15	132.7
21	142.3
21	139.7
21	122.8
23	114.3
25	158.5
25	150.9
35	179.3
41	130.4
43	131.4
45	157.6
50	173.7
50	114.7
50	134.9
50	137.5
55	175.5
55	180.9
55	172.5
55	163.1
55	160.4
75	158.8
75	158.4
85	177.7
85	195.4
85	192.4
95	176.5
95	174.9
95	171.6
95	170.6
110	188.4
250	169.8
250	169.8
650	202.3

SERRATED CYLINDERS

BOB RADIUS = 0.0184 m
CUP RADIUS = 0.021 m

RPM	Shear Stress (Pa)
5	134.5
8	150.3
10	165.7
11	152.9
15	155.3
20	152.4
20	152.9
20	152.6
40	164
40	172.3
40	144.8
50	176.9
70	192.6
70	178.4
80	195.6
80	195.3
90	220.7

TIME-DEPENDENCY DATA USING BACK EXTRUSION. BENTONITE 7%

Force scale = 10 N
length of paper in y-direction = 25 cm
length of paper in x-direction = 38 cm

Length in x-direction corresponding to time (cm)	LENGTH IN y-direction corresponding to force (cm)	Time scale (min)
0.1296	0.0545	10
0.1195	0.0545	10
0.3457	-3.3775	10
0.3609	-3.3977	10
0.3940	-3.5093	10
0.5007	-3.9934	10
0.5871	-4.4649	10
0.7218	-5.1492	10
0.8032	-5.7398	10
0.9226	-6.2924	10
1.0294	-6.9083	10
1.1590	-7.5750	10
1.2530	-8.0870	10
1.3903	-8.8347	10
1.8834	-11.2960	10
2.3917	-13.7470	10
2.8568	-15.9345	10
3.1262	-17.0042	10
3.2813	-17.7671	10
3.2533	-15.0271	10
3.2533	-15.0169	10
3.2558	-14.8319	10
3.2584	-14.5049	10
3.2762	-14.2160	10
3.3143	-13.9321	10
3.3346	-13.7952	10
3.4058	-13.6051	10
3.4744	-13.4860	10
3.5913	-13.2806	10
3.7667	-13.0829	10
3.9268	-12.9689	10
4.0870	-12.8802	10
4.3487	-12.8269	10
4.7986	-12.7179	10
5.1239	-12.6748	10
5.4340	-12.6419	10
5.8407	-12.6394	10
6.1787	-12.6165	10

6.6388	-12.6039	10
6.9946	-12.5912	10
7.4292	-12.5937	10
7.6020	-12.5735	10
7.6986	-12.5557	10
7.7952	-12.5608	10
7.9401	-12.5785	10
9.3024	-12.5608	10
10.7054	-12.5659	10
11.8135	-12.5608	10
14.5077	-12.5684	10
17.0925	-12.5608	10
20.1450	-12.5963	10
22.4960	-12.5912	10
26.4279	-12.6596	10
30.5479	-12.7838	10
32.2889	-12.8269	10
32.2915	-12.8269	10
32.2966	-12.7940	10
32.3296	-12.6444	10
32.3703	-12.5354	10
32.4592	-12.3859	10
32.6473	-12.1349	120
32.8939	-11.9753	120
33.2471	-11.8130	120
33.9334	-11.5545	120
34.6171	-11.3314	120
35.5778	-11.0653	120
36.3606	-10.8853	120
37.6315	-10.5837	120
37.9593	-10.5431	120
0.0381	-10.5178	120
0.0381	-10.5203	120
0.3584	-10.1604	120
1.0065	-9.5926	120
2.2011	-8.4165	120
2.9102	-7.7904	120
3.7464	-7.1948	120
4.2903	-6.8424	120
5.1595	-6.4673	120
6.2041	-6.1023	120
7.0175	-5.8666	120
7.6351	-5.7297	120
8.6365	-5.4788	120
9.4091	-5.3317	120
10.3343	-5.1721	120
10.9799	-5.0529	120
11.9228	-5.0048	120
12.6573	-5.0276	120
13.7604	-5.2202	120
14.8101	-5.5497	120
15.6184	-6.0288	120
15.9971	-6.3178	120
16.6808	-6.9058	120

17.4051	-7.6079	120
17.9389	-8.1732	120
18.6327	-8.9082	120
19.2199	-9.5216	120
20.1475	-10.4215	120
20.2848	-10.5786	120
20.3534	-10.6547	120
20.4043	-10.6116	120
20.4653	-10.6040	120
20.5212	-10.5812	120
20.5618	-10.5761	120
20.6254	-10.5888	120
20.7169	-10.6623	120
20.7804	-10.7206	120
20.8338	-10.6496	120
20.8592	-10.6673	120
21.0066	-10.7991	120
21.2252	-10.8701	120
21.5632	-11.0121	120
22.0868	-11.1312	120
22.5011	-11.2123	120
22.9637	-11.3137	120
23.5000	-11.4151	120
24.0617	-11.4379	120
24.7200	-11.4911	120
25.3986	-11.5317	120
26.2119	-11.5570	120
27.0125	-11.5368	120
27.9529	-11.5951	120
28.8882	-11.5925	120
29.7143	-11.6407	120
30.4666	-11.7497	120
31.1274	-11.7725	120
31.8264	-11.8105	120
32.5660	-11.8130	120
33.1887	-11.8054	120
33.7606	-11.8282	120
34.4493	-11.8156	120
34.8712	-11.8308	120
35.3135	-11.8485	120

APPENDIX B : DERIVATION OF EQUATION [59]

Starting with the equilibrium flow curve is described by the Herschel Bulkley equation

$$\sigma = \sigma_0 + \eta \dot{\gamma}^n \qquad [56]$$

Adding and substracting the term $\sigma_0 \exp(- A \kappa^s)$ into the above equation gives,

$$\sigma = \sigma_0 - \sigma_0 \exp(- A \kappa^s) + \eta \dot{\gamma}^n + \sigma_0 \exp(- A \kappa^s)$$

Using the definition of the equilibrium function of the structural parameter as given by Eq. [58],

$$\kappa_e = (\alpha \dot{\gamma})^{(n-m)} \qquad [58]$$

where:

α = a constant = 1 s

m = exponent defined by this equation, dimensionless

Regrouping yields

$$\sigma = \sigma_0(1 - \exp(- A \kappa^s)) + \eta \kappa \dot{\gamma}^m + \sigma_0 \exp(- A \kappa^s)$$

Using the expression that defines yield stress

$$\sigma_y = \sigma_0 (1 - \exp(- A \kappa^s)) \qquad [55]$$

Then,

$$\sigma = \sigma_y + \eta \kappa \dot{\gamma}^m + \sigma_0 \exp(- A \kappa^s) \dot{\gamma}^m (\dot{\gamma})^{-m}$$

Introducing the definition of the structural parameter gives,

$$\sigma = \sigma_y + \eta \kappa \dot{\gamma}^m + \sigma_0 \exp(- A \kappa^s) \dot{\gamma}^m \kappa^{(m/(m-n)}$$

And finally, after regrouping, the generalized equation of state for a thixotropic fluid is found to be

$$\sigma = \sigma_0(1 - \exp(- A \kappa^s))+\eta \dot{\gamma}^m\left[\kappa+ \frac{\sigma_0 \kappa^{\frac{m}{m - n}}}{\eta}\right]\exp(- A\kappa^s) \qquad [59]$$

APPENDIX C : DIAGRAM OF EQUATIONS SOLVED BY USING REGRESSION CURVE FITTING, AND SOLUTIONS TO SIMULTANEOUS EQUATIONS SYSTEM

REGRESSION CURVE FITTING [Equation number]	SOLUTION TO SIMULTANEOUS EQUATION [Equation number]
[55]	[40]
[56]	[41]
[57]	[43]
[59]	
[67.a]	
[89]	
[101]	
[108]	